University of Alberta

Diffusion Tensor Magnetic Resonance Imaging of Neurodevelopment

by

Lindsay Adrienne Snook 

A thesis submitted to the Faculty of Graduate Studies and Research in partial fulfillment of the requirements for the degree of

Master of Science

Department of Biomedical Engineering

Edmonton, Alberta
Spring 2006

Your file Votre référence
ISBN: 0-494-13890-4
Our file Notre référence
ISBN: 0-494-13890-4

This thesis is dedicated to my family; Gail, Michael, Laelie and Lisa, my fiancé Justin and my future family; Shirley, Don, Matt and Kristin.

ABSTRACT

Diffusion tensor magnetic resonance imaging (DTI) is an MRI technique that takes advantage of the natural Brownian motion of water in the brain and uses it to elucidate information about the microstructure of the brain by allowing the water molecules to diffuse for a sufficient time, probing the local environment. In this body of work we use DTI to study the development of the brain through childhood, adolescence and young adulthood, with nearly 200 subjects between the ages of 5 – 27 years. We use quantitative measures of mean diffusivity (Trace/3 ADC) and fractional anisotropy (FA) to determine patterns of development within gray matter and white matter structures. This is accomplished with two analysis techniques: manual region of interest and automated voxel-by-voxel analysis (e.g. statistical parametric mapping, SPM). This large DTI dataset is a valuable tool for comparative studies of various neurologic, cognitive and genetic disorders that affect the brain's connectivity.

ACKNOWLEDGEMENTS

Thanks firstly to my supervisor Christian, for all the wonderful opportunities and experiences of the last two and a half years. Never did I imagine international travel as part of my graduate work! Thanks for your patience, as well as for pushing me to accomplish all that I could. Thanks to Dawne for all the work we did with the children, and for all the interesting, and thought provoking discussions. Things wouldn't have been the same without you.

Thanks also to each of the graduate students of our research group: Yusuf, for getting me started way back when, Jacob and Alison for being great office-mates, Luis, for all your help with cool brain images and videos, as well as all that anatomy stuff that is just so foreign to me, and Rob for helping me to find more volunteers. A huge thank you goes out to Chris Plewes for your work over the past 3 summers. Without all of your programs, macros, and insights, this thesis would not be the same. Also, thanks to Catherine for being a good friend in the few months we've known each other.

Thanks to my family and friends, for letting me go on and on about things you probably didn't understand.

Thanks also to each and every one of the 219 kids, teenagers and graduate students for allowing me to scan your brains, especially Jacob, Chris and Justin for your repeat visits! I will have memories of flying paperclips and bobby pins, worries over iron in the blood being a metal, and all sorts of other things that only children can provide, for the rest of my life.

Financial support provided by Networks of Centres of Excellence (NCE) – Canadian Language and Literacy Research Network (www.cllrnet.ca), Alberta Heritage Foundation for Medical Research (AHFMR), Canadian Institutes of Health Research (CIHR). MRI infrastructure provided by AHFMR, Canada Foundation for Innovation, Alberta Science and Research Authority and the University Hospital Foundation.

TABLE OF CONTENTS

LIST OF TABLES

LIST OF FIGURES

LIST OF ABBREVIATIONS AND SYMBOLS

$90°_x$	excitation pulse in x direction
$180°_y$	refocusing pulse in y direction
ADC	apparent diffusion coefficient
ALS	amyotrophic lateral sclerosis
B(r,t)	net magnetic field
B_i	magnetic field in any of the Cartesian directions (i = x, y or z)
B_0	main magnetic field along z-direction
b	gradient factor
b0	non-diffusion weighted images (i.e. b = 0 s/mm^2)
Δb	b – b0
C(r)	concentration function
CNS	central nervous system
CSF	cerebrospinal fluid
D	diffusion coefficient
D^{eff}	effective diffusion tensor
<D>	Trace/3 ADC
DTI	diffusion tensor imaging
DWI	diffusion weighted imaging
EPI	echo-planar imaging
FA	fractional anisotropy
fMRI	functional magnetic resonance imaging
FOV	field of view
G	gradient height
GM	gray matter
HIV	human immunodeficiency virus
$\vec{i},\vec{j},\vec{k}$	unit vectors
$\vec{J}$	diffusion flux
M	magnetization
MNI	Montreal Neurological Institute

MR	magnetic resonance
MRI	magnetic resonance imaging
MS	multiple sclerosis
N	number of subjects
NIH	National Institutes of Health
NMR	nuclear magnetic resonance
PET	positron emission tomography
PWS	Prader-Willi syndrome
r	distance
RF	radio frequency
ROI	region of interest
S(t)	echo signal amplitude in the presence of gradients
$S_0(t)$	echo signal amplitude in the absence of gradients
SD	standard deviation
SNR	signal to noise ratio
SPM	statistical parametric mapping
T	Tesla
T1	longitudinal relaxation time
T2	transverse relaxation time
TE	echo time
TR	repetition time
Trace ADC	trace of the apparent diffusion coefficient
Trace/3 ADC	mean diffusivity
v_1, v_2, v_3	eigenvectors
VBM	voxel based morphometry
WM	white matter
x_ρ, y_ρ	rotation frame coordinates
z	direction of main magnetic field
Δ	time elapsed between diffusion pulses
δ	length of diffusion gradient pulse
γ	gyromagnetic ratio

$\lambda_1, \lambda_2, \lambda_3$	eigenvalues
τ	amount of time a particle diffuses

Chapter 1 ♦ Introduction to Thesis

1.1 – Introduction

Nuclear magnetic resonance (NMR) has evolved into one of the most exciting medical technologies of our time, Magnetic Resonance Imaging (MRI). MRI is a non-invasive medical imaging technique that has the ability to image the whole body. Diffusion tensor magnetic resonance imaging, or more commonly referred to as diffusion tensor imaging (DTI), is a newer technique designed to image the brain, providing information from the restricted Brownian motion of the water in the brain due to natural tissue barriers. The diffusion tensor is defined by multi-directional diffusion weighted imaging (DWI). The effect of diffusion on the NMR signal was first described in 1950 (Hahn, 1950) in the first paper on spin echoes. It was later observed that the self-diffusion coefficient as measured by spin echoes was dependent on the parameters of the experiment; in particular, the time between the excitation pulse and the inversion pulse seemed to have a strong bearing on the diffusion coefficient (Woessner, 1963). The idea of using a pulsed gradient as opposed to continuous gradients was proposed in 1965 (Stejskal and Tanner, 1965; Stejskal, 1965), which was advantageous because it offered more control over the experiment, such as how much time the water was allowed to diffuse. Despite MRI being operational in the 1970s, MRI and diffusion were not put together until the mid 1980s (Wesbey et al., 1984a; Wesbey et al., 1984b; Taylor and Bushell, 1985; Le Bihan et al., 1986). Two groundbreaking papers were published in 1990: one on the detection of anisotropic diffusion in the nervous system (Moseley et al., 1990a) and another on the early detection of ischemic stroke in cats (Moseley et al., 1990b), where it was found that the water diffusion drops very early in the ischemic event, which standard T2-weighted imaging methods failed to identify, allowing for earlier detection of stoke.

The most attractive reason to use DTI is the fact that it probes the microstructure of the brain's white matter. By allowing the water molecules to diffuse for sufficient time, they probe the local environment, and thus we can infer microstructural properties of the brain

tissues (Basser, 1995). Differences in DTI measures between controls and subjects are thought to be caused by increases in myelin, and/or white matter fibre tract density. Thus it is an ideal tool for studying brain injury and diseases which specifically affect white matter. Since the discovered use of DWI in stroke, it has been used to study a plethora of brain injuries, diseases, and normal processes. These include multiple sclerosis, Alzheimer's disease, schizophrenia, autism, epilepsy, ALS (amyotrophic lateral sclerosis), dyslexia, tumors, HIV (human immunodeficiency virus), and normal brain development, to name a few (Sundgren et al., 2004; Kubicki et al., 2005; Barnea-Goraly et al., 2004; Tucker et al., 2004; Neil et al., 2002).

The use of DTI in neurodevelopment can provide more detailed information than was previously available. Before the wide use of medical imaging techniques, post-mortem studies were the main method of studying the brain (Flechsig, 1901; Benes et al., 1994; Yakovlev and Lecours, 1967). However, normal development is a tricky subject to study post-mortem because of the small number of subjects without complicating diseases, especially in a young population. Standard T1-weighted imaging studies find limited age related changes in the white matter (Paus et al., 1999; Thompson et al., 2000). DTI allows for the comprehensive study of neurodevelopment *in vivo*, paving the way for studies of a population of young subjects without the complicating factors surrounding death at a young age.

In this investigation DTI is used for the study of "normal" neurodevelopment from 5 years to 27 years of age in male and female subjects with no history of psychiatric disorder or neurological injury. We examine the complex structural and temporal changes occurring in the brain through early childhood, adolescence and into young adulthood. Chapter 1 provides an overview of the principles of diffusion imaging, white matter fibre structure, as well as the known progression of development in the brain. Chapter 2 presents the results of a study comparing the child brain (8 – 12 years of age), and the young adult brain (21 – 27 years of age) (Snook et al., 2005). Chapter 3 presents a comparison of two commonly used analysis techniques in DTI. Chapter 4 presents work in progress of neurodevelopment

covering the whole span of 5 years to 27 years, adding to Chapter 2 a group of younger children and a group of adolescents. Chapter 5 presents a discussion of the individual studies as a whole and provides conclusions, including potential future work and applications of both DTI itself and in the context of neurodevelopment.

1.2 – Principles of Diffusion Tensor Imaging

1.2.1 – Diffusion Physics

Molecular diffusion is the process by which molecules display random spontaneous movements. Robert Brown first observed this, in the 19th century, while studying the fertilization process in a particular species of flower. He observed the pollen in water through a microscope and observed rapid motion of the particles. He went on to observe the same phenomenon in the pollen of other species of flowers, and then many organic and inorganic materials. While this random motion was originally thought to arise from the fact that the particles were alive, Brown refuted this, believing that the particles simply underwent rapid, irregular motions (Nelson, 1967). This microscopic process was further quantified by Einstein nearly 100 years later (Einstein, 1956). Einstein's relation describes the time-distance relationship for a particle undergoing diffusion in free space:

$$D = \frac{1}{6\tau} r^2 \tag{1.1}$$

where D is the diffusion coefficient, τ is the time the particle undergoes diffusion, and r^2 is the mean square distance traveled in time τ. The diffusion coefficient is dependent upon molecular weight, viscosity, temperature, and the local environment (Berg, 1983). In a human system, weight, viscosity and temperature are assumed to be constant in the time frame of a DTI experiment. Thus, we can interpret the diffusion tensor solely in terms of the structure of the local environment (Beaulieu, 2002).

Diffusion in free space is called isotropic diffusion, as it is free to diffuse equally in all directions. However, if there are highly organized barriers to motion, the particles will

move preferentially parallel to these barriers. This directionally dependent diffusion is termed anisotropic diffusion. In such cases it is much more useful to view diffusion from a macroscopic perspective. From Fick's first law, we see the relation for a group of moving particles:

$$\vec{J} = -D\nabla C(r) \tag{1.2}$$

where $\vec{J}$ is a vector representing the flux of particles, D is now diffusion in the direction of particle flux, and C(r) is a function describing the concentration of particles at a given position r (Berg, 1983). Hence, macroscopic diffusion is proportional to the gradient of the particle concentration; the negative sign on the right hand side of equation (1.2) indicates that particles tend to move from areas of higher concentration to areas of lower concentration. The change in this concentration over time is governed by Fick's second law:

$$\frac{\partial C(r)}{\partial t} = D\nabla^2 C(r) \tag{1.3}$$

The standard method of measuring diffusion in biological systems is to introduce a labeled material in order to establish a concentration gradient, and then determine the rate at which the labeled material is transported along the gradient. However, this method may alter the system of interest, as we are introducing a foreign material. DWI avoids these issues by measuring the self-diffusion coefficient. The magnetic field gradient labels one species of atomic nuclei in the system as a function of their position along the gradient (Cooper et al., 1974).

1.2.2 – The Effect of Diffusion on Transverse Magnetization

The simplest method of measuring diffusion in MRI is with the spin echo experiment (Hahn, 1950). In this pulse sequence, a 90° excitation pulse is applied, the spins are allowed to dephase in the $x_\rho y_\rho$ plane, and then a 180° refocusing pulse is applied to create the echo (Figure 1.1). Equal diffusion sensitizing gradients are placed on either side of the

180° pulse, as per Stejskal and Tanner, 1965). These gradients are applied in a specific Cartesian direction, and are able to demonstrate the diffusion along that one direction.

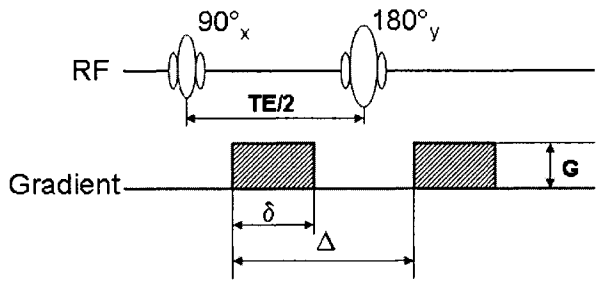

Figure 1.1 – Stejskal-Tanner spin echo sequence showing gradient length (δ), gradient height (G), time between diffusion gradients (Δ) and time between RF pulses (TE/2, where TE is the echo time).

The effect of diffusion on this pulse sequence is a partial refocusing of the spins, due to the distance traveled in the time between gradient pulses. This is best described visually (Figure 1.2). Non-stationary spins will not refocus perfectly because they are displaced within the gradient field, resulting in an attenuated spin-echo.

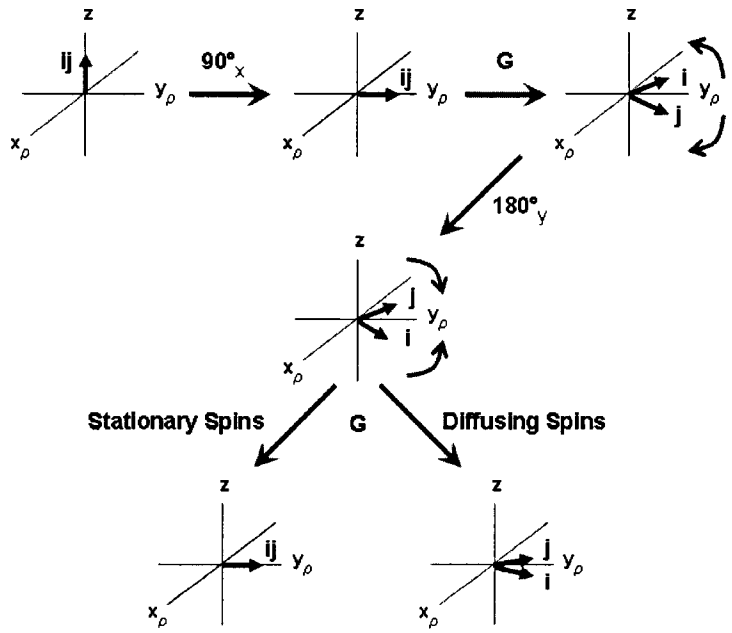

Figure 1.2 – The effect of diffusion on transverse magnetization. In the ideal stationary case, spins i and j refocus completely for a maximum spin echo. However, in the case where the spins are moving, they experience differing levels of the gradient fields causing an attenuated spin echo.

1.2.3 – Bloch-Torrey Equations

The rate of change of the magnetization vector with time can be described by combining Fick's second law and the Bloch equations (Torrey, 1956) which describe the behaviour of a nuclear spin in a magnetic field. Ignoring terms of flow and drift, the Bloch-Torrey equations are:

$$\frac{\partial M}{\partial t} = \gamma\left(M(t)\times B(r,t)\right) - \frac{(M_x\vec{i} + M_y\vec{j})}{T_2} + \frac{(M_0 - M_z)\vec{k}}{T1} + D\nabla^2 M \qquad (1.4)$$

where γ is the gyromagnetic ratio, M is the net magnetization, $M_{x,y,z}$ are the magnetization in their respective Cartesian directions, $\vec{i},\vec{j},\vec{k}$ are the unit vectors, T_2 is the transverse relaxation time, T_1 is the longitudinal relaxation time, and D is the diffusion tensor. Note that B(r,t) ~ B_z since B_x and B_y are effectively zero, therefore; $B(r,t) = B_0 + (G\cdot r)$. The Bloch-Torrey equations can be solved to show:

$$S(t) = S_0(t)\left(-\gamma^2\int_0^t\left\{\left[\int_0^{t'}G(t'')dt''\right]\cdot D\cdot\left[\int_0^{t'}G(t'')dt''\right]\right\}dt'\right) \qquad (1.5)$$

where S(t) is the echo amplitude in the presence of gradients, and $S_0(t)$ is the echo amplitude in absence of gradients, and G(t) is the applied diffusion gradient. Assuming linear gradients, and the absence of local background gradients (i.e. $G_0 = 0$), then we can solve this equation in terms of the constants as defined in Figure 1.1.

$$\ln\left(\frac{S(t)}{S_0(t)}\right) = -\gamma^2\delta^2G^2(\Delta - \delta/3)D = -bD \qquad (1.6)$$

Here we define 'b' as the gradient factor (Le Bihan et al., 1986), and (Δ-δ/3) is the effective diffusion time (Stejskal and Tanner, 1965). The diffusion coefficient in MRI is referred to as the *apparent* diffusion coefficient (ADC), for a few reasons: firstly, water is not diffusing freely, and secondly it is an indirect measure of the diffusion coefficient since in each volume element (voxel) measured in an MRI experiment there is not only many

millions of water molecules, but also the possibility for multiple tissue types (gray matter, white matter and/or cerebrospinal fluid) as well. Thus, the diffusion coefficient as measured by DWI is dependent on the interactions of the diffusing molecule in its environment. ADC is the slope of a graph of $\ln\left(\frac{S(t)}{S_0(t)}\right)$ versus gradient factor, b.

Determining an appropriate b value is important for achieving reliable and accurate measures of the ADC. Xing et al determined that the optimum value for the gradient factor depends on the diffusion coefficient (Xing et al., 1997):

$$\Delta bD = 1.1 \tag{1.7}$$

where $\Delta b = b - b0$, is the difference between the b-value of a non-diffusion weighted image ($b0 \sim 0$ s/mm^2) used to acquire $S_0(t)$, and the diffusion weighted images ($b \neq 0$ s/mm^2). Diffusion coefficients (D) of water in biological tissues are of the order of 10^{-3} mm^2/s, thus Δb should be on the order of 1000-1500 s/mm^2 (Le Bihan et al., 2001). Let us consider the case of $\Delta b < 1000$ s/mm^2; since b is proportional to the effective diffusion time, for small b values we are not allowing the spins to dephase for very long, thus we are forced to estimate the ADC based on a very small difference. However, in the case of $\Delta b > 1000$ s/mm^2, once we reach the physical limits to increase G (since b is also proportional to the square of the gradient strength) we need to increase either δ or Δ, thereby increasing the echo time (Figure 1.1). By increasing TE we allow the signal to attenuate due to spin-spin (T_2) relaxation (Neil, 1997). Also, at high b the diffusion decay is non-linear, thus equation (1.6) fails, and ADC can no longer be estimated from the slope. Thus, in the DTI experiment, typically a value of $b_1 \cong 0$ s/mm^2 is used and then b_2 ranges anywhere from 700 – 1000 s/mm^2 (in reality, a number of studies use b_2 values between 400 and 700 s/mm^2, although far from ideal).

1.2.4 – The Diffusion Tensor

Up to this point we have been discussing the basic science behind diffusion weighted imaging (DWI). By applying the gradients as per Figure 1.1 in multiple directions, we can define a diffusion tensor of rank 2 which will describe diffusion in 3-dimensions (D^{eff}).

$$D^{eff} = \begin{bmatrix} D_{xx} & D_{xy} & D_{xz} \\ D_{yx} & D_{yy} & D_{yz} \\ D_{zx} & D_{zy} & D_{zz} \end{bmatrix} \tag{1.8}$$

For Gaussian diffusion, this tensor is symmetric: $D_{xy} = D_{yx}$, $D_{yz} = D_{zy}$ and $D_{xz} = D_{zx}$ (Basser et al., 1994a). Therefore, it can be fully defined by applying the diffusion gradients in 6 non-coplanar directions as well as one without diffusion sensitizing gradients in order to acquire $S_0(t)$ and solve equation (1.6). Once the diffusion tensor is obtained, we diagonalize the tensor (equation 1.9) to determine the diffusion ellipsoid (Figure 1.3) (Basser et al., 1994b).

$$D = \begin{bmatrix} \lambda_1 & 0 & 0 \\ 0 & \lambda_2 & 0 \\ 0 & 0 & \lambda_3 \end{bmatrix} \tag{1.9}$$

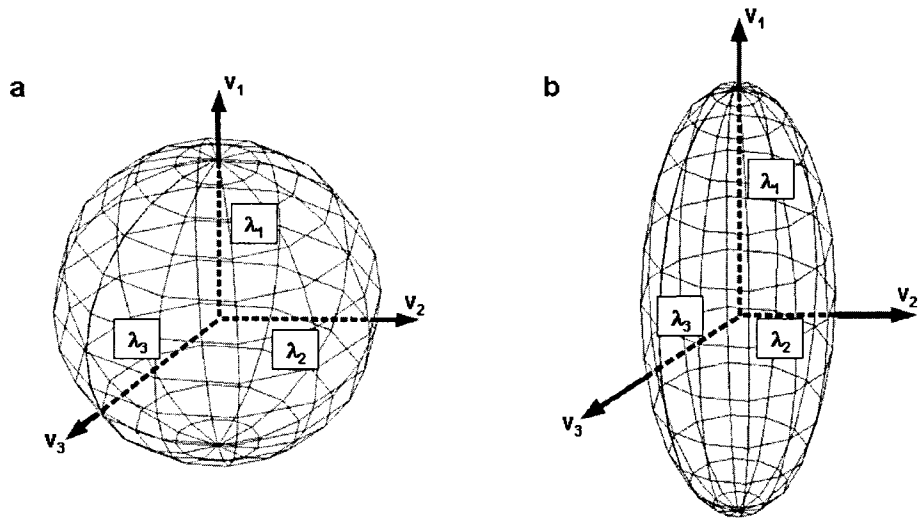

Figure 1.3 – Diffusion illustration in two types of media: a) a sphere representing isotropic diffusion, all eigenvalues are equal in magnitude, b) an ellipsoid representing anisotropic diffusion, $\lambda_1 > \lambda_2, \lambda_3$.

The tensor has three eigenvectors (v_1, v_2, and v_3) and their associated eigenvalues (λ_1, λ_2 and λ_3). The eigenvalues are then sorted from largest to smallest. By transforming the coordinates of the ellipse in this way, the ellipse becomes useful in the physical interpretation of the diffusion tensor. The major axes of the ellipsoid are the mean diffusion distances in the three principle directions of diffusion. The largest eigenvalue (λ_1) is assumed to be along the axon, giving us an idea as to the directionality of the fibre tract. The 2 smaller eigenvalues (λ_2, λ_3) are perpendicular to the axon and give us an indication of the density of fibres in the local environment. Thus, in the imaging of white matter tracts in the brain, the ellipsoid represents the fibre tract direction and the mean diffusion distances (Basser et al., 1994b).

From the eigenvectors and eigenvalues we can derive several quantities with which one can extract information from the diffusion tensor. The two most common measures of interest are mean diffusivity, which characterizes the mean diffusion distances (i.e. the relative size of the diffusion ellipsoid), and the degree of anisotropy, which characterizes the

directionality of water diffusion due to highly organized barriers within the local environment (i.e. quantifies the eccentricity of the ellipse) (Le Bihan et al., 2001).

For mean diffusivity to be a true evaluation of the mean diffusion in a region, it must be invariant, in other words, it must be independent of the orientation of the reference frame (Basser et al., 1994b). One of those combinations is the trace of the diffusion tensor (Trace ADC) (equation 1.10). The mean diffusivity $\langle D \rangle$ is then given as Trace/3 ADC, where:

$$\langle D \rangle = \frac{Trace\ ADC}{3} = \frac{\lambda_1 + \lambda_2 + \lambda_3}{3} \tag{1.10}$$

Several indices have been suggested to measure the degree of anisotropy. However, the most commonly used, and again invariant, measure is the fractional anisotropy (FA).

$$FA = \sqrt{\frac{3}{2}} \left(\frac{\sqrt{(\lambda_1 - \langle D \rangle)^2 + (\lambda_2 - \langle D \rangle)^2 + (\lambda_3 - \langle D \rangle)^2}}{\sqrt{(\lambda_1^2 + \lambda_2^2 + \lambda_3^2)}} \right) \tag{1.11}$$

The FA index is a dimensionless constant which measures the fraction of the diffusion tensor that we can ascribe to anisotropic diffusion (Basser and Pierpaoli, 1996). For the situation of isotropic diffusion, FA = 0 (i.e. $\lambda_1 = \lambda_2 = \lambda_3$). For highly anisotropic diffusion, FA approaches 1 (i.e. $\lambda_1 >> \lambda_2, \lambda_3$).

1.2.5 – Single-Shot EPI DTI sequence

Commonly, echo-planar imaging (EPI) sequences are used for DTI in order to decrease acquisition time. Unlike single line acquisition strategies used in conventional imaging, all the information is encoded in a single step (Mansfield, 1977; Schmitt et al., 1998) by creating a train of spin echoes after only one excitation pulse (Figure 1.4).

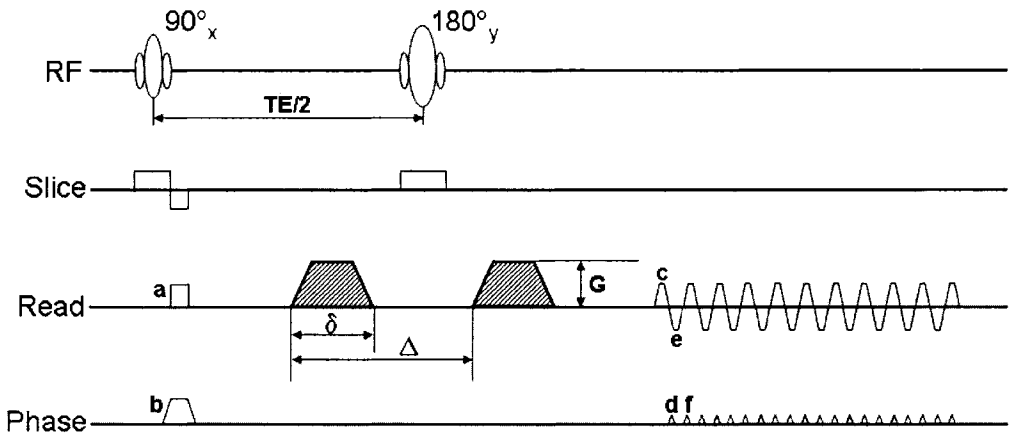

Figure 1.4 – Single-shot echo-planar diffusion imaging sequence. Letters in red show k-space trajectory (see Figure 1.5).

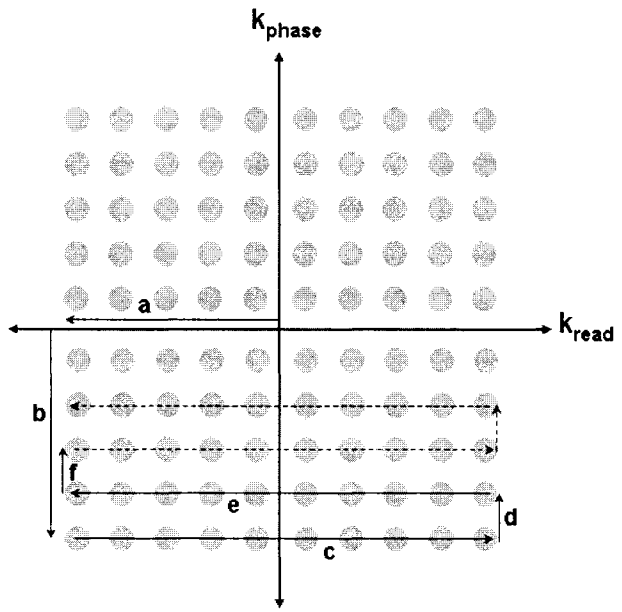

Figure 1.5 – K-space trajectory for single-shot EPI sequence. Letters in red represent the order of k-space point collections, as determined by the pulse sequence (see Figure 1.4).

The echo train allows for the collection of all points of k-space with only one excitation pulse. With conventional imaging, multiple rf / phase sampling repetitions are required, acquiring only one line of k-space per excitation pulse (Figure 1.5). The positive-negative read gradients take us back and forth through k-space, in the frequency read-out, while the

small pulsed phase gradients bring us up one line in the phase direction for each full line in the frequency direction.

While EPI is preferred because it minimizes the appearance of ghosting artifacts arising from the motion of the subject (Turner et al., 1990), there are two major drawbacks to this technique. Firstly, EPI is prone to problems with geometric distortions and susceptibility artifacts. While every effort is made to make the magnetic fields of an MRI homogenous, there will always be some inhomogeneities. The amount of local distortion in an image is proportional to both the amount of field inhomogeneity and the data acquisition time (Schmitt et al., 1998). With a small amount of inhomogeneity in a conventional imaging sequence, this is fairly minimal, but with the extended read-out period of single-shot EPI, this can be a major issue. And it is particularly a problem in regions of large magnetic susceptibility differences, such as the sinus cavities, and at the base of the skull (Ito et al., 2002). Secondly, eddy current effects are of a concern due to the large diffusion sensitizing gradients. A distortion correction scheme for more robust tensor estimation has been suggested (Mangin et al., 2002) to deal with this particular issue. Or, more recently, a twice-refocused spin echo sequence was proposed (Reese et al., 2003) that greatly reduces the eddy current distortions (Figure 1.6) which normally vary substantially with diffusion gradient direction. Using this method, no postprocessing is needed to correct for eddy current distortions.

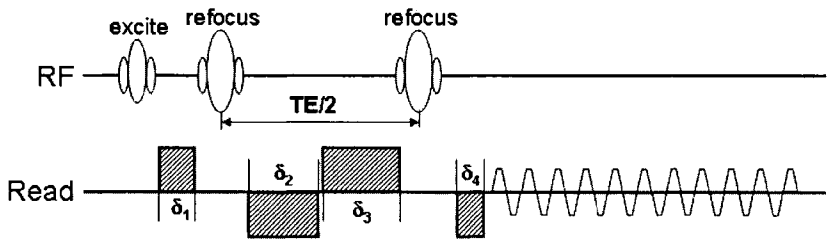

Figure 1.6 – Twice-refocused spin echo sequence for eddy current correction. The length of the first two diffusion gradients is equal to the length of the second two gradients ($\delta_1 + \delta_2 = \delta_3 + \delta_4$). Slice and phase gradients are not shown, but would be similar to those of Figure 1.4.

In this study, we are using a Siemens Sonata 1.5T MRI scanner, using the twice-refocused single shot EPI method. One set of DWI images is acquired with no diffusion weighting (i.e. b = 0 s/mm^2) and 6 sets are acquired at b = 1000 s/mm^2 in the following non-coplanar directions: (x,y,z) = (1,0,1), (-1,0,1), (0,1,1), (0,1,-1), (1,1,0) and (-1,1,0). Some sample raw DWI images, Trace/3 ADC maps and FA maps are presented in Figures 1.7, 1.8 and 1.9 respectively. Note the homogeneity of the Trace/3 ADC maps (although this is not true of neonates (Miller et al., 2003)) as compared to the heterogeneous FA maps. Thus, the FA maps better define the white matter tracts from the cortical gray matter regions.

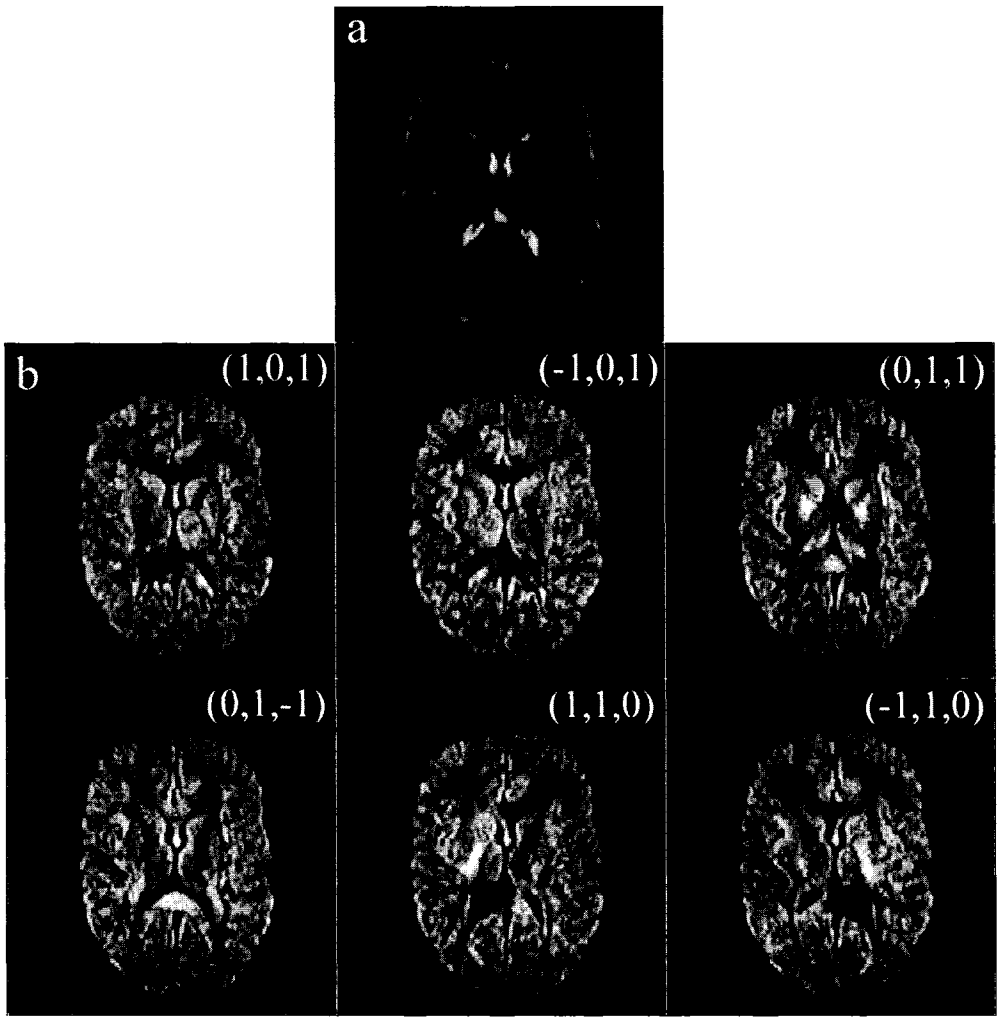

Figure 1.7 – Raw DWI images for a 22 year old male subject. a) b = 0 s/mm^2, b) all six images at b = 1000 s/mm^2, with diffusion gradient directions marked in top right corner.

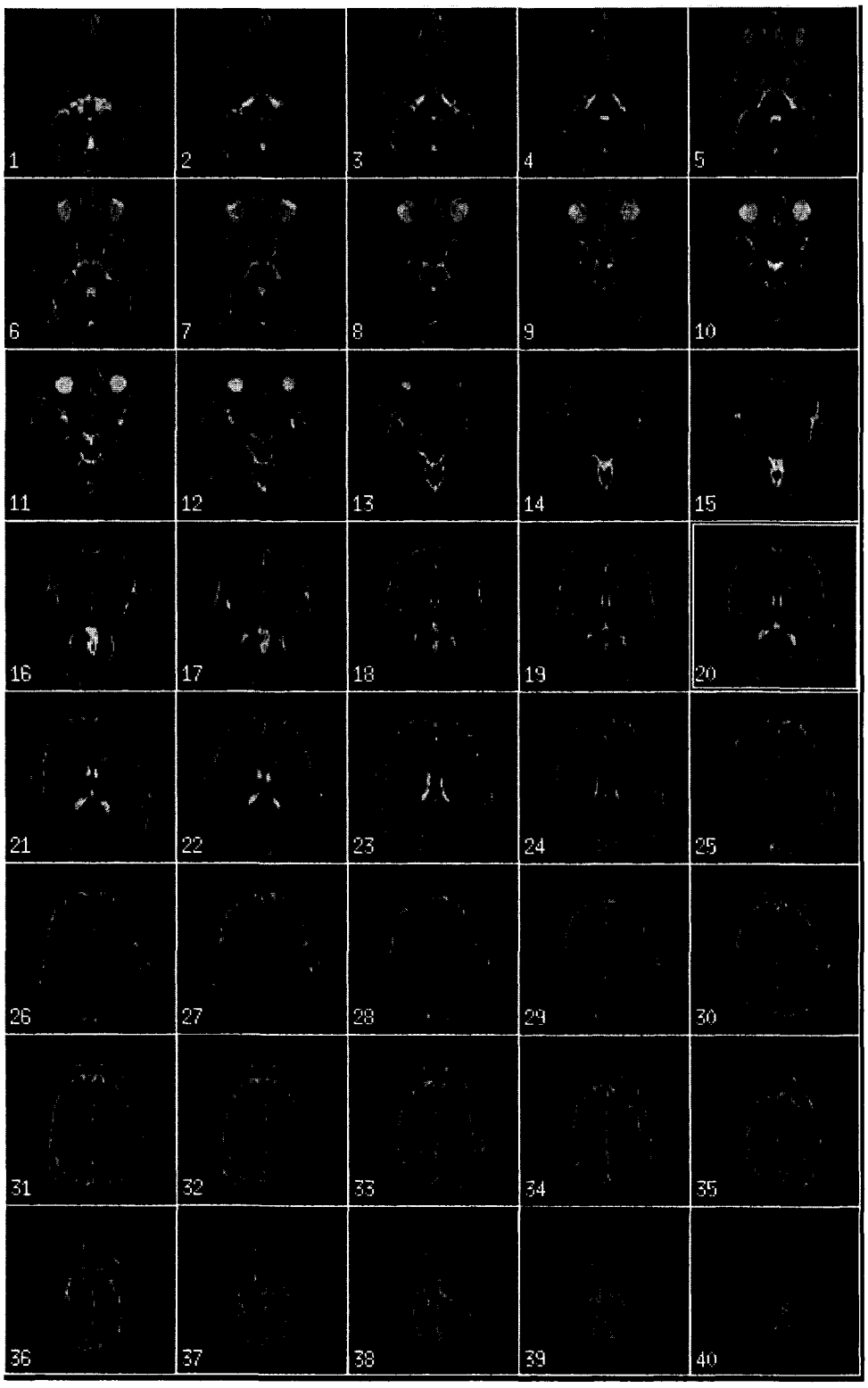

Figure 1.8 – Mean diffusivity (Trace/3 ADC) maps for a 22 year old male subject.

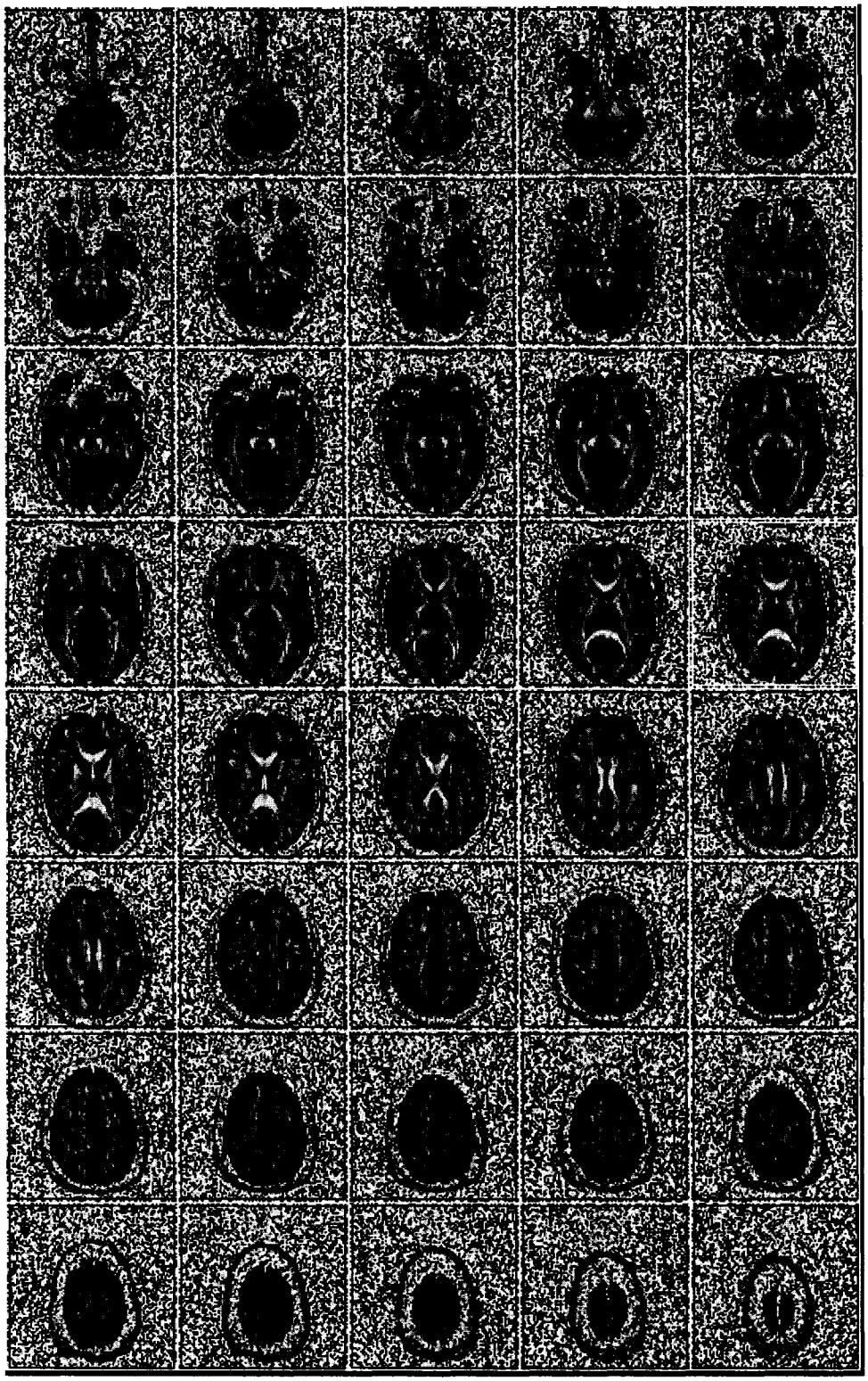

Figure 1.9 – Maps of the degree of anisotropy (FA) for a 22 year old male subject.

1.3 – Brain Tissues and the Known Progression of Neurodevelopment

1.3.1 – Structure of White Matter

The brain is made up of 3 main tissue classes: white matter, gray matter and cerebrospinal fluid (CSF). Gray matter is composed of millions of neurons, and when viewed after dissection, appears pinkish-gray. White matter is composed of the axons extending from the gray matter neurons, covered in a myelin sheath (Figure 1.10) and many white matter axons together form a white matter fibre tract, also known as a fasciculus.

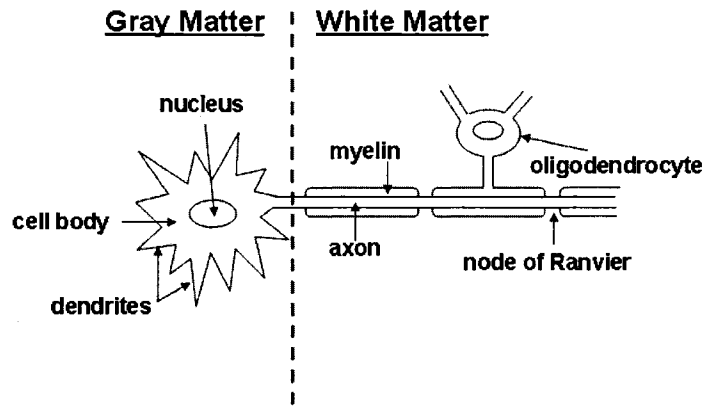

Figure 1.10 – Diagram of a neuron. The axons leading away from the cell body form the white matter. Many of these axons combined form a white matter fibre tract.

White matter fibres can be from 1 mm to 1 meter in length, with axon diameters ranging from 0.2 – 20 μm (Filley, 2001). In general, the larger the axon diameter, the faster nerve impulses can travel down the axon. However, myelination of the axons greatly increases the speed of nerve impulse conduction without taking up too much space (take for example the unmyelinated giant squid axon of 500 μm diameter versus the myelinated frog axon of 12 μm diameter which both have conduction speeds of 25 m/s (Barkovich, 2000)). This is accomplished by the fact that the sodium channels occur only at the nodes of Ranvier. The myelin layer has a very high resistance, so electrical impulses flow along the axon and out the next node 1mm or farther away. The increased diameter decreases the capacitance of the axon, allowing for fast conduction of action potentials.

Myelin is formed by oligodendrocytes in the central nervous system (CNS). Oligodendrocytes are neuroglia cells (or glia). Glia are far more numerous than neurons in the brain, however their purpose is not fully understood. They may provide nutritional, ionic and mechanical support as well as regulate neuronal shape and synaptic activity (Greenstein and Greenstein, 2000). The one well supported theory of glia function is in the formation of myelin (Lindsley and Holmes, 1984). During development the oligodendrocytes send out processes. When a process encounters an axon it wraps itself around that axon, thereby creating a myelin sheath. The myelinated sections are separated by small segments of unmyelinated bare axon, called nodes of Ranvier. A myelinated axon will contain many layers of myelin. Myelin forms lipid bilayers (i.e. two lipid layers separating long chain fatty acids) (Barkovich, 2000). One oligodendrocyte may provide myelin to many axons (Greenstein and Greenstein, 2000). These complex fasciculi create a substantial barrier to the motion of water. Logically, then, water will diffuse greater in directions parallel to these tracts, and less in directions perpendicular (Beaulieu, 2002). It is this anisotropic diffusion that we measure with DTI.

Myelin accounts for 50 – 60 % (by weight) of white matter in the CNS (Hildebrand et al., 1993). However, in all white matter structures, there exist some unmyelinated axons. The exact proportion of myelinated to unmyelinated axons is not well documented. For instance, one light microscopy study suggested that the corpus callosum has very few unmyelinated fibres, except in the genu, where they formed approximately 16% of the structure (Aboitiz et al., 1992). However, it has been suggested that microscopy results underestimate the total portion of unmyelinated fibres (Jancke and Steinmetz, 2003), and that electron microscopy shows that half or more of all callosal fibres are unmyelinated (Innocenti, 1986).

1.3.2 – Organization of White Matter in the Brain

White matter makes up about 40 – 50 % of the brain tissue by volume in an adult brain. These white matter fibre tracts can be organized into 3 main groups: projection, commissural and association fibres (Filley, 2001).

1.3.2.1 – Projection Fibres

Projection fibre tracts are the long fibres that run between the spinal cord and the lower brain (called coticopetal) and those that run in the opposite direction (corticofugal). Some common examples of these fibres include the thalamocortical connections, which link the thalamus with the somatosensory and the visual cortices, and the corticospinal tracts, which connect the motor cortices with the lower motor areas (Filley, 2001).

1.3.2.2 – Commissural Fibres

Commissural fibres connect the two hemispheres of the brain. The most common and important commissural fibre tract is the corpus callosum. Other examples include the anterior commissure and the hippocampal or fornical commissure (Filley, 2001).

1.3.2.3 – Association Fibres

Association fibres connect cortical areas within one hemisphere. There are 2 types of association fibres: the short or arcuate (U fibres) and the long fibres. The short fibres connect adjacent gyri, while the long fibres connect cortical areas which are further apart. The long fibres include the arcuate fasciculus, inferior fronto-occipital fasciculus, and cingulum to name a few. Interestingly, the long association fibres are all known to terminate in the frontal lobes, thus organizing the brain to facilitate frontal lobe interactions with all other cortical areas (Filley, 2001).

In DTI, the anatomical orientation of the fibres is often demarcated by a colour map, where green represents anterior-posterior, red represents left-right and blue represents superior-inferior oriented fibres.

1.3.3 – Some Important Brain Structures

1.3.3.1 – Corpus Callosum

The corpus callosum is the largest white matter tract in the brain (Filley, 2001). It is a wide band of fibres running left-right which connects homologous cortices of the left and right hemispheres, making it a commissural fibre. It allows for communication among sensory, motor and association areas, and is essential for the integration of information (Lindsley and Holmes, 1984). Thus, it is an important structure for sensory experience, memory and learned behaviour (Greenstein and Greenstein, 2000).

1.3.3.2 – Brain Stem

The brain stem is the structure through which all projection fibres travel in order to pass sensory and motor information to and from the brain and spinal cord. It is a very complex structure, which contains the reticular formation: a complex and dense network of nerve cells, as well as the cranial nerves. The brain stem consists of the medulla, the pons and the midbrain. The medulla is involved in the cardiovascular and respiratory systems. The pons is also involved with respiration, making the respiratory rhythm smooth and regular (Lindsley and Holmes, 1984). The midbrain (containing the cerebral peduncles) receives the occulomotor and trochlear nerves. It is also involved with dopamine regulation in the brain (Greenstein and Greenstein, 2000). The cerebral peduncles each contain a large fibre bundle that travels down the entire length of the spinal cord, called the cortico-spinal tract (Lindsley and Holmes, 1984).

1.3.3.3 – Internal and External Capsules

The internal and external capsules are projection fibres that come up from the brain stem. The internal capsule is formed by two parts: the anterior limb which is concerned with thalamic radiation, as well as carrying connections between the frontal lobes and the pons, and the posterior limb, which is concerned with motor pathways and somatosensory pathways (Greenstein and Greenstein, 2000). The external capsule is not a very well documented fibre tract, and is sometimes referred to as projection fibres and sometimes as association fibres. However, recent histological research has shown that it is in fact projection fibres that connect up with the fibres of the posterior limb of the internal capsule before entering the brain stem (Haghir et al., 2001).

1.3.3.4 – Corona Radiata and Centrum Semiovale

These are also projection fibres that continue on from the internal capsule (Greenstein and Greenstein, 2000). The fibres of the corona radiata fan out into the cortex after coming out of the internal capsule, and the centrum semiovale is a continuation of this even higher in the brain (Filley, 2001).

1.3.3.5 – Inferior and Superior Fronto-Occipital Fasciculi

These are association fibre bundles. The inferior runs between the occipital and frontal lobes, and the central portion of it is bundled with the uncinate fasciculus. The superior is more complex, and connects the parietal and frontal lobes involved with visuospatial perception, as well as the parietal with the prefrontal and the cingulate gyrus and is involved with spatial attention (Filley, 2001).

1.3.3.6 – Inferior and Superior Longitudinal Fasciculi

These are association fibre bundles. The inferior (like the inferior occipito-frontal fasciculus) runs between the temporal and occipital lobes, connecting the gray matter areas involved in face and object recognition. The superior connects the occipital and frontal

lobes. Part of the superior longitudinal fasciculus is the arcuate fasciculus, which breaks off from the main bundle to connect to the temporal lobe (Greenstein and Greenstein, 2000). It is thought that the arcuate fasciculus is highly involved in language skills (connecting the Wernicke's and Broca's language areas) (Dronkers and Baldo, 2001).

1.3.3.7 – Limbic System

The limbic system is a group of structures that borders the thalamus and hypothalamus. The structures in this system are the amygdala, the hippocampus, the septum, the fornix, the hypothalamus, the mammillary body, the uncinate and the cingulate gyrus (Greenstein and Greenstein, 2000). The limbic system is known to be involved with emotions, personality, learning and memory.

1.3.3.8 – The Cerebellum

The cerebellum is a mass that emerges from the peduncles of the components of the brain stem. It is the only structure of the brain that is not separated into two hemispheres. It is made up of gray matter, white matter, deep nuclei and masses of input and output fibres. It receives connections from the cortex, brain stem and auditory system. It is involved with fine motor control and coordination (Lindsley and Holmes, 1984).

1.3.3.9 – Thalamus and Basal Ganglia

The thalamus is a gray matter structure that acts as a "relay station". Myelinated fibres pass in and out of it to the sensory areas, cortex, cerebellar nuclei and reticular formation to name a few. The main purpose of the thalamus seems to be to process information as these fibres pass through (Lindsley and Holmes, 1984). The substantia nigra is the motor center of the thalamus.

The lentiform is made up of the globus pallidus and the putamen. The putamen and the caudate together are named the corpus striatum. All of these together form the basal

ganglia. They form connections with the thalamus, with fibres moving around and through the internal capsule. The basal ganglia are involved with motor function (Lindsley and Holmes, 1984).

Combining the thalamus and the basal ganglia we get many circuits of information flow (Behrens et al., 2003). For example, the direct pathway facilitates impulses through the thalamus and the indirect pathway inhibits impulses through the thalamus. At least 5 parallel circuits have been identified in the basal ganglia. These are the motor, limbic, dorsolateral prefrontal, lateral orbitofrontal and occulomotor. These complex patterns of fibres traveling in and out of the thalamus and basal ganglia create a higher level of anisotropy than is seen in the cortex and allows us to make measurements with DTI in these gray matter structures.

1.3.4 – Known Progression of Neurodevelopment: Post Mortem Evidence

Until the advent of MRI, our knowledge of brain development was limited to a few classic post-mortem studies (Flechsig, 1901; Yakovlev and Lecours, 1967). From these studies we learn that myelination begins in utero in the middle trimester, and continues well into adulthood, although by year 2 the myelin is approximately 90% formed (Filley, 2001). Yakovlev et al suggested that the myelination of the association fibres continues on into the 30s, and beyond, although he does not indicate at what point this may end. A more recent study (Benes et al., 1994) indicates, in fact, that myelination may continue into the 50s and 60s.

In general, it is known that myelination follows a caudal-rostral progression of development. Firstly, the brain stem and cerebellum myelinate, followed by the diencephalon and the cerebral hemispheres, as well, the occipital and parietal lobes myelinate before the temporal and frontal lobes. This follows from the fact that the more ancient parts of our brains develop before the more modern portions (Filley, 2001).

In terms of specific white matter fibre tracts, the association fibres and the commissural fibres are the last to myelinate. Thus, the intra-cortical connections both within each hemisphere and between the hemispheres are the final connections to be made, and likely continue to change and develop throughout life. It is thought that this late development of intra-cortical areas combined with the later development of the frontal lobes is the main reason that personality is not fully developed until adulthood, and that subtle changes in personality throughout adulthood are likely due to the changes in myelin occurring into the 50s and 60s (Filley, 2001).

Interestingly, Yakovlev and Lecours suggested that the reticular formation continues to develop until at least the 2nd decade of life, if not later (Yakovlev and Lecours, 1967). The reticular formation consists of tiny structures of the brain stem in the medulla, pons and midbrain, and their respective connections to the brain. And while the brainstem is known to myelinate before anything else in the brain, it is interesting that portions of it continue to myelinate quite late in life (Lindsley and Holmes, 1984).

1.3.5 – Neurodevelopment and MRI

An extensive amount of work has been done studying gray matter development using conventional T1-weighted MRI. These studies generally use high resolution, 3D volumetric analysis to look at changes in cortical thickness with age. In general, it was found that cortical thickness decreases between childhood and young adulthood, in agreement with earlier reports of reduction in synaptic density. Most of these changes occur in more dorsal regions: greater decreases were seen in the frontal lobes than in the temporal lobes. Changes in the frontal lobe thickness have been linked to changing cognitive abilities (Sowell et al., 2004; Thompson et al., 2005).

It is therefore logical to think that if such drastic changes are occurring in the gray matter, that the connections between these cortical areas are also developing. This is also supported by our knowledge of continuing myelination in young adulthood (Yakovlev and Lecours, 1967). White matter development was then studied using 3D T1- weighted high

resolution imaging. This method involves creating 3D maps of white matter "density" and then correlating them with subject age on a voxel-by-voxel basis. One neurodevelopment study found increases in white matter "density" over 4 – 17 years in the internal capsule and the left arcuate fasciculus (Paus et al., 1999).

Before the formalism of DTI was fully described, there were some neurodevelopment studies using DWI in the early 1990s (Rutherford et al., 1991; Sakuma et al., 1991; Nomura et al., 1994). Despite the fact that DTI was fully described by 1994 (Basser et al., 1994b), researchers continued to use DWI due to the complexity of measuring the entire diffusion tensor (Huppi and Barnes, 1997; Takeda et al., 1997; Ramenghi et al., 1998; Morriss et al., 1999). In these studies, anisotropy is measured by performing DWI in the three Cartesian directions. In general, it was seen that ADC decreases, and that anisotropy increases with age. The biggest drawback to this method is that we do not get the full 3 dimensional picture of anisotropy. This is something that only DTI offers, by measuring the full diffusion tensor. DTI studies of neurodevelopment are described in detail in the following chapters. However, in general they find much more widespread changes than T1- weighted imaging and DWI studies of white matter.

Chapter 2 ♦ Diffusion Tensor Imaging of Children and Young Adults[1][2]

2.1 – Introduction

Magnetic resonance imaging (MRI) has opened the door to localizing maturational changes in the brain (Paus et al., 2001). Post-mortem studies, although quite enlightening, are often limited in the numbers of young subjects who are free of complicating diseases, making it difficult to study the normal aging brain (Sowell et al., 2004). T1- and T2-weighted MR imaging studies have shown differences in overall brain volumes with age and gender (Giedd et al., 1999; Courchesne et al., 2000; Sowell et al., 2002). In order to look at more specific tissues rather than just global volume differences, three-dimensional T1-weighted scans have been post processed to look at regional growth rates and tissue density. One longitudinal study found a rostro-caudal wave of growth in the corpus callosum of young children (Thompson et al., 2000). Using voxel based morphometry, age related "white matter density" increases have been reported in the internal capsule and the left arcuate fasciculus over 4 – 17 years of age (Paus et al., 1999). The T1-weighted imaging studies tend to find changes in a limited number of brain regions, and the relationship between the signal intensity on the T1-weighted images and the underlying microstructure is unclear. Diffusion tensor imaging (DTI) of water mobility in tissue may provide a more sensitive measure of the changes in the brain's microstructure with maturation (Le Bihan, 2003).

DTI is sensitive to the Brownian motion of water as it diffuses in the brain. Diffusion is said to be isotropic when it occurs equally in all directions (e.g. when there are no barriers). However, when there is a barrier to impede the motion of the water, such as membranes in

---

[1] A version of this chapter has been published. Snook, L., Paulson, L. A., Roy, D., Phillips, L. and Beaulieu, C., 2005. Diffusion tensor imaging of neurodevelopment in children and young adults. Neuroimage. 26, 1164-1173

[2] A preliminary version of this was presented at the Annual Meeting of the International Society of Magnetic Resonance in Medicine (ISMRM), Kyoto, Japan, May 15 – 21, 2004.

a white matter tract, the diffusion is no longer equal in all directions and it is said to be anisotropic (Chenevert et al., 1990; Moseley et al., 1990a). The standard tissue diffusion parameters derived from DTI are the average apparent diffusion coefficient (Trace/3 ADC) and fractional anisotropy (FA) (Basser, 1995). Trace/3 ADC is a rotationally-invariant measure of the magnitude of diffusion and it is fairly homogenous throughout the brain, with the exception of neonates (Miller et al., 2003), when diffusion-weighted images are acquired at lower diffusion sensitivity factors (i.e. b-values up to ~ 1000 s/mm^2). FA is a measure of the directionality of diffusion with values ranging from 0 (isotropic diffusion) to 1 (highly anisotropic diffusion) and has far greater variability throughout the brain than Trace/3 ADC. Although the interpretation of water diffusion parameters, particularly anisotropy, is not straightforward (Beaulieu, 2002), higher FA values could indicate an increase in fibre bundle density and/or increased myelination with development. The eigenvalues of the diffusion tensor, which yield the apparent diffusion coefficients either parallel (λ_1) or perpendicular (λ_2, λ_3) to the white matter tracts, are not often reported but can yield insight into the microstructural changes of the tissue.

DTI has been applied to better understand neurodevelopment in several studies from neonates up to the 8th decade of life (Neil et al., 2002; Moseley, 2002). In adult studies (ages 20 years and above), general maturational trends of increasing Trace/3 ADC and decreasing FA were found (Pfefferbaum et al., 2000; Abe et al., 2002; Bhagat and Beaulieu, 2004). Studies of neonates and children have found opposite trends of decreasing mean diffusivity and increasing anisotropy with age, with the exception of the cortex in preterm infants which shows decreases in anisotropy (McKinstry et al., 2002). More specifically, these increases of FA have been observed in the corpus callosum, internal capsule, caudate head, lentiform nucleus, and thalamus over 1 day – 11 years (Mukherjee et al., 2001), the internal capsule, corticospinal tract, left arcuate fasciculus, and right inferior longitudinal fasciculus over 5 – 18 years (Schmithorst et al., 2002), and the pons, crus, centrum semiovale, and subcortical white matter over 1 day – 16 years (Schneider et al., 2004). The first and third studies demonstrated that most of the diffusion changes occur within the first four years of life. These analyses have been performed with

a limited number of ROIs (between 7 and 11) and with thicker slices (5mm for the first two and 4mm for the last), and in addition they did not investigate the transition into young adulthood. A separate study investigated this transition period and demonstrated that anisotropy increased from childhood (8-12 years) to adulthood (20-31 years) in the frontal white matter; however, no other brain regions were investigated (Klingberg et al., 1999). No comprehensive DTI studies have examined the potential brain changes occurring between late childhood and young adulthood although it is known that the brain experiences a protracted progression of myelination and axonal growth during adolescence and young adulthood based on histological autopsy studies (Yakovlev and Lecours, 1967) as well as linear increases of total white matter volume on longitudinal T1-weighted in vivo MRI scans (Giedd et al., 1999).

The purpose of this study is to determine what regions of the brain are continuing to develop through late childhood (8 – 12 years, N=32) and into young adulthood (21 – 27 years, N=28) using diffusion tensor imaging. FA and Trace/3 ADC were measured in a large number of brain regions to assess micro-structural changes associated with brain maturation. Two types of analyses were performed: (i) linear regression within the 8 – 12 year old children and also within the 21 – 27 year old young adults and (ii) group comparisons between the children and young adults. We also report apparent diffusion coefficients parallel and perpendicular to the fibre bundles (i.e. eigenvalues of the diffusion tensor) in the children to interpret any observed changes of diffusion anisotropy with maturation.

2.2 – Methods

2.2.1 – Subjects

Two groups of healthy volunteers were used in this study, namely: 32 children aged 11.1 ± 1.3 (range 8 - 12 years, 18 female, 14 male, 30 right handed, 2 left handed) and 28 young adults aged 24.4 ± 1.8 (range 21 – 27 years, 14 female, 14 male, 25 right handed, 3 left handed). All subjects gave informed consent, and parent/guardian consent was given for

all volunteers under 18 years of age. Volunteers had no history of psychiatric disease or neurological injury.

2.2.2 – Image Acquisition

Subjects were scanned with a 1.5 Tesla Siemens Sonata MRI scanner for approximately 26 minutes for anatomical and DTI imaging. The DTI data was acquired using a dual spin-echo, single shot echo-planar imaging sequence with 3 mm slice thickness, no inter-slice gap (interleaved acquisition), TR = 6400 ms, TE = 88 ms, field-of-view 220 x 220 mm^2, 6 non-collinear diffusion-sensitizing gradient directions with diffusion sensitivity b = 1000 s/mm^2, 8 averages, and a matrix of 96 x 128 zero filled to 256 x 256 for a resulting voxel size of 0.85 x 0.85 x 3.0 mm^3. Total DTI acquisition time was 6:06 minutes with 40 contiguous axial slices for full brain coverage. Slices were positioned along the anterior commissure-posterior commissure line. The mean SNR of brain parenchyma on the non-diffusion-weighted images was 75 ± 6 for the children and 71 ± 6 for the young adults. Representative FA maps of the children and young adults are shown in Figure 2.1.

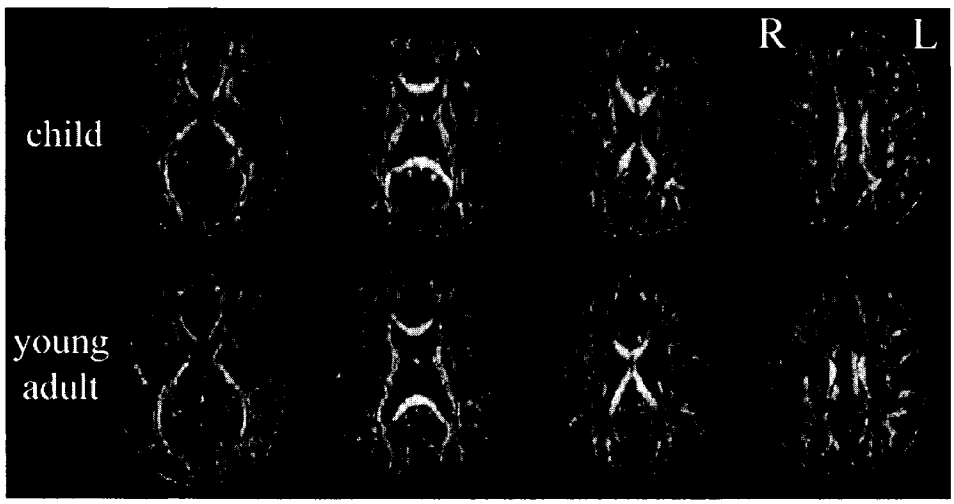

Figure 2.1 - Representative fractional anisotropy (FA) maps of four transverse slices of a 12 year old female volunteer (above) and a 26 year old male volunteer (below).

2.2.3 – Region-of-Interest Data Collection

Trace/3 ADC and FA values were collected from 30 regions of interest (ROIs), in 13 distinct brain regions, which can be divided into 4 tissue type categories. 1. Major White Matter: genu of corpus callosum, splenium of corpus callosum, anterior limb of the internal capsule, posterior limb of the internal capsule, external capsule, corona radiata and centrum semiovale, 2. Subcortical White Matter in Gyri: a sample of 5 gyri including the right superior frontal gyrus, right supra marginal gyrus, right middle occipital gyrus, left superior temporal gyrus and the left postcentral gyrus, 3. Cortical Gray Matter: a thin band around the subcortical white matter gyri, and 4. Deep Gray Matter: thalamus, globus pallidus, putamen, and head of the caudate nucleus. The five subcortical white matter regions in the gyri were combined to yield mean diffusion parameters, as were the five cortical gray matter regions.

ROIs were drawn on the slice of the FA map where the structures were visualized to be at their thickest, with the exception of the globus pallidus, putamen, and caudate for which the ROIs were placed initially on the non-diffusion-weighted images ($b = 0$ s/mm^2). Using image analysis software (MRVision, Winchester, MA), the structure in question was outlined following its contours. However, the corona radiata, centrum semiovale, globus pallidus, putamen, and caudate, had small ROIs placed on central regions of the structure (Figure 2.5 shows all regions, with the exception of 2 small circles drawn on the lower ventricles, and the small band of gray matter around the subcortical white matter gyri). ROIs were then translated onto the corresponding FA and Trace/3 ADC maps. ROIs were also translated onto the eigenvalue maps of all structures that showed significant correlation of FA with age in the children. Where appropriate left and right measurements were taken separately. To avoid inclusion of cerebrospinal fluid (CSF) in the ROIs, non-diffusion-weighted images and Trace/3 ADC maps were used to better visualize and avoid the CSF spaces. The ROI method was chosen so as to avoid any problems due to normalization of the brain into stereotactic space, and so that summary data on entire brain structures could

be analyzed as opposed to a voxel by voxel analysis. Furthermore, the structures we analyzed are readily identified on the 2D MR images.

2.2.4 – Statistical Analysis

2.2.4.1 – Left/Right Asymmetry

Left and right FA and Trace/3 ADC values were compared using paired t-tests (significant with $p<0.05$). Where no significant left/right differences exist, the values are averaged for all further analyses. Absolute differences of less than $0.01 \times 10^{-3} mm^2/s$ for Trace/3 ADC or 0.01 for FA between left and right are not reported.

2.2.4.2 – Correlation Analysis

Linear regression was performed for both FA and Trace/3 ADC versus age within the 8 – 12 year age range of the children and within the 21 – 27 year age range of the young adults (significant with $p<0.05$).

2.2.4.3 – Group Analysis

Unpaired t-tests were performed to compare each brain region individually between the child group and the young adult group (significant with $p<0.05$).

2.2.4.4 – ROI Reliability

Three subjects (aged 17, 22, and 23 years) were scanned on 4 different occasions over the course of 4 months. ROIs were drawn in the genu, corona radiata, thalamus, and caudate. The mean FA values for each structure for each of the three subjects (mean over 4 scans ± SD) were: genu of the corpus callosum (0.78 ± 0.01, 0.76 ± 0.01, 0.84 ± 0.02), corona radiata (0.61 ± 0.02, 0.65 ± 0.02, 0.68 ± 0.01), thalamus (0.30 ± 0.01, 0.34 ± 0.03, 0.34 ± 0.02), and head of the caudate nucleus (0.20 ± 0.01, 0.20 ± 0.02, 0.23 ± 0.02). These intra-

subject standard deviations are in general less than the inter-subject variability. Figure 2.2 shows the variability of all four regions for one of the subjects (22 year old male).

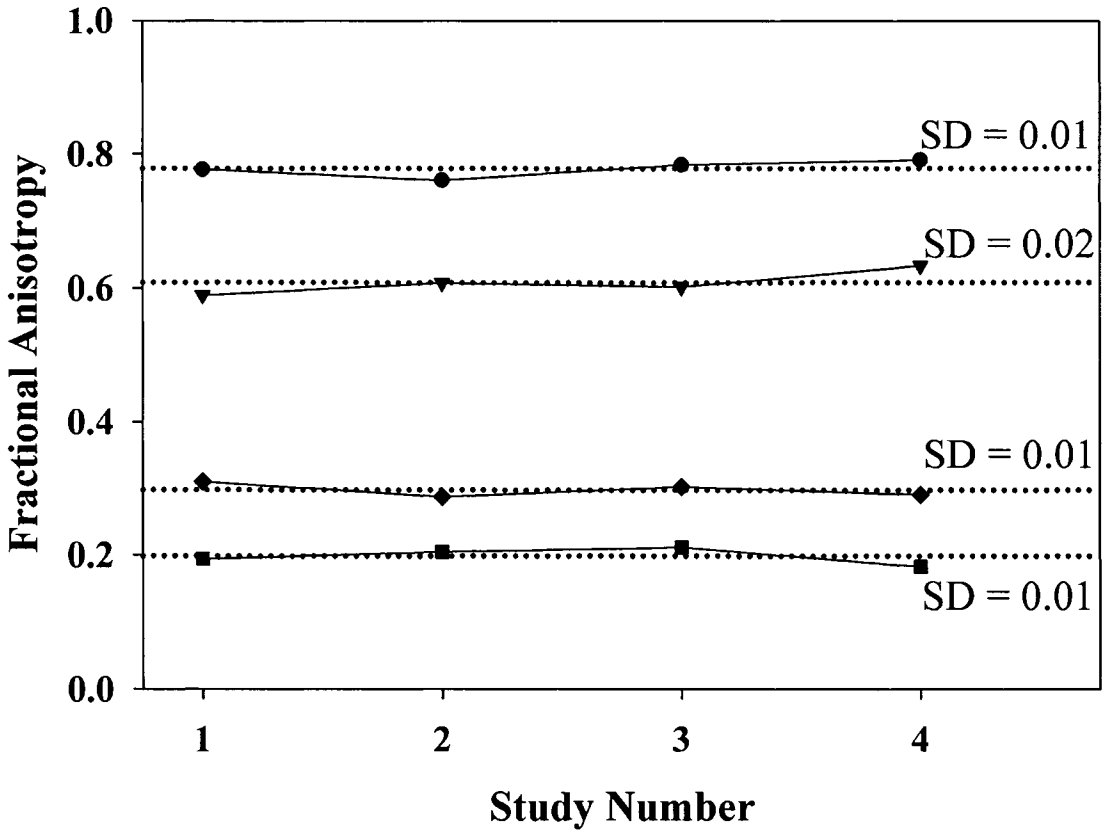

Figure 2.2 - Variability of ROI measurements of fractional anisotropy for one subject over 4 scans taken within a period of 4 months for the genu of the corpus callosum (FA range = 0.76 - 0.79, SD = 0.01), corona radiata (0.59 – 0.63, 0.02), thalamus (0.29 – 0.31, 0.01) and head of the caudate nucleus (0.18 – 0.21, 0.01). The dashed lines represent the mean of the 4 measurements. The variability shown in this graph is very small, suggesting a high level of consistency in both imaging and ROI methods.

2.3 – Results

2.3.1 – Left/Right Asymmetry

Overall, there was very little hemispheric asymmetry in either Trace/3 ADC or FA, and even when asymmetry was present, its magnitude was small. FA was greater on the left in the anterior limb of the internal capsule (mean over 32 volunteers ± SD: left 0.59 ± 0.05,

right 0.57 ± 0.05, p=0.05), and centrum semiovale (left 0.48 ± 0.03, right 0.46 ± 0.03, p=0.05) in the 8 – 12 year old children. In the young adults, the centrum semiovale also showed leftward asymmetry of FA (mean over 28 volunteers ± SD: left 0.47 ± 0.05, right 0.44 ± 0.05, p=0.0001), but the globus pallidus had rightward asymmetry (left 0.27 ± 0.04, right 0.29 ± 0.05, p=0.002).

2.3.2 – Correlation Analysis (within 8 – 12 years and within 21 – 27 years)

Significant increases of FA were seen in 5 of 13 regions, namely the genu of the corpus callosum (p=0.002, r=0.54), splenium of the corpus callosum (p=0.02, r=0.42), corona radiata (p=0.02, r=0.40), putamen (p=0.05, r=0.35), and head of the caudate nucleus (p=0.0007, r=0.57) (Figure 2.3a). No significant decreases of FA were seen with age in the children. On the other hand, a significant decrease in Trace/3 ADC was seen in 9 of 13 brain regions in children over this 5 year age span, with the exception of the genu of the corpus callosum, posterior limb of the internal capsule, thalamus, and cortical gray matter (Figure 2.3b-d). In young adults, there was very little change within the larger time span of 21 – 27 years of age and it was limited to a significant increase of Trace/3 ADC in the left globus pallidus (r=0.41, p=0.03) and a significant increase of FA in the right centrum semiovale (r=0.44, p=0.02).

The eigenvalues of the diffusion tensor were evaluated for correlation with age in the 5 brain regions that had significant linear increases of FA over the 8 – 12 year old age range (Figure 2.4). In the genu of the corpus callosum, splenium of the corpus callosum, corona radiata, and head of the caudate nucleus, the "parallel" diffusivity (λ_1) stayed constant, whereas the "perpendicular" diffusivity (λ_2 and λ_3) decreased significantly ($p<0.01$) from 8 – 12 years. In contrast, all three eigenvalues decreased significantly for the putamen with age over 8 – 12 years ($p<0.001$).

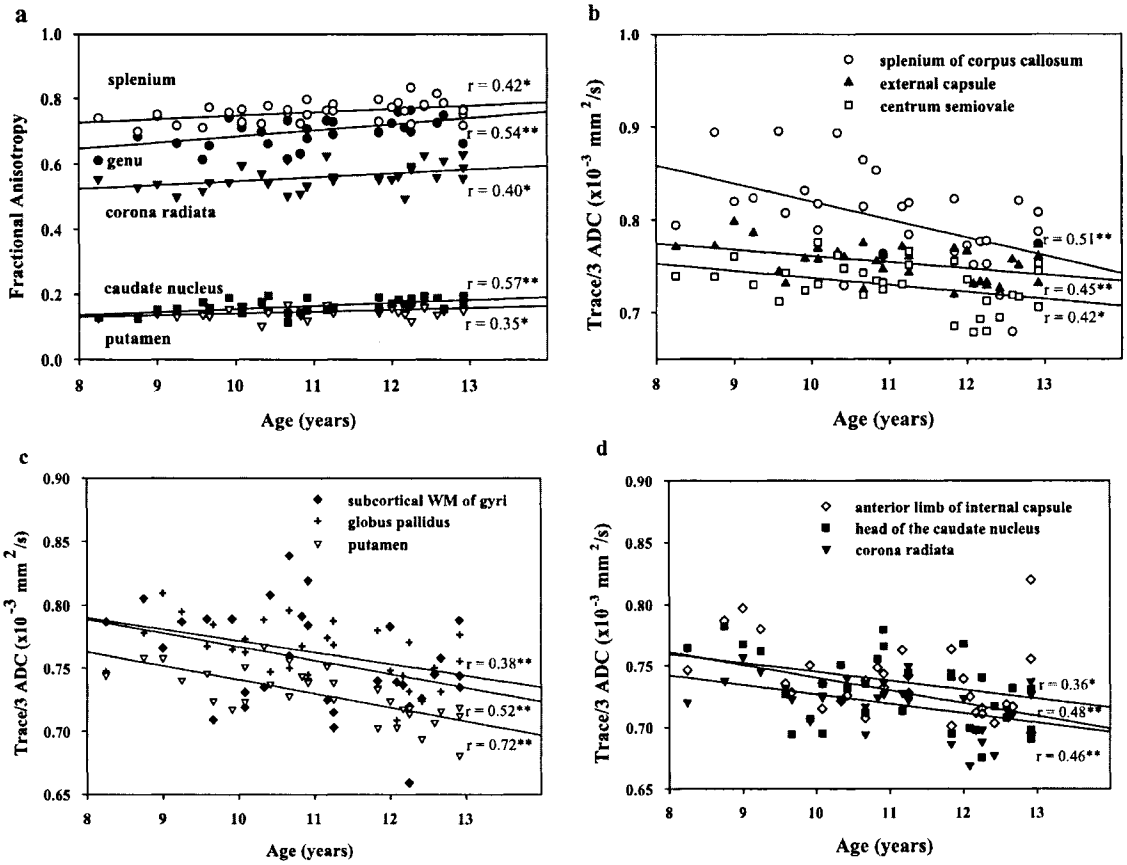

Figure 2.3 - Correlation Trends within 8 – 12 years. Linear regression of FA and Trace/3 ADC values with age in the 8 – 12 year child age range. a) Of the 13 distinct brain regions measure, positive correlations of FA were observed in five regions, listed from top to bottom: splenium of corpus callosum, genu of corpus callosum, corona radiata, head of the caudate nucleus, and putamen. Negative correlations of Trace/3 ADC were observed in nine regions, listed from top to bottom: b) splenium of corpus callosum, external capsule, and centrum semiovale, c) subcortical white matter in the gyri, globus pallidus, and putamen, d) anterior limb of the internal capsule, head of the caudate nucleus, and corona radiata. Fewer regions of the brain demonstrate positive correlations of fractional anisotropy within the narrow 8 – 12 year old age range than negative correlations of Trace/3 ADC (* = $p < 0.05$, ** = $p < 0.01$).

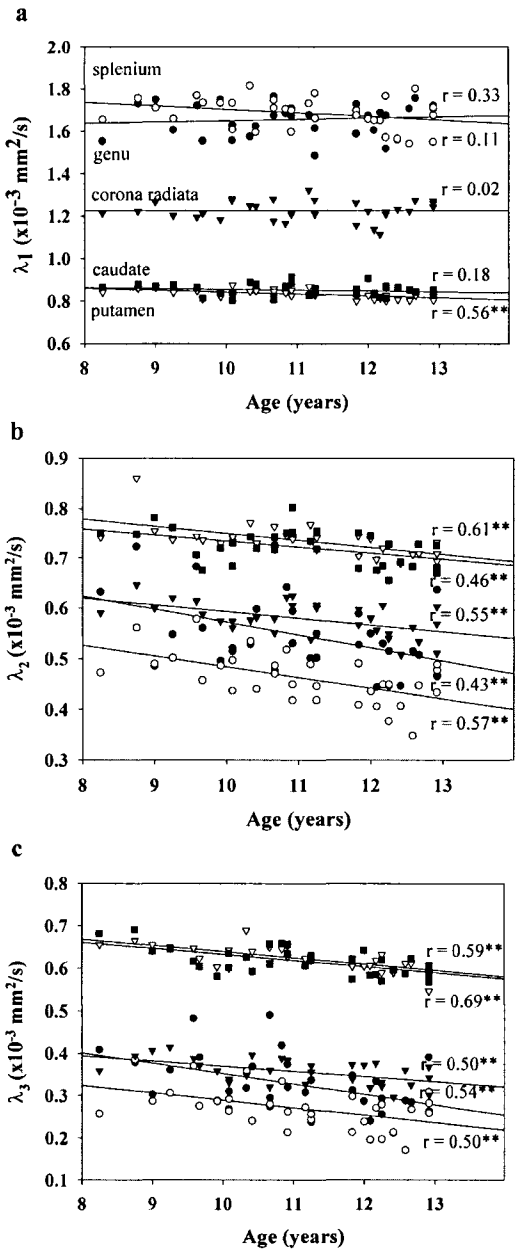

Figure 2.4 - Eigenvalue correlations within 8 – 12 years. In the five brain regions that showed a significant increase of fractional anisotropy over ages 8 – 12 years, linear regression of the three eigenvalues of the diffusion tensor with age demonstrates that: a) the parallel diffusivity (λ_1) is approximately constant in all structures except the putamen which has a small decline with age, (b, c) whereas the perpendicular diffusivity (λ_2,λ_3) decreases significantly with age in all five structures.

2.3.3 – Group Analysis (8 – 12 years versus 21 – 27 years)

When comparing the children to the young adults, increases in FA were seen in 11 of 13 structures; however, a decrease of FA was seen in the right centrum semiovale (Table 2.1).

Table 2.1 – Group analysis statistics for fractional anisotropy (FA) – children versus young adults

Region	Fractional Anisotropy		p	Difference (%)
	Children[3] (mean ± SD)	Young Adults[4] (mean ± SD)		
White Matter				
genu of corpus callosum	0.70 ± 0.05	0.78 ± 0.03	<0.0001	11
splenium of corpus callosum	0.76 ± 0.03	0.81 ± 0.03	<0.0001	7
anterior limb of internal capsule	0.58 ± 0.04	0.66 ± 0.05	<0.0001	14
posterior limb of internal capsule	0.66 ± 0.03	0.70 ± 0.03	<0.0001	6
external capsule	0.47 ± 0.03	0.51 ± 0.03	<0.0001	9
corona radiata	0.56 ± 0.04	0.62 ± 0.04	<0.0001	11
centrum semiovale[5]	0.47 ± 0.02	0.46 ± 0.05	0.15	----
subcortical WM of gyri	0.44 ± 0.06	0.49 ± 0.06	<0.0001	11
Gray Matter				
thalamus	0.31 ± 0.03	0.33 ± 0.03	0.007	7
globus pallidus	0.25 ± 0.02	0.28 ± 0.04	<0.0001	12
putamen	0.15 ± 0.02	0.17 ± 0.02	<0.0001	13
caudate	0.16 ± 0.02	0.21 ± 0.03	<0.0001	31
cortical GM	0.18 ± 0.03	0.18 ± 0.03	0.94	----

[3] 8 – 12 years, N=32

[4] 21 – 27 years, N=28

[5] Left/right combined value is presented for centrum semiovale: left FA 0.48 ± 0.03 children, left FA 0.47 ± 0.05 young adults, p=0.30; right FA 0.46 ± 0.03 children, right FA 0.44 ± 0.05 young adults, p=0.02.

The trend of decreasing Trace/3 ADC, as seen in the correlational analysis, was seen in 12 of 13 structures ($p<0.01$, absolute difference ranging from 3% - 10%), (Table 2.2). The cortical gray matter showed no trends for either FA or Trace/3 ADC.

Table 2.2 – Group analysis statistics for mean diffusivity (Trace/3 ADC) – children versus young adults

Region	Trace/3 ADC		p	Difference (%)
	Children[6] (mean ± SD) $x10^{-3}$ mm^2/s	Young Adults[7] (mean ± SD) $x10^{-3}$ mm^2/s		
White Matter				
genu of corpus callosum	0.83 ± 0.06	0.75 ± 0.03	<0.0001	-10
splenium of corpus callosum	0.80 ± 0.05	0.75 ± 0.03	<0.0001	-6
anterior limb of internal capsule	0.74 ± 0.03	0.70 ± 0.02	<0.0001	-5
posterior limb of internal capsule	0.74 ± 0.02	0.72 ± 0.02	0.004	-3
external capsule	0.75 ± 0.02	0.73 ± 0.02	<0.0001	-3
corona radiata	0.72 ± 0.02	0.69 ± 0.02	<0.0001	-4
centrum semiovale	0.73 ± 0.03	0.71 ± 0.03	0.01	-3
subcortical WM of gyri	0.77 ± 0.04	0.73 ± 0.05	<0.0001	-5
Gray Matter				
thalamus	0.78 ± 0.03	0.74 ± 0.02	<0.0001	-5
globus pallidus	0.76 ± 0.02	0.73 ± 0.03	<0.0001	-4
putamen	0.73 ± 0.02	0.69 ± 0.02	<0.0001	-6
caudate	0.73 ± 0.03	0.66 ± 0.03	<0.0001	-10
cortical GM	0.82 ± 0.04	0.82 ± 0.05	0.44	----

[6] 8 – 12 years, N=32

[7] 21 – 27 years, N=28

Putting together the correlation and group analyses, FA is observed to continually increase from 8 years to young adulthood in 5 of 13 structures whereas Trace/3 ADC continues to drop over this age range in 9 of 13 structures (Figure 2.5).

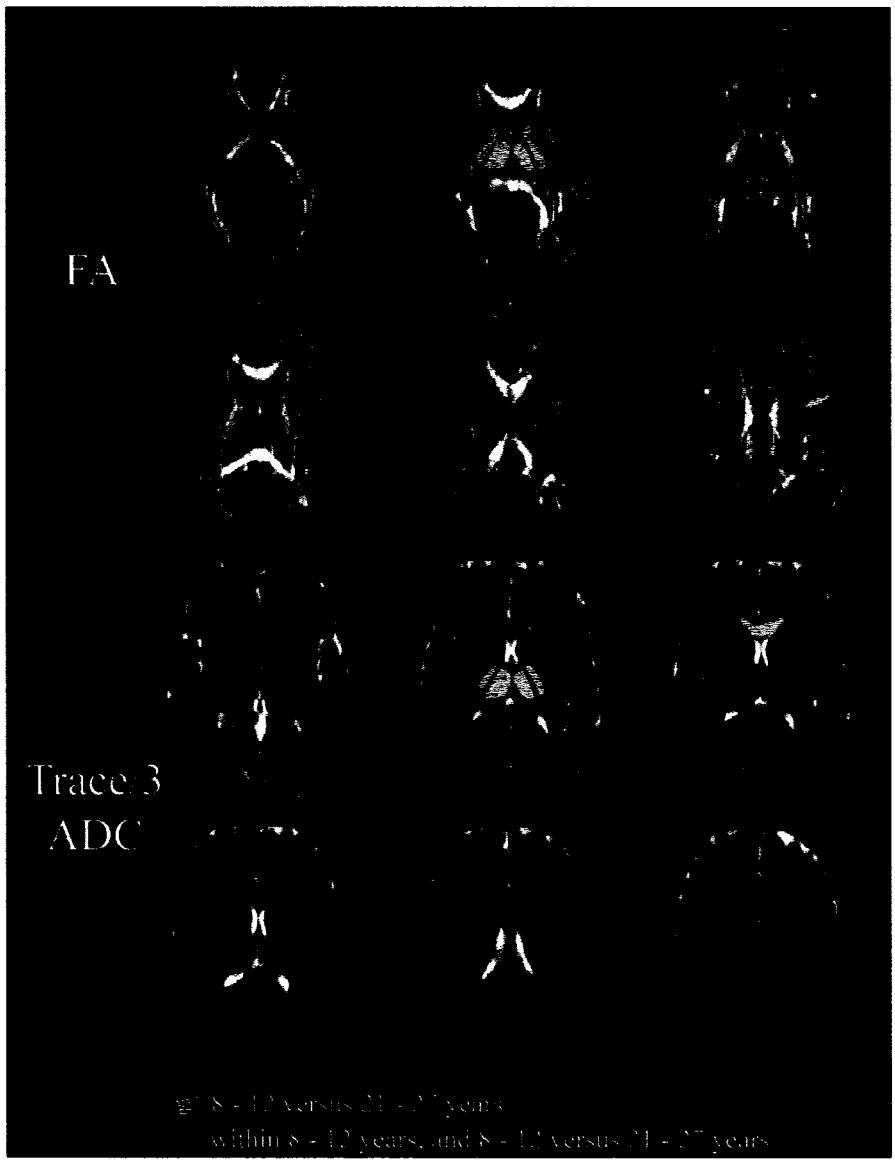

Figure 2.5 - Regional changes in maturation. FA and Trace/3 ADC maps of six slices in a 12-year-old female volunteer. ROIs are drawn as per the analysis method. Red regions show both significant correlations within 8 – 12 years and significant differences between childhood and young adulthood. Yellow regions only show significant changes between childhood and young adulthood, suggesting development during adolescence. Note that the splenium of the corpus callosum, corona radiata, head of the caudate nucleus, and putamen show continued changes with age for both FA and Trace/3 ADC (i.e. red on both maps). The remaining structures demonstrate different progression of FA and Trace/3 ADC.

2.4 – Discussion

High-resolution diffusion tensor imaging in 60 healthy subjects has demonstrated maturational changes in the brain throughout late childhood (8 – 12 years) and in the progression towards young adulthood (21 – 27 years). The timing of these changes in the water diffusion parameters implies a marked development of regional-specific brain microstructure from pre-adolescence to young adulthood.

Left/Right asymmetry was seen in very few structures. It has been suggested that this difference may be due to coherence of fibre bundles as opposed to differences in myelination (Klingberg et al., 1999). The most interesting left/right difference was seen in the centrum semiovale, with higher FA values on the left side, not only in the children, but also in the young adults. In fact, the left/right difference became more pronounced and more significant with age, increasing from 3% ($p=0.05$) to 7% ($p=0.0001$), due to a unilateral reduction of FA between childhood and young adulthood in the right centrum. However, the interpretation of this asymmetry in a complex fibre-crossing region such as the centrum semiovale is uncertain. Significant left/right differences were reported in the superior longitudinal fasciculus in a recent study (Büchel et al., 2004) with higher FA in the left hemisphere, similar to our findings.

In the children (8 – 12 years), we saw widespread changes in mean diffusivity (i.e. Trace/3 ADC) and a smaller number of brain regions with changes in diffusion anisotropy (i.e. FA). Decreases in Trace/3 ADC were observed in 9 of 13 structures measured in the children in agreement with previous reports of reduced ADC with development (Schneider et al., 2004; Schmithorst et al., 2002). Increases of FA were observed in 5 of 13 structures, mainly in the central parts of the brain such as the genu and splenium of the corpus callosum, corona radiata, caudate nucleus, and putamen. The significant diffusion trends of these white matter regions in the 8 - 12 year olds suggest that diffusion MRI is more sensitive to underlying microstructural changes associated with brain maturation, since these same regions did not demonstrate "white matter density" changes on T1-weighted

images (Paus et al., 1999), even though the age range in that study was greater at 4 – 17 years.

It is known that myelination follows a posterior – anterior progression with development, and that the projection fibres develop first followed by the commissural and finally associational fibres (Filley, 2001). We see changes in both projection fibres (e.g. internal capsule and corona radiata) as well as commissural fibres (corpus callosum) through childhood. It is of interest that the internal capsule is one of the first structures to myelinate in infancy, and that the posterior limb is known to myelinate much earlier than the anterior limb (Yakovlev and Lecours, 1967; Barkovich et al., 1988). This timing difference appears to agree with the greater change of FA in the anterior limb of the internal capsule than in the posterior limb of the internal capsule between childhood and young adulthood (Table 2.1). As well, it is of note that the corona radiata is made up of the projection fibres that radiate out of the brain stem via the internal capsule (Greenstein and Greenstein, 2000). The diffusion changes may be reflecting the continued development of the internal capsule out into the corona radiata in later childhood. Although the posterior limb of the internal capsule and corona radiata appears to be fully myelinated (i.e. highest myelin staining grade) by 2 years of age in autopsy studies (Brody et al., 1987), there are significant increases of FA due to axonal growth and/or myelination between childhood and young adulthood in these two structures.

The commissural fibres are known to develop next after the projection fibres, and in fact continued development of the corpus callosum through early adolescence has been described by a wave of growth from posterior to anterior in the corpus callosum (Thompson et al., 2000). The slope of FA increase is greater for the genu (0.02 FA units per year) than for the splenium (0.01 FA units per year), which would be consistent with the greater anterior development of the corpus callosum over this age span of 8 – 12 years (Figure 2.3a). Also, the genu has a greater increase from childhood to adulthood for FA (Table 2.1) and a greater decrease for Trace/3 ADC (Table 2.2) than the splenium.

Eigenvalue analysis shows a reduction of diffusion perpendicular to the fibre tracts (λ_2 and λ_3), whereas diffusion parallel to the tracts (λ_1) is fairly constant, with the exception of the putamen over the range of 8 – 12 years. Hence increases in FA are not caused by an increase in the parallel eigenvalue, but rather by a decrease in the perpendicular eigenvalues. A greater reduction in the two perpendicular eigenvalues has been observed with maturation (between children of 1 – 10 years and young adults) in the frontal and parietal lobe white matter (Suzuki et al., 2003) as well as in the basal ganglia, internal capsule, and corpus callosum in children aged 31 gestational weeks to 11 years, with the majority of the change occurring in the first 2 years of life (Mukherjee et al., 2002). This observation of reduced perpendicular diffusivity is consistent with either an increase in the compactness or density of the fibre bundles and/or increased myelination.

In stark contrast to these changes, there were very few changes seen within 21 – 27 years of age. We saw an increase in Trace/3 ADC in the left globus pallidus, which could be an indication of the increasing trends in mean diffusivity previously reported with aging in adulthood (Pfefferbaum et al., 2000; Abe et al., 2002; Bhagat and Beaulieu, 2004). We also saw an increase of FA in the right centrum semiovale. This was not paralleled in the left centrum semiovale, nor was it observed in the children. However, the centrum semiovale is a complex structure composed of numerous crossing projectional, commissural, and associational fibres. Since standard DTI cannot resolve crossing fibres within a voxel, the pattern of FA changes (or lack thereof), including a decrease of FA in the right centrum between childhood and young adulthood followed by an increase of FA in the same region during young adulthood, may be artificial and misleading for the centrum semiovale. More sophisticated methods of resolving multiple crossing fibres in a single voxel such as Q-Ball imaging (Tuch, 2004), which uses a greater number of diffusion-encoding directions and specific post-processing methods, may be necessary to detect the complicated growth patterns within areas such as the centrum semiovale. However, it is important to note that when considering an increase in the number of encoding directions in a DTI sequence, the duration of the scan must be considered, particularly when imaging children.

Although most of the gray and white matter structures we measured did not show any change in FA over 21-27 years (only exception was increase in right centrum semiovale), histological studies have provided evidence that associative cortical regions of the human brain continue to myelinate well beyond childhood (Benes et al., 1994). However, we did not measure the associational fibres (e.g. U fibres) since our 2D region-of-interest analysis targeted readily identifiable areas that are straightforward to outline, primarily deep central white matter, such as the corpus callosum or internal capsule. It would be more difficult to outline the various associational fibres on the 2D images and then measure robust, reproducible FA values. Future analysis using 3-dimensional fibre tracking techniques could be useful for the assessment of these peripheral white matter fibres (Mori et al., 1999; Jones et al., 1999; Conturo et al., 1999). Furthermore, it is possible that on-going changes in myelination and axonal growth do not manifest themselves as large enough changes of FA with age to detect with the 6-direction DTI method used in our study at 1.5T. DTI obtained with higher angular resolution (i.e. more diffusion-sensitizing gradient directions), better spatial resolution, and larger static magnetic field could both improve the accuracy and reduce the variability of the diffusion parameters.

Group analysis of the diffusion parameters showed that much has changed between childhood and young adulthood. More widespread changes were seen in both Trace/3 ADC and FA than was seen in either correlational analysis. To summarize, 11 of 13 structures showed increases in FA and 12 of 13 structures showed decreases in Trace/3 ADC. Figure 2.5 shows the regions in which developmental changes were apparent. Red regions show increases both within 8 – 12 years as well as between childhood and young adulthood. Yellow regions show increases only between childhood and young adulthood but do not demonstrate any measurable changes within 8 – 12 years. Due to the fact that more regions are developing between childhood and young adulthood (i.e. only the genu of the corpus callosum, splenium of the corpus callosum, corona radiata, putamen and head of the caudate nucleus show FA changes within childhood as well as young adulthood, whereas the posterior limb of the internal capsule, anterior limb of the internal capsule, external capsule, subcortical white matter of the gyri, thalamus, and globus pallidus all

show FA changes only between childhood and young adulthood), we believe that more significant and widespread brain changes are occurring throughout the teenage years between our child and young adult groups. These temporal differences in maturation are highlighted in Figure 2.5 by the fact that there are more yellow regions than red regions on the FA maps. In contrast to FA, note that the Trace/3 ADC continually decreases through childhood and adolescence, shown by more red regions in Figure 2.5. These findings confirm those of a previous T1-weighted imaging study that reported significant brain growth between adolescence and adulthood, but very little growth between childhood and adolescence (Sowell et al., 2001).

No significant changes were seen in the diffusion properties of cortical gray matter, in either anisotropy or mean diffusivity. Hence, either the structure of the cortex is fairly static by the time puberty is reached, or DTI is insufficient for detecting microstructural changes that are related to volume increases/decreases that occur in cortical gray matter over this time frame (Giedd et al., 1999; Sowell et al., 2004). However, some of the largest changes seen were in the deep (subcortical) gray matter. Increases of FA were seen in the caudate head and the putamen within 8 – 12 years of age. Between childhood and adulthood all deep gray matter regions measured showed large increases of FA: 7% increase in the thalamus, 12% in the globus pallidus, 13% in the putamen, and 31% in the head of the caudate nucleus. Consistent with our findings, a small linear increase in the head of the caudate nucleus and the lentiform nucleus (comprising the putamen and globus pallidus) was reported (Mukherjee et al., 2001) as the only region which showed continued increase over 1 day – 11 years. There is a paucity of gray matter DTI studies due to low FA values (<0.25 FA units); however, it is clear from our data that major changes are occurring that are detectable using DTI. The DTI findings agree with 3D T1-weighted MRI studies that have demonstrated marked gray matter density changes in the striatum, primarily in the putamen and the globus pallidus, between adolescence (12 – 16 years) and young adults (23 – 30 years) (Sowell et al., 1999). These findings could be related to an increase in motor coordination with maturation or cognitive development associated with brain regions that are linked to these deep gray matter structures. Higher density, more

coherent organization, and/or a greater degree of myelination of fibres (i.e. axons) going into and out of these gray matter relay stations could all contribute to the increases of FA. Small increases of anisotropy in the basal ganglia have been attributed previously to internal white matter pathways (Mukherjee et al., 2001), as opposed to changes of the diffusion parameters of the gray matter neurons.

2.5 – Conclusions

Non-invasive diffusion tensor magnetic resonance imaging of water demonstrates that many regions of the brain continue to develop through late childhood. Relative to the younger age range (8 – 12 years), a greater number of brain regions demonstrate increases of diffusion anisotropy and decreases of mean diffusivity during the adolescent period in the transition from childhood to young adulthood suggesting a progressive pattern of myelination/axon growth during this critical time period of neurodevelopment.

Chapter 3 ♦ Voxel Based Analysis versus Region of Interest Analysis in Diffusion Tensor Imaging of Neurodevelopment[8]

3.1 – Introduction

Diffusion tensor magnetic resonance imaging (DTI) is a valuable tool in studying the microstructure of the brain *in-vivo*. It has been used in the study of neurodevelopment (Neil et al., 2002; Snook et al., 2005) and shows more widespread white matter changes with age than previous T1-weighted studies (Paus et al., 1999; Thompson et al., 2000). However, the spatial extent of the brain changes with age depends on the analysis method employed, namely either manual region of interest (ROI) analysis or automated voxel based analysis (VBM). SPM is frequently associated with fMRI studies where ROI analysis is not usually used. However, for maps where quantitative analysis is desirable, such as DTI data, ROI analysis is an acceptable analysis tool. A direct comparison of ROI and VBM analysis has been studied in detail for gray matter volume differences with variable conclusions. Some studies suggested that while VBM is a valid tool for this type of analysis, it is not a replacement for ROI analysis, and the two should be used in tandem to extract a more complete story (Kubicki et al., 2002; Testa et al., 2004; Giuliani et al., 2005; Suzuki et al., 2005). One study suggested that caution needs to be used for VBM analysis due to the differences seen between VBM and ROI analysis (Suzuki et al., 2005), while another study suggested that VBM provided more information than ROI analysis (Tapp et al., 2006); however, the new region-specific changes were in regions not measured in their previous ROI study (Tapp et al., 2004).

The ROI analysis method involves defining an area of interest in the brain within which to make measurements. However, this method has a large number of drawbacks. There can be some user bias in defining the regions of interest. Not all structures of the brain can be readily defined on a 2D FA map, such as the fornix and cingulum. Note that some of these

[8] A preliminary version of this chapter was presented at the ISMRM Diffusion Workshop, Lake Louise, Alberta, Canada, Mar. 13 – 16, 2005.

structures can be identified on 2D colour maps (Hermoye et al., 2006). The placement of the regions can also have a marked effect on the results of the analysis. By defining the ROIs according to the shape of the structure partial voluming effects of the ROI can be avoided (Schneider et al., 2004; Snook et al., 2005). However, the standard method is to place circles, squares, or ovals over a certain area, which often involves crossing fibre regions (Shimony et al., 1999; Abe et al., 2002; Suzuki et al., 2003; Yoshiura et al., 2005). In these cases, the white matter structure of interest is being sampled along with other fibre tracts, or even gray matter and CSF, causing an artificially decreased or increased FA value. Finally, ROI analysis has the simple limitation in that it is not feasible to measure every region of the brain given time constraints.

The voxel based analysis method, essentially voxel-by-voxel statistical comparisons throughout the brain, may resolve some of these issues. Typically, this method is accomplished by spatially normalizing each set of brain images to a template, and thus assigning an "address" to each voxel. Then, a voxel-by-voxel comparison of the subject brains can be performed, with the assumption that each individual voxel represents the same anatomic location between subjects. While this method does resolve the ROI method issues of user bias as well as a priori knowledge by essentially checking every possible location of the brain, it does have some drawbacks that are not present with an ROI based method of analysis. Since this method performs so many statistical comparisons, the chance of an error due to multiple comparisons is very high, and therefore the statistical power of the results is reduced. Additionally, the standard method of spatial normalization using the program statistical parametric mapping (SPM) (Ashburner and Friston, 2000) warps the *boundaries* of the brain (i.e. the skull) to a template brain, which does not take into account differences in the internal structures of the brain. While one can pass the normalized images through a low pass filter, which will help alleviate some of the imperfections of the spatial normalization process, one must still question whether a location 'X' is indeed the same location in multiple subjects. Despite these issues, voxel based analysis methods have been widely accepted in the imaging community due to its

simplicity of use, although not without criticism (Bookstein, 2001; Ashburner and Friston, 2001; Davatzikos, 2004).

It was previously shown that neurodevelopmental changes in white matter are evident in fractional anisotropy (FA) and mean diffusivity (Trace/3 ADC) within 8 - 12 years of age, as well as between a young (8 – 12 years) and an older age group (21 – 27 years) using ROI analysis (Snook et al., 2005). The statistical tests employed in that study are repeated here using voxel based analysis (hereon in referred to as the SPM analysis method). The purpose of this study is to determine whether these two analysis methods lead to different conclusions of neurodevelopment in the same DTI data set.

3.2 – Methods

3.2.1 – Subjects

Subjects were healthy boys and girls aged 8 – 12 years (N=32, 18 female, 14 male, 30 right handed) and young men and women 21 – 27 years (N=28, 14 female, 14 male, 25 right handed), as previously reported in Snook et al., 2005. All subjects gave informed written consent, and parental consent was given where appropriate. Volunteers had no history of psychiatric disease or neurological injury.

3.2.2 – Image Acquisition

DTI data was acquired using a dual spin-echo, single shot echo-planar imaging sequence on a 1.5T Siemens Sonata scanner with 3mm slice thickness, no inter-slice gap, TR = 6400 ms, TE = 88 ms, FOV = 220 x 220 mm^2, 6 non-collinear diffusion-sensitizing gradient directions with diffusion sensitivity b = 1000 s/mm^2, 8 averages, and a matrix of 96 x 128 zero filled to 256 x 256 for a resulting pseudo-voxel size of 0.85 x 0.85 x 3.0mm^3. Total DTI scan time was 6:06 minutes for 40 contiguous slices for full brain coverage. Slices were positioned along the anterior commissure-posterior commissure line. The mean SNR

of brain parenchyma on the non-diffusion-weighted images was 75 ± 6 for the children and 71 ± 6 for the young adults.

3.2.3 – Region of Interest Analysis

Region of interest analysis was performed as described in a previous publication. Mean diffusivity (Trace/3 ADC) and fractional anisotropy (FA) values were collected from 30 regions in 13 distinct brain structures. For comparison to SPM2 data, we will consider only those regions with an FA value greater than 0.2 FA units. This remains 14 regions in 8 distinct brain structures, mainly: genu of the corpus callosum, splenium of the corpus callosum, anterior limb of the internal capsule, posterior limb of the internal capsule, external capsule, corona radiata, centrum semiovale, and thalamus. ROIs were defined on the FA map where the structure was visualized to be at its thickest. Using image analysis software (MRVision, Winchester, MA), the structure in question was outlined following its contours, with the exception of the corona radiata and centrum semiovale in which only central regions were measured in order to avoid partial voluming effects with the adjacent subcortical white matter. ROIs were subsequently translated onto trace/3 ADC maps.

Three statistical tests were performed for both FA and Trace/3 ADC data. **Test 1**: linear correlation with age within 8 – 12 years. **Test 2**: two sample un-paired t-tests to compare the children and young adults. **Test 3**: linear correlation with age within 21 – 27 years. Significance was set at $p<0.05$ for all tests.

3.2.4 – Statistical Parametric Mapping Analysis

All Statistical Parametric Mapping (SPM) analysis was done using the SPM2 package (Wellcome Department of Cognitive Neurology, Institute of Neurology, London, UK). The non-diffusion-weighted (b0) images were normalized to the Montreal Neurological Institute (MNI) EPI template that is supplied with the SPM2 package. The FA and Trace/3 ADC maps were then spatially transformed according to the normalized b0 images. Normalized images were re-sliced into 69 slices with 2 x 2 x 2 mm^3 voxels.

While not the focus of this study, FA maps were smoothed with 4 mm, 6 mm and 8 mm isotropic Gaussian kernels, due to a recent study (Jones et al., 2005). This study suggests that different smoothing kernels can lead to different conclusions. While the size of the clusters SPM identified tended to increase with increased smoothing, no clusters "appeared" or "disappeared". Thus, all data analysis is performed on the $4x4x4mm^3$ smoothed data, following the 'rule of thumb' as developed for fMRI and PET studies that states that the smoothing kernel is of at least 2 – 3 times the voxel dimension (Worsley et al., 1992). We feel this small smoothing kernel is desirable over a very large one due to the heterogeneous nature of fractional anisotropy.

To compare to ROI analysis, the statistical tests were repeated for the SPM analysis. **Test 1 & Test 3**: correlative analysis was performed using the "simple linear regression (correlation)" analysis tool, with age as covariate within 8 – 12 years and 21 – 27 years using the FA maps, looking for positive correlations. **Test 2**: group analysis was performed using the "two sample t-test" tool. These tests were repeated for Trace/3 ADC, looking for negative correlations with age. All tests on fractional anisotropy were performed using an absolute threshold of $FA > 0.2$, such that if a voxel had an FA value less than 0.2 FA units in any one subject, that voxel is not considered for analysis. A total brain mask was used so that no voxels outside the volume of the brain are considered. Significance was placed at $p<0.05$, and an extent threshold of 10 voxels.

After SPM analysis was completed, the normalized FA maps were imported into a 3D image processing software package (Amira, Template Graphics Software, Inc., San Diego, CA), and overlaid with a mask comprised of the significant SPM clusters. Each cluster was located according to the voxel of highest significance, as determined by SPM2, in order to determine its anatomic location, with the help of a neuroanatomy atlas (Greenstein and Greenstein, 2000) and fibre tracking atlas (Wakana et al., 2004). We also used this software to run movie loops of the normalized FA maps of all the subjects in order to appraise the clusters. The clusters of FA were checked for several criteria: 1) does the anatomic location make sense and does the cluster involve two or more white matter tracts?

2) Is the cluster consistently in the same region for all subjects or is the cluster right on the edge of a structure? 3) Is the cluster right on the edge of the brain or in an area of severe susceptibility artifact? In general, only 20 - 25% of clusters output by SPM were kept after this rigorous visual inspection. Within 8 – 12 years, 9 of 35 clusters were kept (including 6723 / 7431 voxels (90%)), between childhood and young adulthood, 2 of 9 clusters were kept (including 14012 / 14201 voxels (99%)) and within 21 – 27 years, 10 of 42 clusters were kept (including 1132 / 1935 voxels (59%)).

3.3 – Results

3.3.1 – Mean Diffusivity

Trace/3 ADC was found to be negatively correlated with age in splenium of the corpus callosum, anterior limb of the internal capsule, external capsule, corona radiata, centrum semiovale, subcortical white matter of the gyri, globus pallidus, putamen, and head of the caudate nucleus within 8 – 12 years as measured with the ROI method. With SPM analysis, Trace/3 ADC decreased with age in the entire brain (Figure 3.1a). Between childhood (8 – 12 years) and young adulthood (21 – 27 years), all structures measured with ROI analysis with the exception of the cortical gray matter showed decreases with age. Similarly, with SPM analysis, we see widespread decreases of Trace/3 ADC with age, although a little sparser in the right hemisphere (Figure 3.1b). Within 21 – 27 years no decreases in mean diffusivity were seen with ROI analysis; however, with SPM analysis, significant decreases of Trace/3 ADC were seen throughout the brain, mainly in the peripheral white matter (Figure 3.1c).

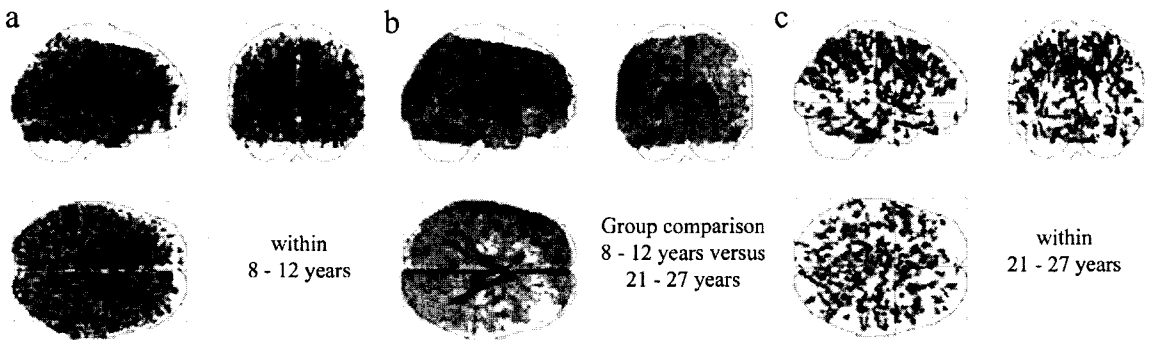

Figure 3.1 - SPM results for Trace/3 ADC analysis with age. Collapsed brain views of the SPM significant clusters: a) negative correlation analysis within 8 – 12 years, b) un-paired t-test analysis between young and older groups, and c) negative correlation analysis within 21 – 27 years. All analyses show global decreases in Trace/3 ADC with age, although into the 20s the clusters become sparser.

3.3.2 – Fractional Anisotropy

3.3.2.1 – Test 1: Correlations within 8 – 12 years

In children 8 – 12 years (N=32), only 3 (of a possible 8) white matter regions were found to have increases of FA with age in ROI analysis. These were the genu of the corpus callosum, splenium of the corpus callosum and the corona radiata. However, with SPM analysis, much more widespread changes were seen. In fact, a cluster of 6422 voxels ($p<0.0001$, $r=0.65$ at the voxel of highest significance) was found to have significant positive correlation with age (Figure 3.2). This cluster includes the cerebellar peduncles, brain stem, inferior fronto-occipital fasciculus, uncinate, inferior longitudinal fasciculus, frontal white matter, internal and external capsules (with the exception of the right external capsule), thalamus, genu of the corpus callosum, the body of the corpus callosum, cingulum, and the corona radiata up to the top of the brain.

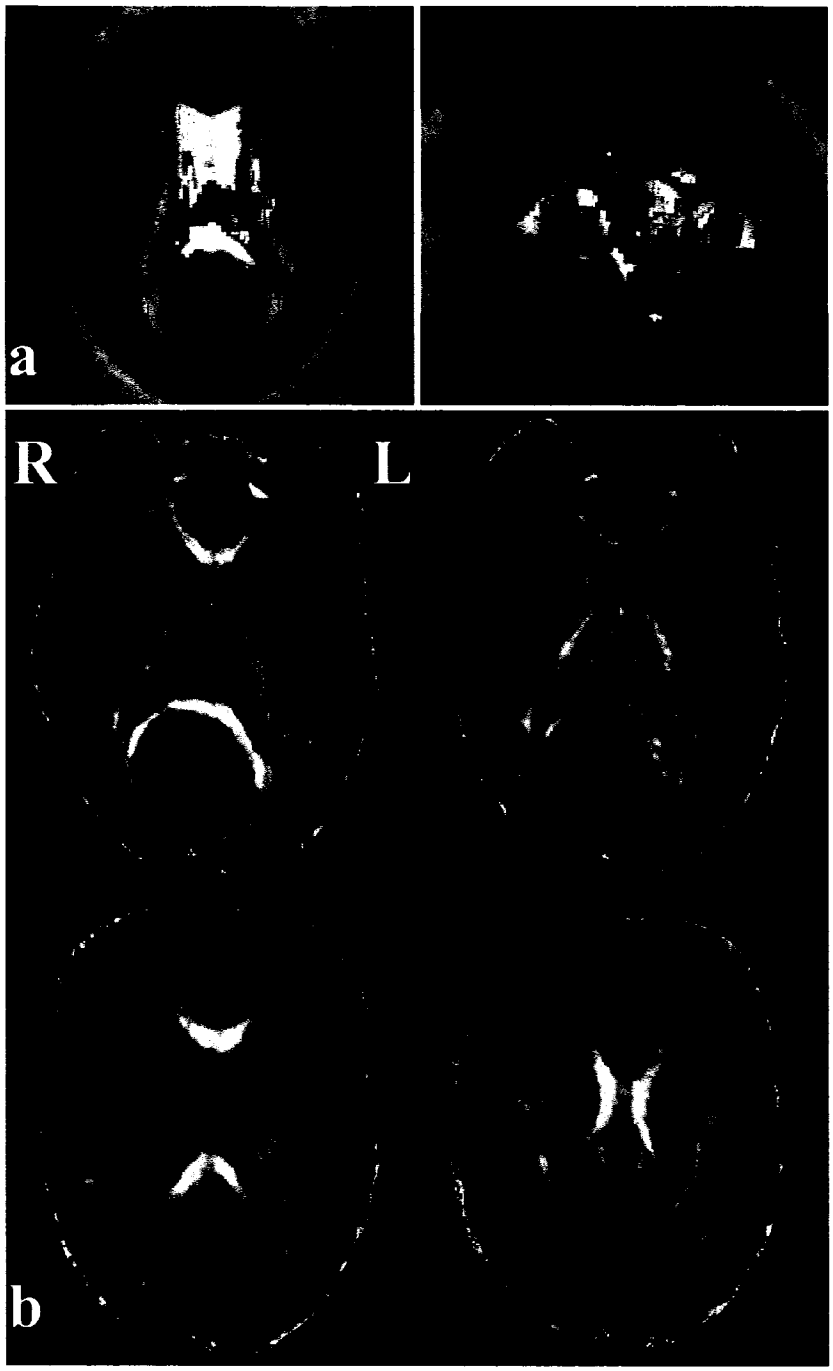

Figure 3.2 – Results for correlation of FA with age within 8 – 12 years: a) SPM significant clusters in orange and b) ROI significant regions in green and non-significant regions in blue. ROI analysis underestimates the extent of the changes occurring over this age range.

There were also a few isolated clusters most of which were contralateral to parts of the large cluster. These were in the left cerebellar peduncle (16 voxels, p=0.01, r=0.45), the right cerebral peduncle (34 voxels, p=0.01, r=0.44), left frontal white matter (34 voxels, p=0.004, r=0.49), right inferior longitudinal fasciculus (15 voxels, p=0.02, r=0.40), right optic radiation (25 voxels, p=0.02, r=0.41), a central portion of the splenium of the corpus callosum (119 voxels, p=0.01, r = 0.45), part of the cingulum and corpus callosum body on the right side (22 voxels, p=0.01, r=0.45) and in the left corona radiata high in the brain (36 voxels, p=0.02, r=0.42).

3.3.2.2 – Test 2: Group Analysis (8 – 12 years versus 21 – 27 years)

Group analysis showed the most robust changes in FA with age. With ROI analysis 7 of 8 measured structures showed increases in FA between childhood and young adulthood with the exception of the centrum semiovale (Table 3.1). Similarly, with SPM analysis, one significant cluster of 13988 voxels was found, comprised of the cerebellum, cerebellar peduncles, brain stem, cerebral peduncles, frontal white matter, inferior longitudinal fasciculus, inferior fronto-occipital fasciculus, internal capsule, external capsule, a small portion of the genu of the corpus callosum, body of the corpus callosum, a small portion of the splenium of the corpus callosum, cingulum, hippocampus, superior fronto-occipital fasciculus, superior longitudinal fasciculus and the corona radiata up to the top of the brain (at max voxel $p=10^{-13}$, difference of 35%) (Figure 3.3). There was also one isolated cluster in the right inferior longitudinal fasciculus (24 voxels, p=0.001, difference of 20%). SPM analysis, like ROI analysis, did not find any significant difference between the child and young adult centrum semiovale. The centrum semiovale is a very complex region of crossing fibres, and therefore very low FA for white matter. Thus, accurate measures of the change in FA in this region may require higher resolution imaging, or different analysis techniques.

Table 3.1 – Group analysis statistics and percentage fractional anisotropy (FA) differences in children versus young adults for ROI and SPM analysis

Region	ROI Analysis[9]		SPM Analysis[10]	
	p	FA Difference (%)[11]	p	FA Difference (%)[11]
cerebellum	N/A	N/A	0.01	15
brain stem	N/A	N/A	0.01	7
inferior longitudinal fasciculus	N/A	N/A	0.001	13
cingulum and corpus callosum	N/A	N/A	0.007	12
hippocampus	N/A	N/A	0.005	16
superior fronto-occipital fasciculus	N/A	N/A	0.001	10
superior longitudinal fasciculus	N/A	N/A	<0.0001	15
genu of corpus callosum	<0.0001	11	0.02	11
splenium of corpus callosum	<0.0001	7	0.05	11
anterior limb of internal capsule	<0.0001	14	<0.0001	31
posterior limb of internal capsule	<0.0001	6	0.0002	15
external capsule	<0.0001	9	0.009	8
corona radiata	<0.0001	11	0.05	7
centrum semiovale	>0.05	None	>0.05	None
thalamus	0.007	7	<0.0001	14

[9] N/A = structure not measured with ROI analysis

[10] SPM results are presented for a voxel from the central portion of each structure within the large cluster

[11] FA difference = $\frac{FA\,adult - FA\,child}{FA\,child} \times 100$

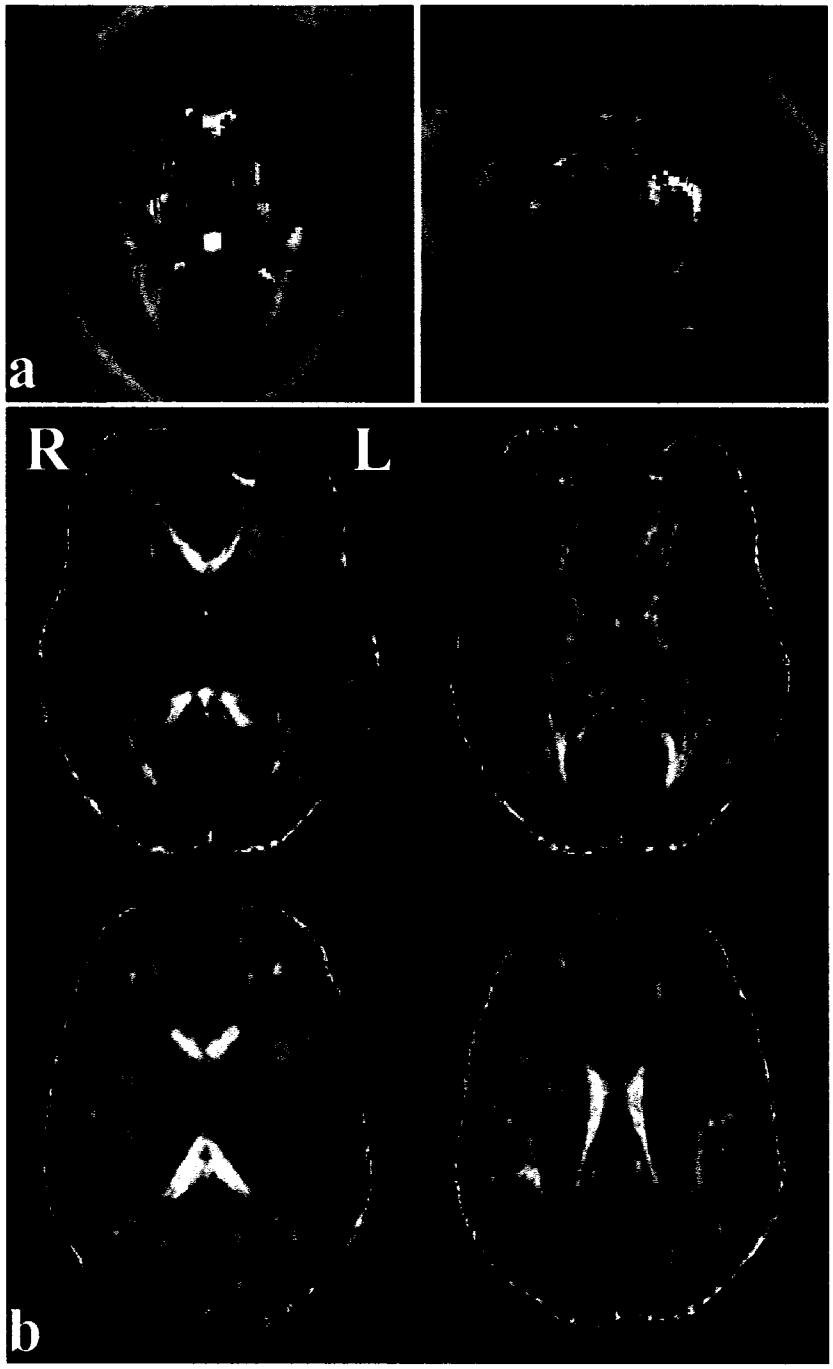

Figure 3.3 - Results for group analysis between children (8 – 12 years) and young adults (21 – 27 years): a) SPM significant clusters in orange and b) ROI significant regions in green and non-significant regions in blue. Although both methods demonstrate widespread increases in FA with age, SPM analysis misses the largest portions of the genu and splenium of the corpus callosum likely due to imperfect spatial normalization. On the other hand, ROI analysis underestimates the extent of the changes in FA with age.

3.3.2.3 – Test 3: Correlations within 21 – 27 years

In young adults aged 21 – 27 years (N=28) only the right centrum semiovale showed significant increase in FA with age using ROI analysis. Using SPM analysis, increases in FA were seen in the left centrum semiovale (two clusters:407 voxels, p=0.0005, r=0.61 and 157 voxels, p=0.009, r=0.49) and right centrum semiovale (285 voxels, p=0.0001, r=0.66), left anterior limb of the internal capsule (63 voxels, p=0.0005, r=0.61), right frontal white matter (12 voxels, p=0.02, r=0.43), right parietal white matter (18 voxels, p=0.02, r=0.45), upper left corona radiata (two clusters: 93 voxels, p=0.003, r=0.53 and 18 voxels, p= 0.01, r=0.48), upper right corona radiata (68 voxels, p=0.001, r=0.59) and the right thalamus (10 voxels, p=0.02, r=0.43).

3.4 – Discussion

3.4.1 – Mean Diffusivity with Age

SPM and ROI analyses were very consistent for the more robust correlations such as Trace/3 ADC with age, where similar trends were seen with both analysis methods. And while SPM analysis did find more regions than were measured using the ROI analysis, the general result was the same: mean diffusivity decreases during development throughout the brain, during childhood and adolescence, in agreement with previous studies which showed a decrease in diffusion coefficient throughout childhood (Mukherjee et al., 2001). However, within 21 – 27 years, SPM indicated that Trace/3 ADC continues to decrease with age, whereas ROI analysis found no decreases with age. Much less of the brain shows this decreasing trend than in childhood (Figure 1) indicating that this decreasing trend may be coming to an end. Previous studies of adult aging suggest that from 20 years and older, mean diffusivity increases (Pfefferbaum et al., 2000; Abe et al., 2002; Bhagat and Beaulieu, 2004), however, very few studies have been performed on the 20s alone. One can infer, then, that the trend of decreasing mean diffusivity with age comes to an end in the beginning of adulthood, and then the trend reverses. While this does not entirely support the results of ROI analysis, it does not entirely contradict it, either. The two analysis

methods thus, tend to lead to the same conclusions of neurodevelopment. The uniform appearance of the various structures on Trace/3 ADC maps obtained with b = 1000 s/mm^2 may also be partly responsible for this good agreement. However, conclusions on regional variations with age of the heterogeneous FA maps differed between ROI and SPM.

3.4.2 – Fractional Anisotropy with 8 – 12 years

The results of fractional anisotropy within 8 – 12 years differed the most between ROI and SPM. While both analyses showed changes in the genu of the corpus callosum and the corona radiata, SPM analysis yielded a much larger number of regions. Most of these regions, such as the cortico-spinal tracts, limbic system and association fibres, were not measured using ROI analysis due to both time constraints and difficulties in identifying structures on 2D FA maps. However; the internal capsule, external capsule and the thalamus were measured using ROIs and were not found to be significant, although they were found to be significant in SPM analysis. Perhaps averaging over all the voxels in the 2D slice of a structure with ROI analysis averages out the differences. This is supported by the fact that FA is known to vary along a given structure (Partridge et al., 2005) hence a portion of the structure may be changing with age, but not the structure as a whole.

On the other hand, ROI analysis identified significant changes in the splenium of the corpus callosum, while SPM analysis found only a very small central portion showing increases in FA over the age range of 8 – 12 years which may be due to improper spatial normalization (Figure 3.4). The splenium of the corpus callosum has a large variety in shape due to natural human variation, even in a spatially normalized state. The central portion is consistent, whereas the ends vary dramatically. This level of variation makes this structure particularly sensitive to the absolute FA threshold, as it would be more likely for voxels to contain gray matter in one individual, and white matter in another.

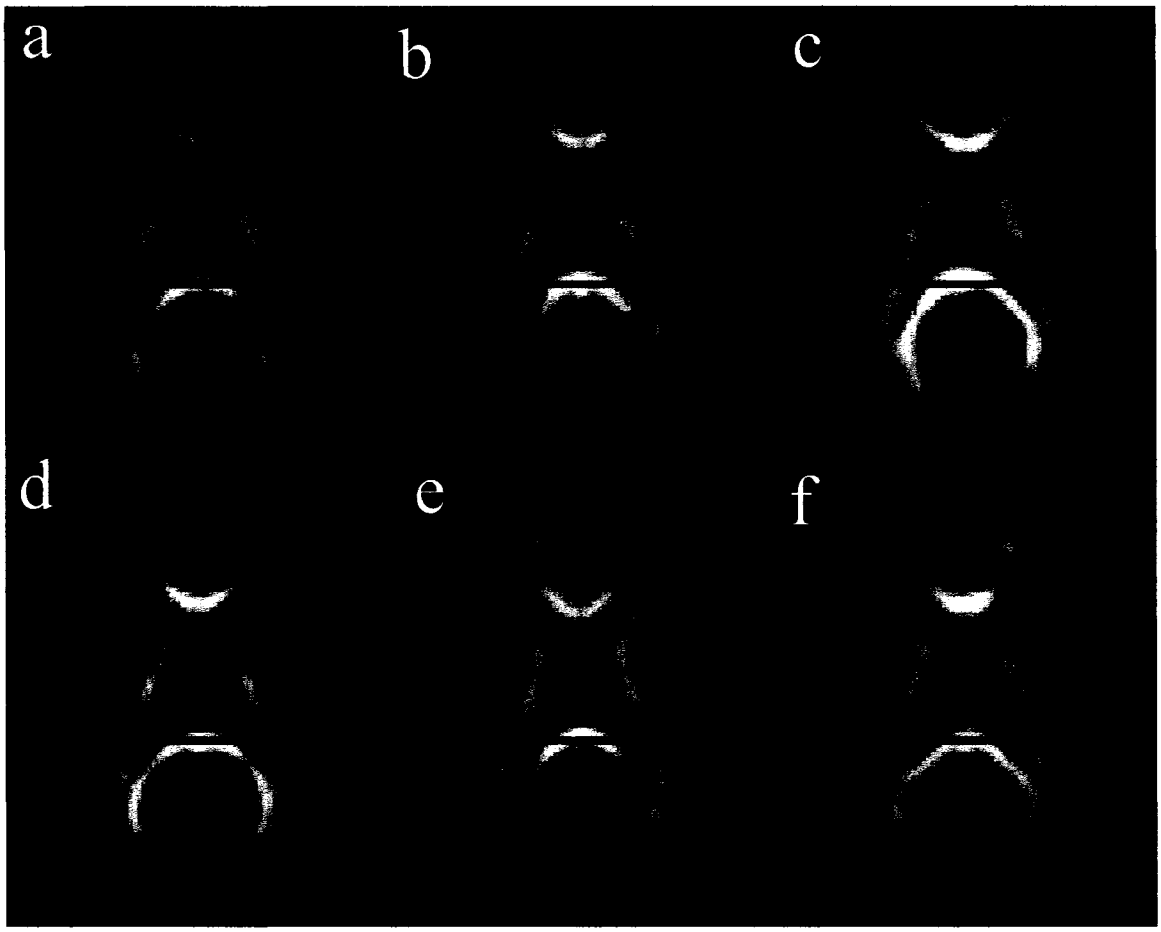

Figure 3.4 - Normalized images from six individuals at the same slice level. The red line shows that the central portion of the splenium lines up for most individuals. However, it is evident that the rest of the structure is quite different from person to person: b) and e) are quite truncated, while c) and d) are elongated, and a) and f) are somewhere in between.

3.4.3 – Fractional Anisotropy between 8 – 12 years and 21 – 27 years

Group analysis comparing the children and young adults agreed quite well between analysis methods. Both methods identified the majority of the white matter having increases in FA with age, with the exception of the centrum semiovale. SPM analysis identified all of the 7 structures that ROI analysis identified. However, the SPM clusters in the genu and splenium of the corpus callosum, as well as the corona radiata did not encompass the entire structures, likely due to imperfect spatial normalization (Figure 3.4)

and biological variability in their shapes. These clusters also had much lower statistical significance than with ROI analysis (with SPM p-values of 0.02, 0.05 and 0.05 respectively, with ROI all were $p<0.0001$). On top of these 7 structures, SPM analysis identified a large number of structures not measured using ROI analysis, including the cortico-spinal tracts, the limbic system and association fibres.

3.4.4 – Fractional Anisotropy with 21 – 27 years

Correlations within 21 – 27 years showed very little change in FA for both SPM and ROI analyses. ROI analysis only identified the right centrum semiovale as having increasing FA with age. SPM analysis also identified the centrum semiovale, although bilaterally, as well as a few other structures not identified with ROI analysis. The significant clusters found in the thalamus and anterior limb of the internal capsule are quite small (10 voxels and 63 voxels respectively). By averaging all the voxels within these structures on one 2D slice with ROI analysis these small regional differences may have been lost. The remaining clusters were in areas not measured with ROI analysis. And while the specific results of these analysis methods did differ, the conclusions of neurodevelopment remain consistent: that the structure showing the most development beyond adolescence is the centrum semiovale. Again, this is a very difficult structure to measure, and so changes may be artifactual.

3.4.5 – General Comments on Neurodevelopment Analysis Techniques

SPM analysis gives a more complete picture of the brain's development through childhood and into young adulthood than does ROI analysis. The continued development of the limbic system and the association fibres are not surprising. Yakovlev and Lecours suggested that the limbic system would continue to develop beyond the 1st decade of life, and that the association fibres continue to myelinate beyond the 30s (Yakovlev and Lecours, 1967). And, in fact, Paus et al identified the arcuate fasciculus association fibre in a study of white matter density with T1-weighted images within 4 – 17 years (Paus et al., 1999), and Schmithorst et al identified both the cortico-spinal tract and association fibres in

a VBM study of 5 – 18 years (Schmithorst et al., 2002). However, these two latter studies severely under-estimated the spatial extent of the developmental changes occurring in the brain. Several studies did not measure these regions with 2D ROIs including our previous study (Klingberg et al., 1999; Schneider et al., 2004; Snook et al., 2005). This is likely due to the difficulties associated with identifying these structures on 2D slices. The use of tractography to study neurodevelopment of those tortuous tracts may be another option (Partridge et al., 2005). This study also showed that tractography based analysis could reduce intra-operator variability and improve reproducibility as compared to manual ROI analysis.

While SPM analysis seems to give a more complete story than is possible with ROI analysis alone, there remains one major concern. Of the clusters that SPM identified as being significant, 75% were thrown away. In group analysis, this only accounted for 1% of the total voxels identified and as such is not much of a concern. However, for correlative analysis, this accounted for up to 41% of the total voxels. While it is quite easy to take the SPM results at face value, visual inspection of all the clusters is an important step in the SPM analysis process.

3.5 – Conclusions

While the ROI method and voxel based method of analysis are both widely used, each method has its advantages and disadvantages. Without any a priori knowledge of the affected areas of the brain, ROI analysis quickly becomes limited by time constraints, and thus seems to under-estimate the extent of the white matter changes occurring with neurodevelopment. However, SPM analysis is limited by the inaccuracies of spatial normalization. These two analysis methods in general tend to agree with one another, but neither method alone gives the complete story of neurodevelopment as assessed by diffusion tensor imaging. Perhaps combining the two methods would give a more complete story of neurodevelopment.

Chapter 4 ♦ Neurodevelopment over the Span of Childhood to Young Adulthood – Works in Progress

4.1 – Introduction

The 8 – 12 year old subjects recruited and scanned for Chapters 2 and 3 above were recruited for a reading study being conducted by our research group (Beaulieu et al., 2005). In order to study neurodevelopment, we recruited the young adults (21 – 27 years) as per Chapters 2 and 3. The reading study was extended younger, and so we had an added opportunity to study neurodevelopment from the age of 5 years, instead of only 8 years. Thus we had children between the ages of 5 – 12 years, as well as young adults between 21 – 27 years of age. Given the large number of changes seen in FA and Trace/3 ADC between childhood and young adulthood (Table 2.1 and 2.2), it was only natural that we should fill the age gap, and recruit and scan teenagers between the ages of 13 – 21 years in order to look at the entire span of neurodevelopment. Our inclusion/exclusion criteria were: 1) no history of psychiatric disorder including depression and attention deficit disorder, 2) no history of neurologic injury or diseases including cerebral palsy, epilepsy, and meningitis, 3) no birth trauma such as premature birth, or injury in which oxygen was required. Also, all subjects were screened for MRI safety, including metal and/or electronic implants, injuries with metal to the eyes, body piercings and tattoos, as well as pregnancy. In total, 219 subjects were scanned. Of those, we had successful scans of 196 subjects (Figure 4.1), giving us roughly a 90% success rate.

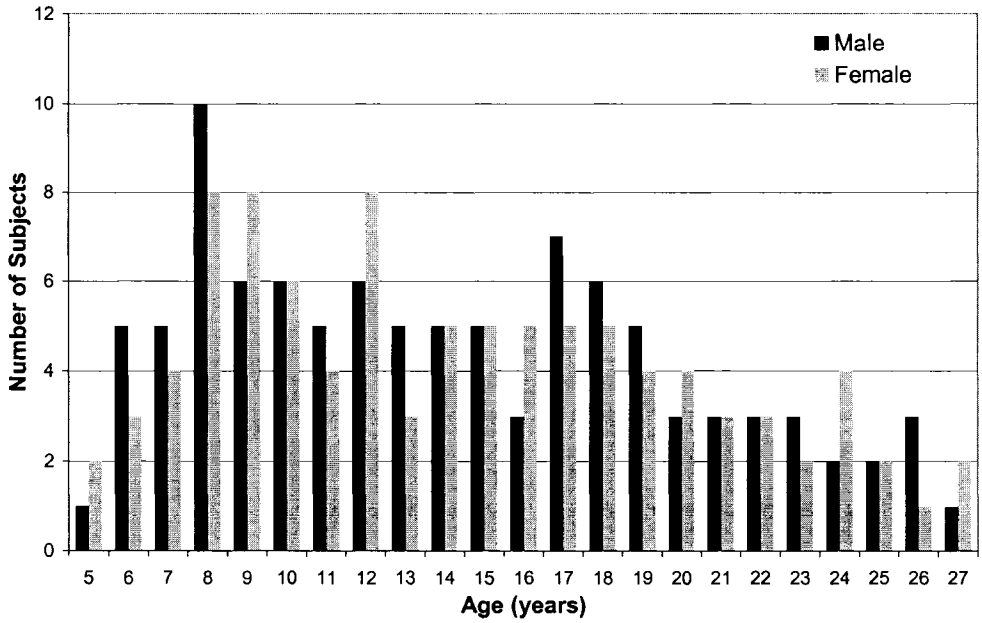

Figure 4.1 – Summary of subjects scanned (successful scans only).

Ideally, we will scan 2 more 13 year old females, 2 more 16 year old males and 1 more 19 year old female in order to have a total of more than 200 subjects, with a minimum of 5 per age per gender through the teenage years, to fully describe the dynamic adolescent years.

The largest portion of unsuccessful scans came from children between the ages of 5 – 7 years (10 subjects) in which the children were simply unable to sit still long enough for the DTI scan (6:06 minutes). The other subjects that were not used were due to a combination of MRI scanner errors (such as RF artifacts), and motion artifacts and their ages ranged anywhere from 9 years to 29 years. Of the successful 196 subjects scanned, 142 (71 female and 71 male) have had a full ROI analysis performed to date (Figure 4.2).

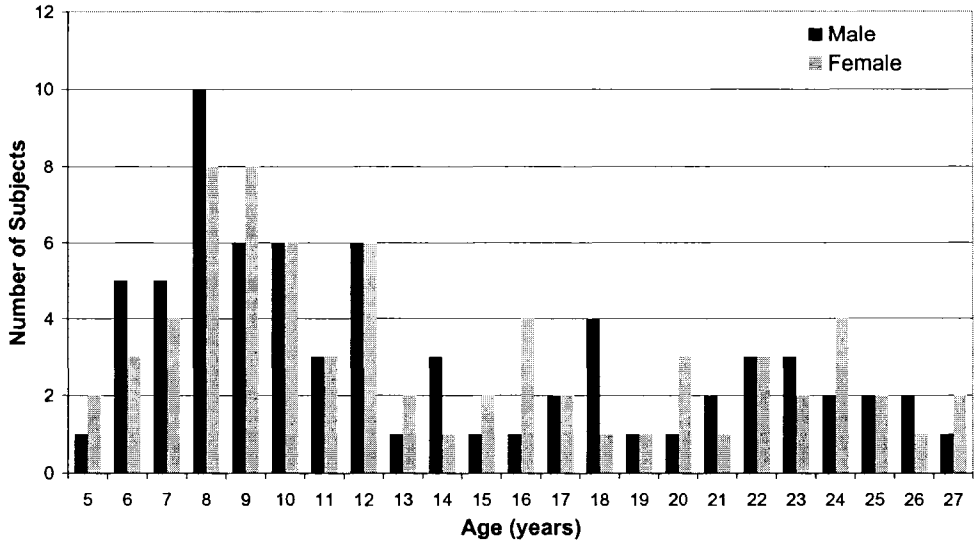

Figure 4.2 – Subjects analyzed to date.

4.2 – Motivation

A large number of MRI studies of maturation have been performed on children, adolescents and young adults. However, the majority of them are looking at volumetric data in the cortex using T1- weighted imaging (Sowell et al., 2004). Considering the evidence of continued myelination through the young adult years (Yakovlev and Lecours, 1967; Benes et al., 1994) it is somewhat surprising that DTI studies have been limited to the childhood and early adolescent years, or the opposite end, looking at the aging brain, into the 70s and 80s. Many DTI studies of neurodevelopment are interested in the first year of life, where major developmental changes are occurring (McKinstry et al., 2002; Maas et al., 2004; Partridge et al., 2004; Hermoye et al., 2006). The largest jumps in FA and ADC are seen in this first year of life. Another large chunk of these studies focus on the first 4 years of life, again where large increases of anisotropy and decreases of mean diffusivity are observed (Morriss et al., 1999; Schneider et al., 2004). However, small changes continue to occur through the older child, adolescent and young adult years. A few studies which look at adolescents simply underestimate the magnitude of change occurring in the brain as compared to our studies, perhaps due to a small number of subjects (Schmithorst et al., 2002) and/or a small number of regions measured (Schmithorst et al., 2002; Ben Bashat

et al., 2005). A recent study of 6 – 19 year olds has shown some interesting results, with increases of FA in the arcuate fasciculus, motor areas, internal capsule, prefrontal regions, corpus callosum, basal ganglia, thalamocortical connections and ventral-visual pathways (Barnea-Goraly et al., 2005), however, they only had 34 subjects. With our nearly 200 subjects over this developmentally highly dynamic age range, it will be interesting to see if we can reproduce the results of these previous studies, as well as analyze other issues, such as gender differences, which is not possible with the small number of subjects in the earlier reports.

The National Institutes of Health (NIH) is undergoing a large scale project of neurodevelopment including both cross sectional and longitudinal information, performing not only DTI, but also anatomical imaging and spectroscopy, as well as a large battery of cognitive and behavioural tests. This study includes subjects of 0 – 18 years (N = 500) with 188 DTI data sets in children 7 – 18 years of age. This is a multi-centre collaborative project with a budget of over $28 million (US dollars). Their motivations are much like ours: a need for studies with larger sample sizes, and more than just T1- weighted imaging. However, the one advantage we have is that our DTI data sets (a comparable number of them) are all acquired with the same scanner. Multi-centre projects tend to have issues with the images being acquired on different MRI scanners, which have their own characteristics in field inhomogeneities, and such. Thus, each centre will have its own set of artifacts, complicating the final analysis of all the subjects from the different centres (Evans, 2005).

With the results of Chapters 2 and 3, which show a large number of changes between childhood and young adulthood in both FA and Trace/3 ADC, then there must be changes occurring in the teenage years in between. The question thus remains what the course of FA and Trace/3 ADC development will look like during the teenage years.

4.3 – Preliminary Results

4.3.1 – Mean Diffusivity

Negative linear correlations were performed for Trace/3 ADC with age over 5 – 27 years (N=142). Mean diffusivity showed continued decreases with age in all 13 measured structures (Figure 4.3a – m, statistics indicated in the top right corner of the graph, m=slope). In 12 of the 13 structures, the statistical significance was very high ($r > 0.45$ and $p < 0.0001$). In the cortical gray matter, the correlation reached significance ($p = 0.0005$), however, it was not a very good correlation ($r = 0.13$) (Figure 4.3m). This is in good agreement with the results of Chapter 2 which showed group decreases of mean diffusivity between childhood and young adulthood in all structures but the cortical gray matter (Table 2.2). Note that while this data fits a linear decrease, were we to include children less than 4 years old it would likely be a biexponential decrease (Schneider et al., 2004).

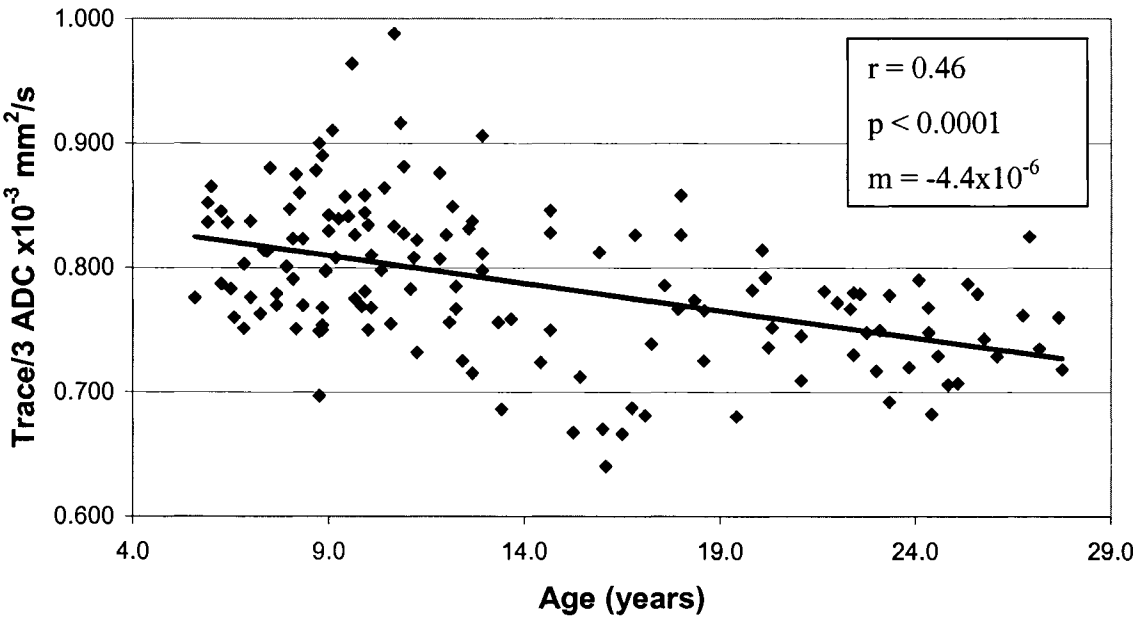

Figure 4.3a – Trace/3 ADC trends for the genu of the corpus callosum.

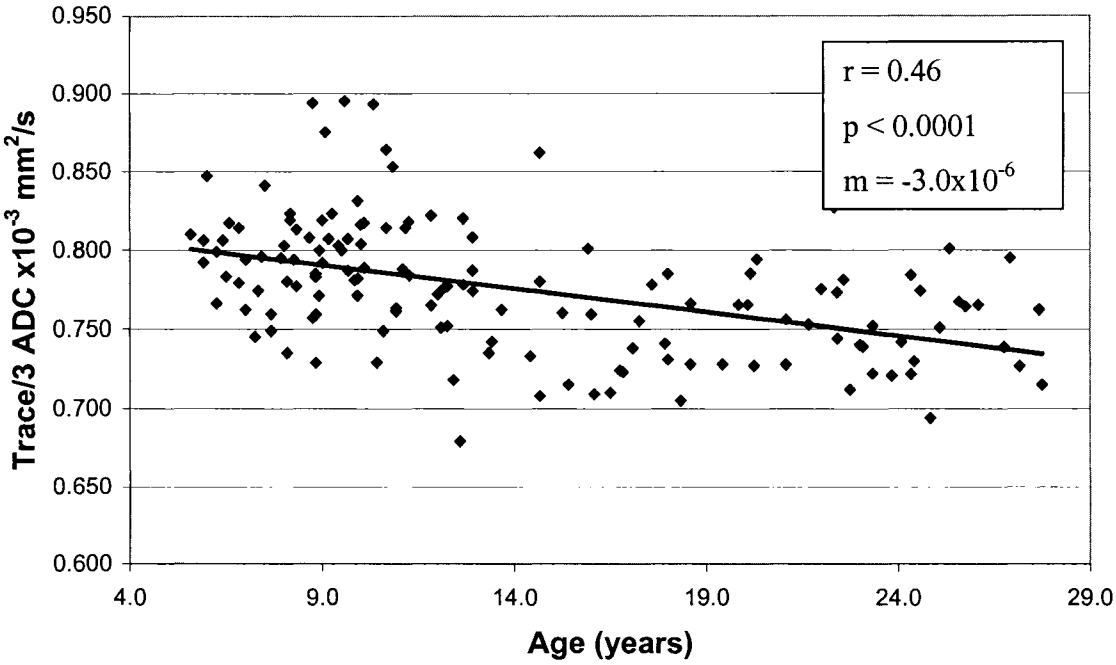

Figure 4.3b – Trace/3 ADC trends for the splenium of the corpus callosum.

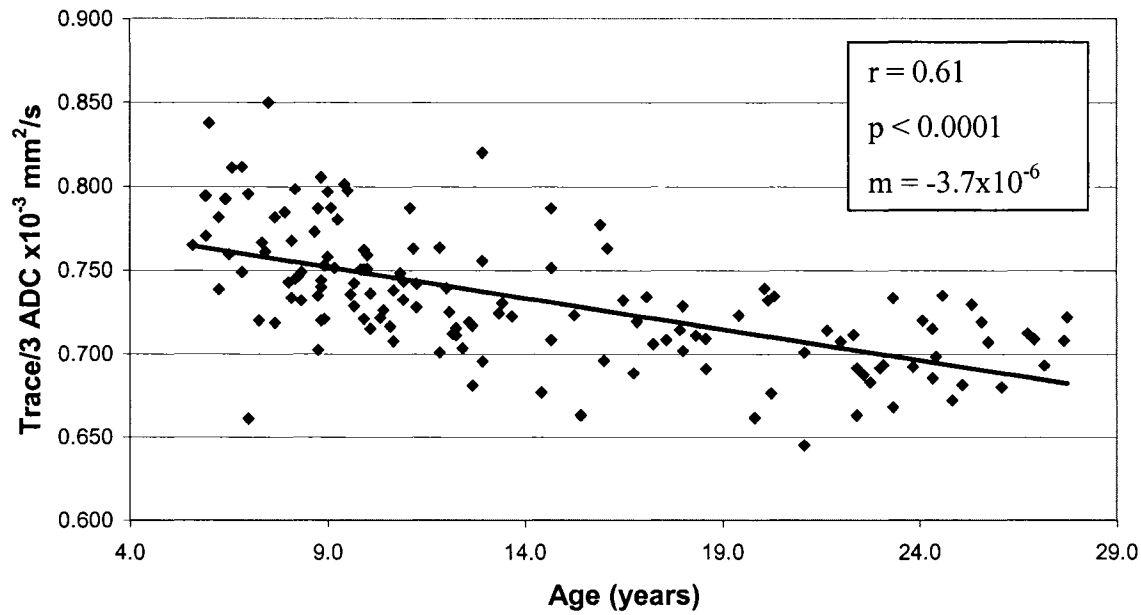

Figure 4.3c – Trace/3 ADC trends for the anterior limb of the internal capsule.

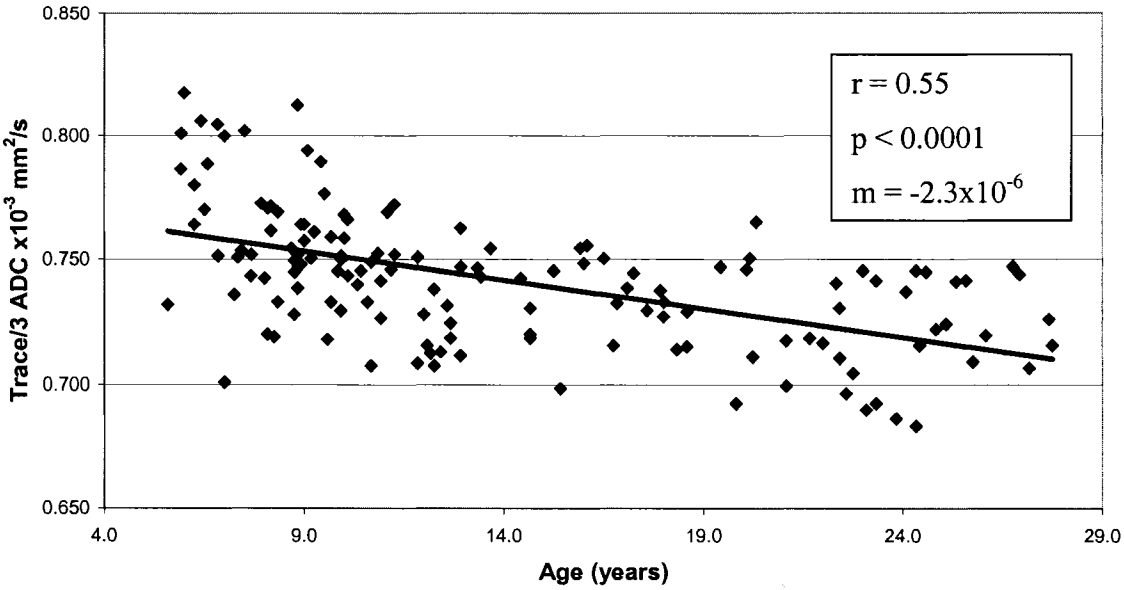

Figure 4.3d – Trace/3 ADC trends for the posterior limb of the internal capsule.

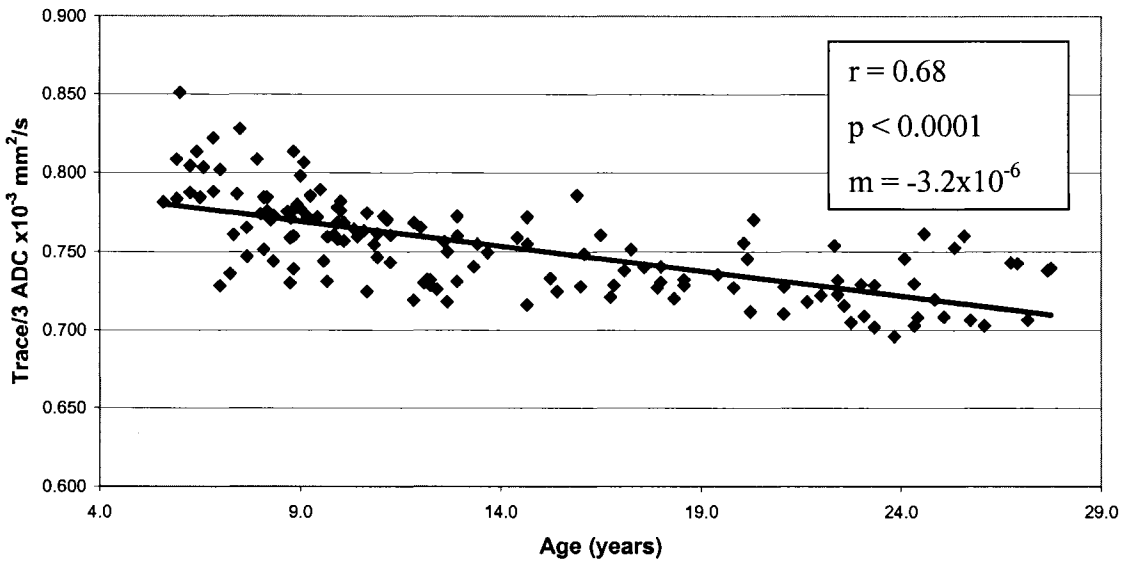

Figure 4.3e – Trace/3 ADC trends for the external capsule.

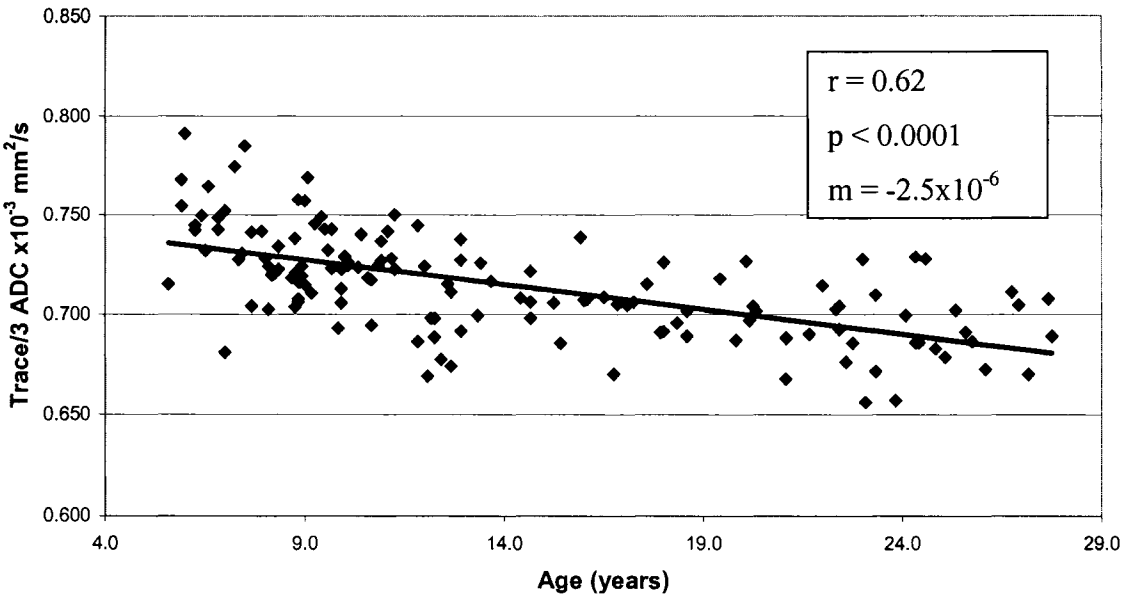

Figure 4.3f – Trace/3 ADC trends for the corona radiata.

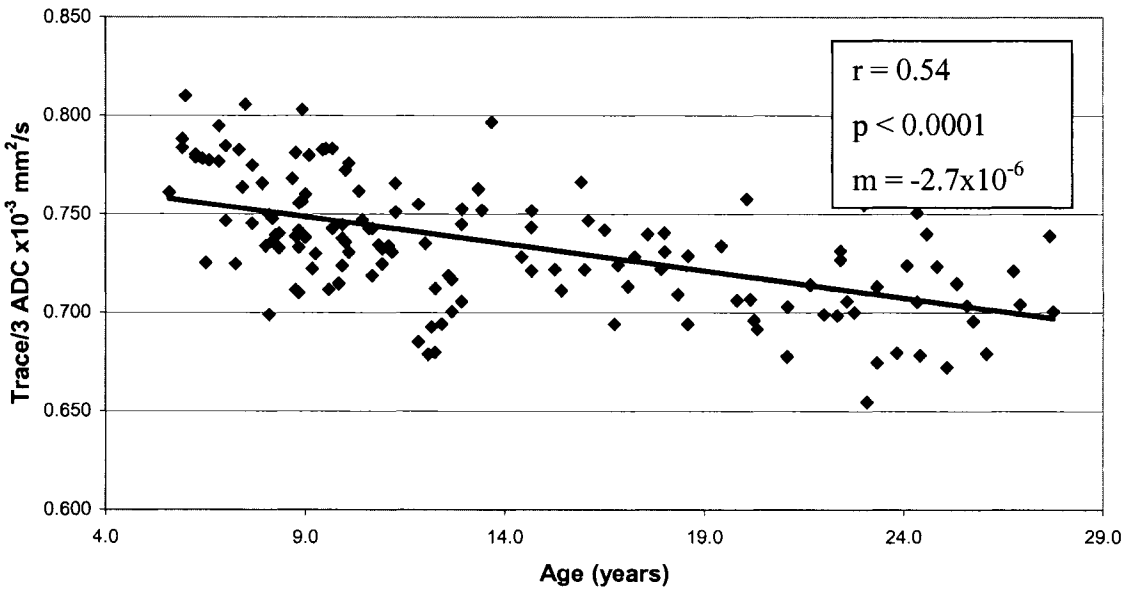

Figure 4.3g – Trace/3 ADC trends for the centrum semiovale.

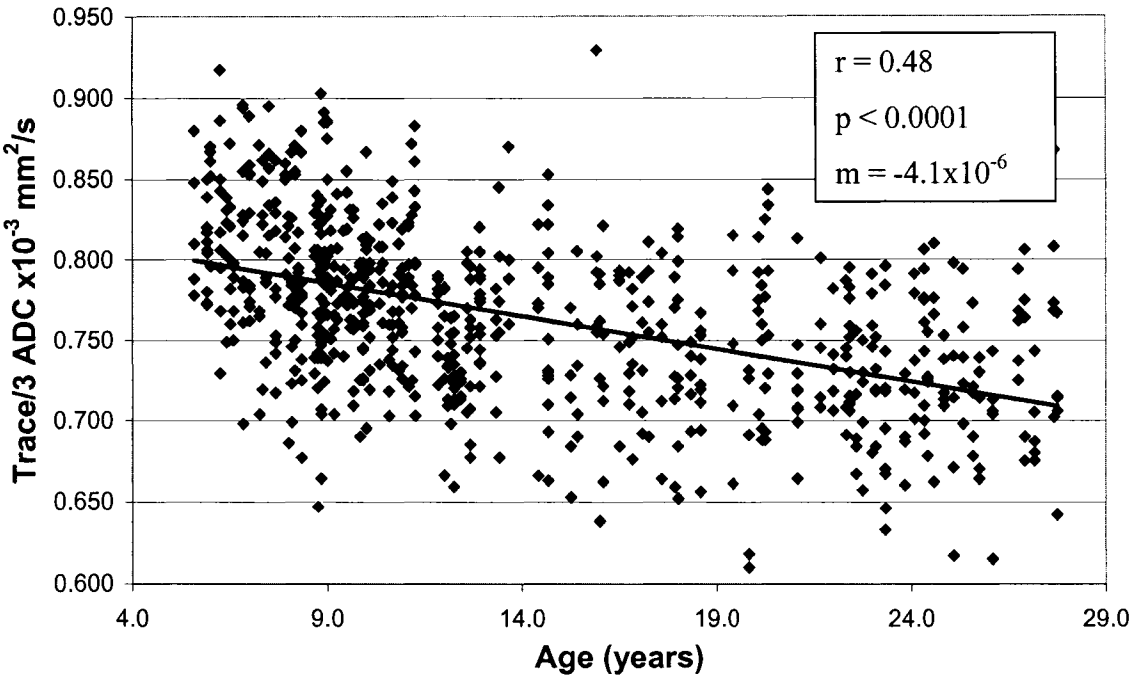

Figure 4.3h – Trace/3 ADC trends for the subcortical white matter in the gyri (superior frontal gyrus, right supra marginal gyrus, right middle occipital gyrus, left superior temporal gyrus and the left postcentral gyrus).

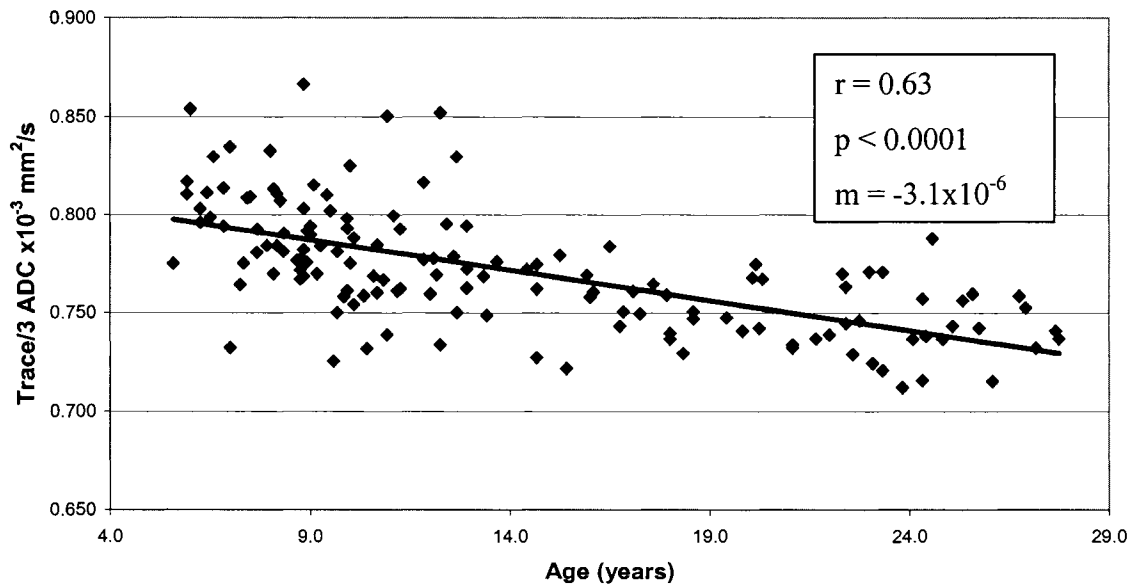

Figure 4.3i – Trace/3 ADC trends for the thalamus.

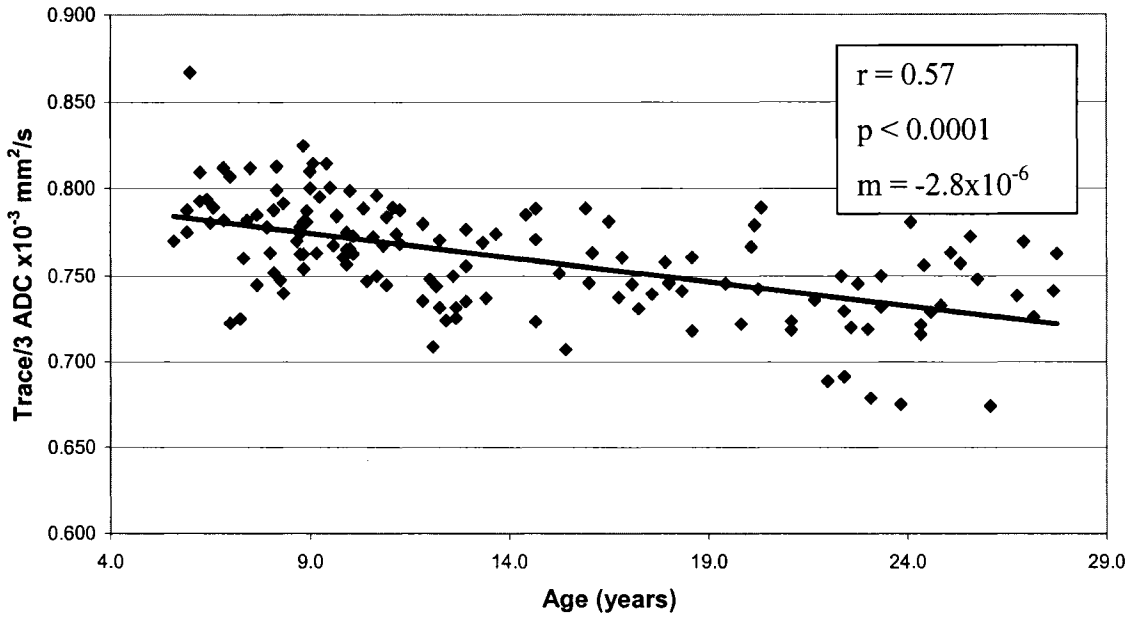

Figure 4.3j – Trace/3 ADC trends for the globus pallidus.

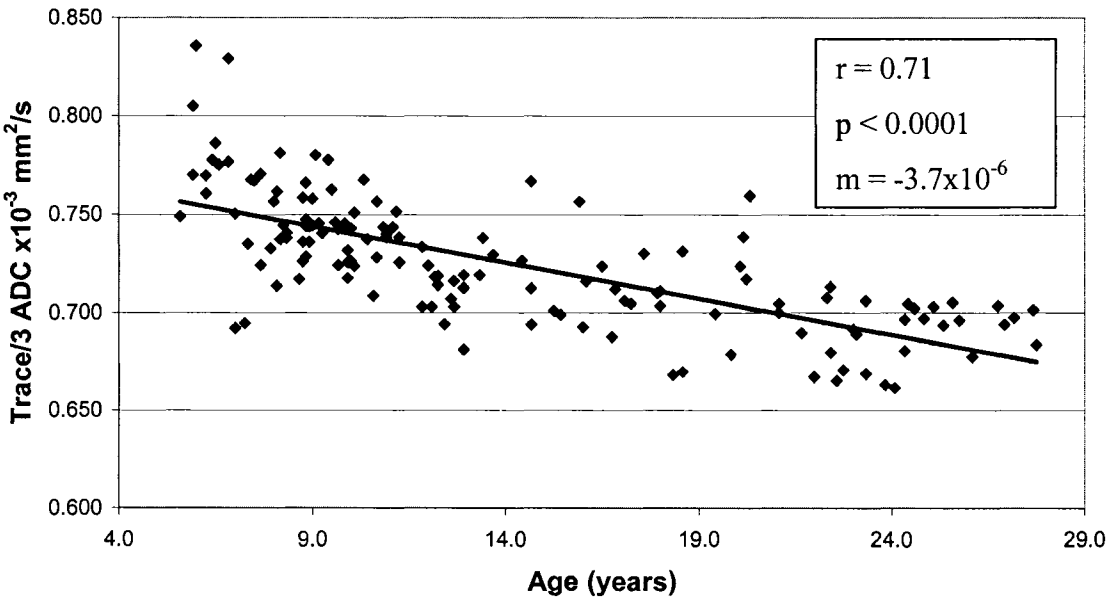

Figure 4.3k – Trace/3 ADC trends for the putamen.

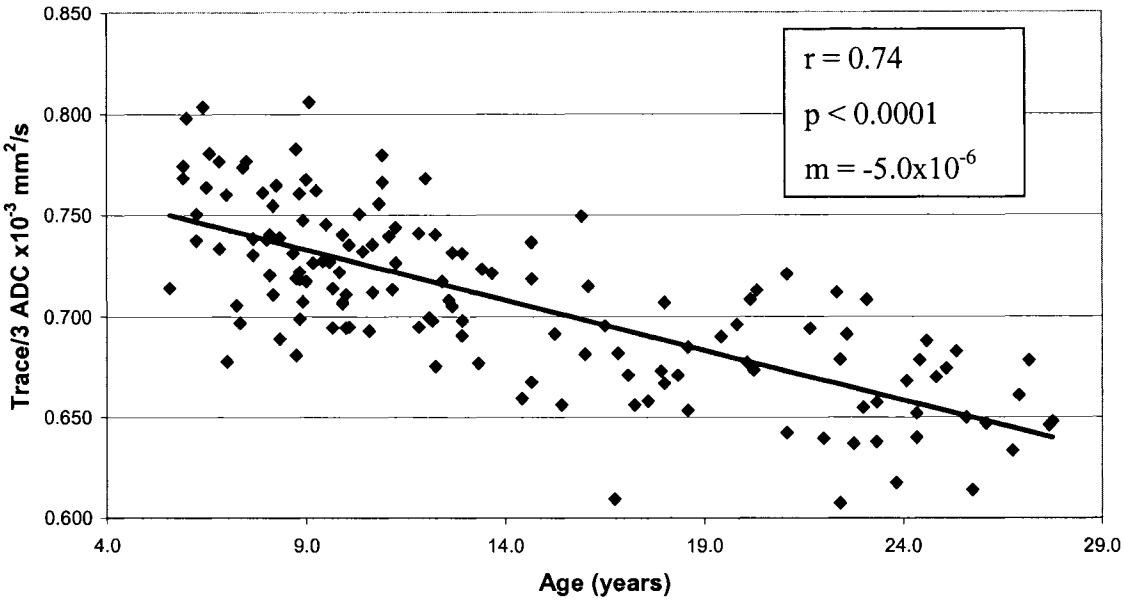

Figure 4.3l – Trace/3 ADC trends for the caudate nucleus.

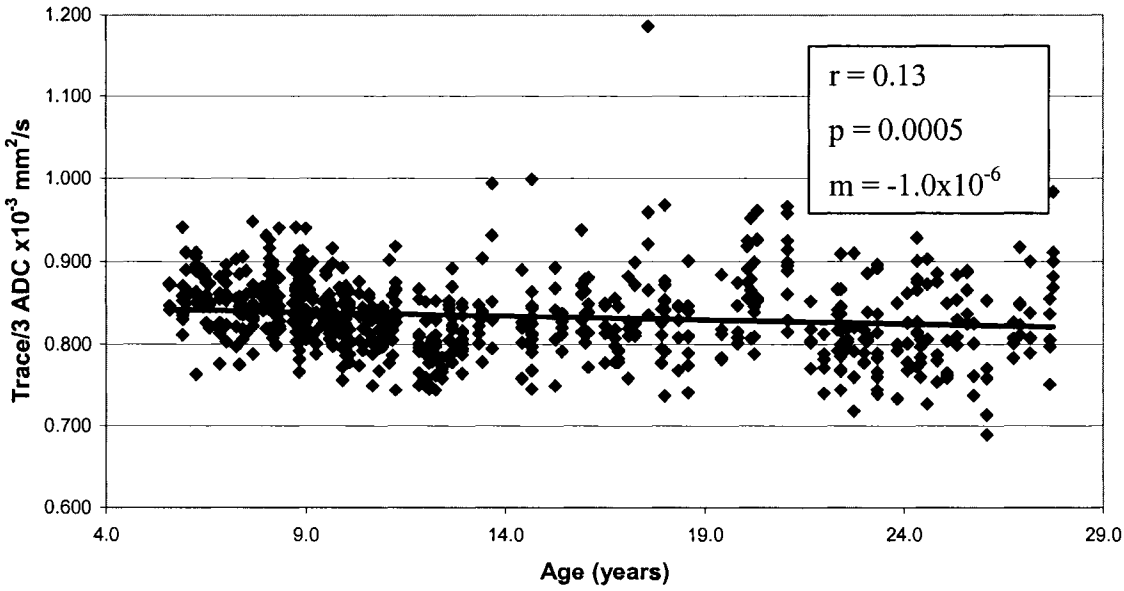

Figure 4.3m – Trace/3 ADC trends for the cortical gray matter surrounding 5 gyri (superior frontal gyrus, right supra marginal gyrus, right middle occipital gyrus, left superior temporal gyrus and the left postcentral gyrus).

4.3.2 – Fractional Anisotropy

Fractional anisotropy shows more complex trends with age than does Trace/3 ADC. All structures were fitted for natural logarithmic and linear regression lines. A lower p value determined which trend was more statistically significant. In the case of the same p value, a higher r value was used to determine which trend was more significant. The majority of structures appear logarithmic in nature (Table 4.1). Plots are shown in Figure 4.4.

Table 4.1 – Logarithmic and Linear Trends of FA with Age (5 – 27 years)[12]

Region	Linear			Logarithmic	
	slope	r	p	r	p
White Matter					
genu of corpus callosum*	0.002	0.29	0.0006	0.27	0.001
splenium of corpus callosum*	0.002	0.40	<0.0001	0.38	<0.0001
anterior limb of internal capsule#	0.003	0.30	0.0003	0.36	<0.0001
posterior limb of internal capsule#	0.002	0.31	0.0002	0.31	0.0001
external capsule#	0.003	0.50	<0.0001	0.53	<0.0001
corona radiata*	0.002	0.31	0.0002	0.27	0.001
centrum semiovale	---	0.02	0.81	0.03	0.69
subcortical WM of gyri#	0.003	0.32	<0.0001	0.35	<0.0001
Gray Matter					
thalamus#	0.003	0.57	<0.0001	0.61	<0.0001
globus pallidus#	0.004	0.58	<0.0001	0.62	<0.0001
putamen#	0.002	0.44	<0.0001	0.46	<0.0001
caudate nucleus#	0.003	0.47	<0.0001	0.48	<0.0001
cortical GM	0.001	0.18	<0.0001	0.22	<0.0001

[12] While the plot may be suggestive of either a logarithmic or a linear curve, our data is not good enough to differentiate between linear or logarithmic trends.

* more closely fits a linear trend, # more closely fits a logarithmic trend

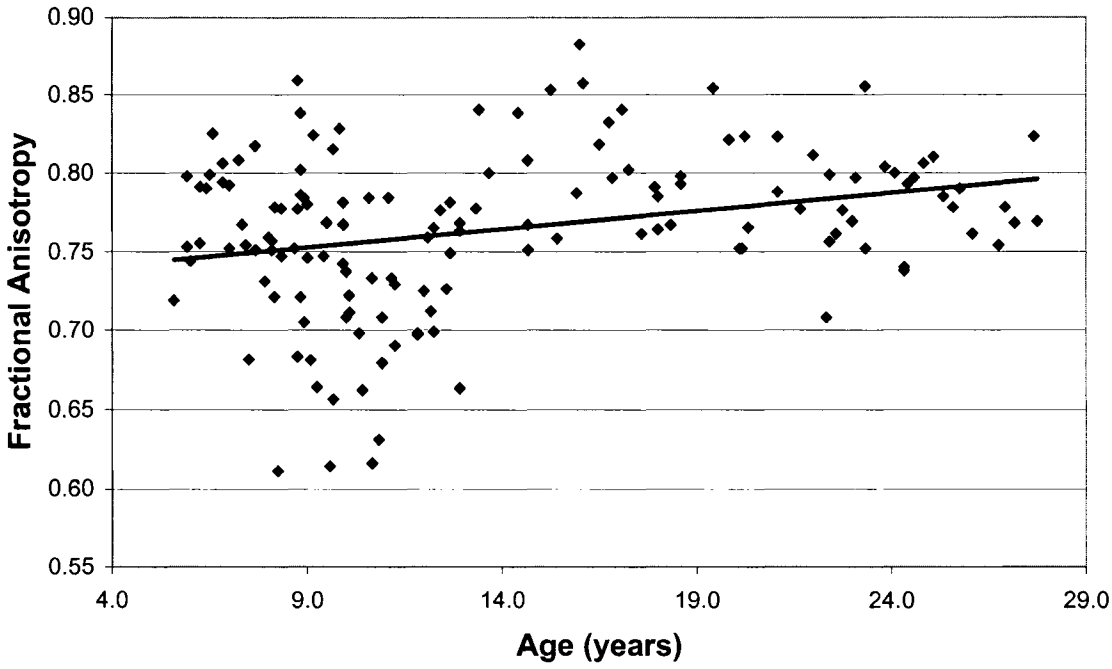

Figure 4.4a – FA trends for the genu of the corpus callosum.

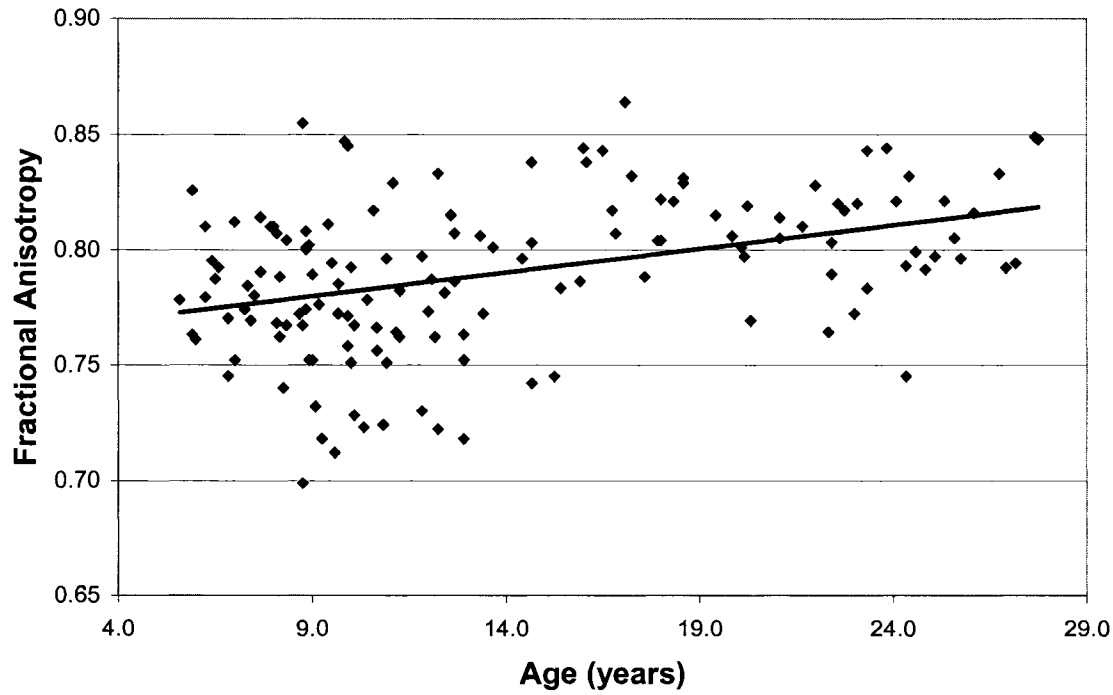

Figure 4.4b – FA trends for the splenium of the corpus callosum.

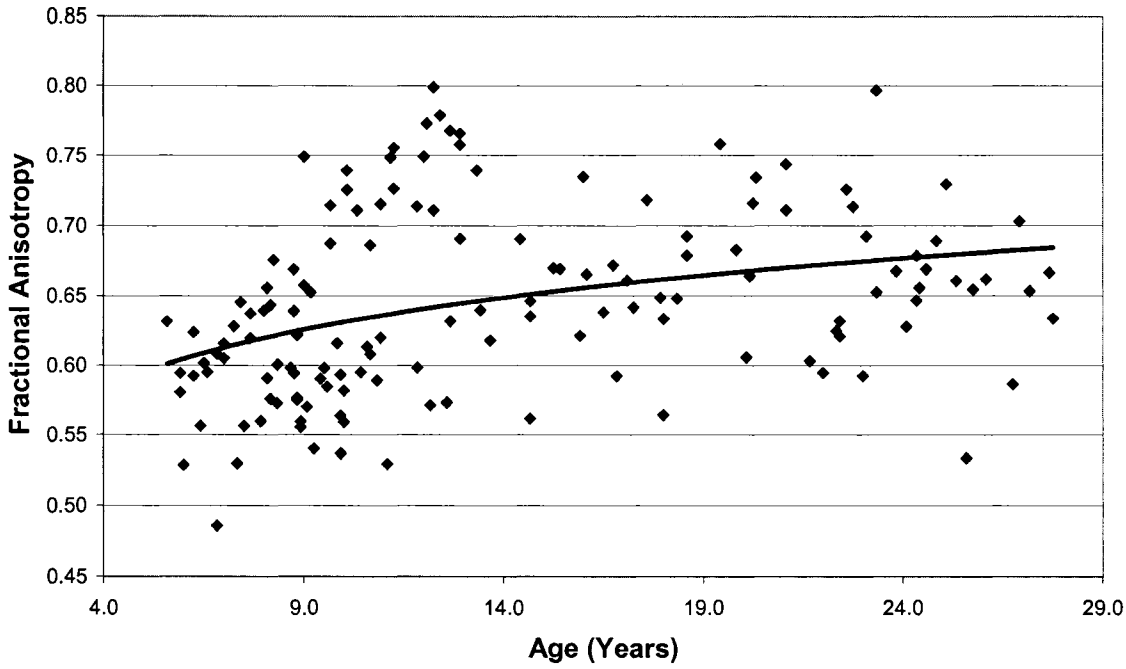

Figure 4.4c – FA trends for the anterior limb of the internal capsule.

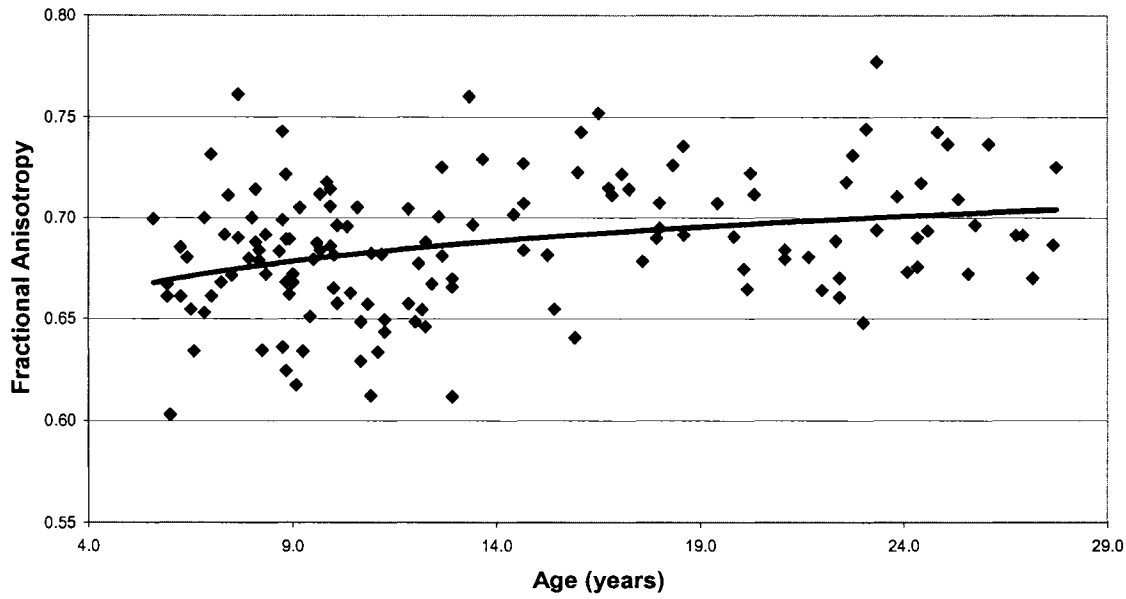

Figure 4.4d – FA trends for the posterior limb of the internal capsule.

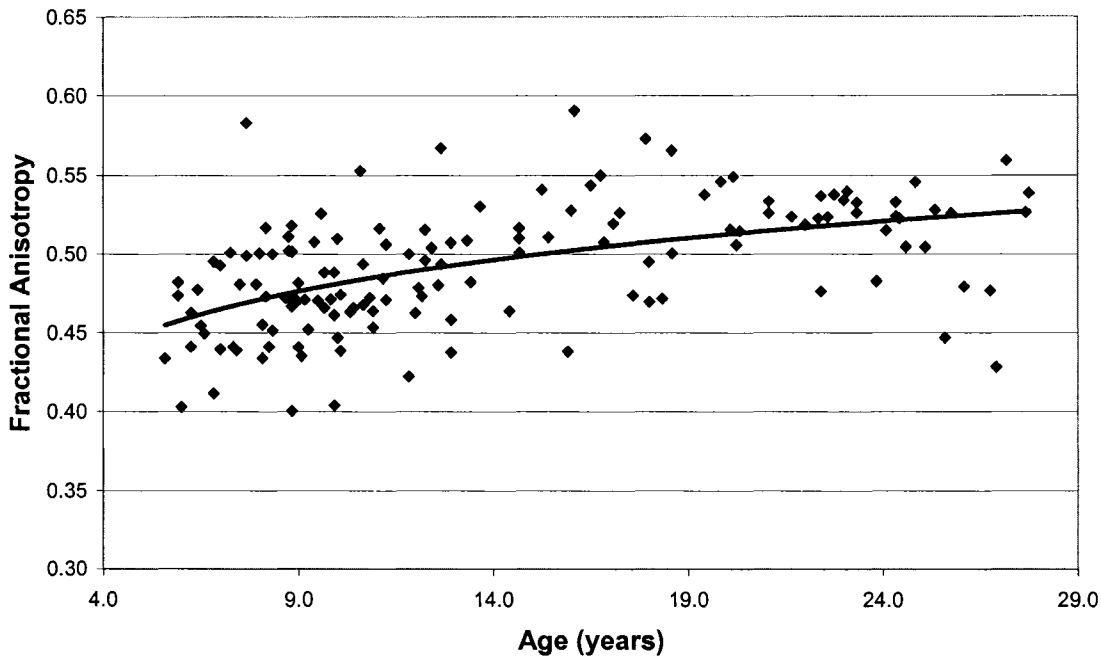

Figure 4.4e – FA trends for the external capsule.

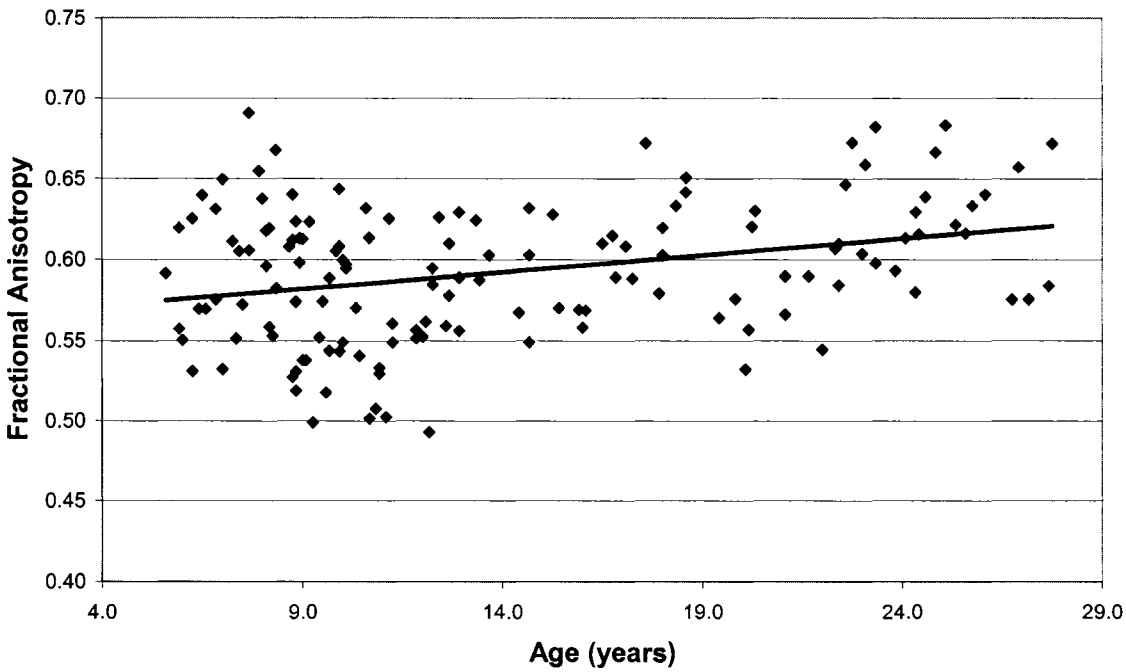

Figure 4.4f – FA trends for the corona radiata.

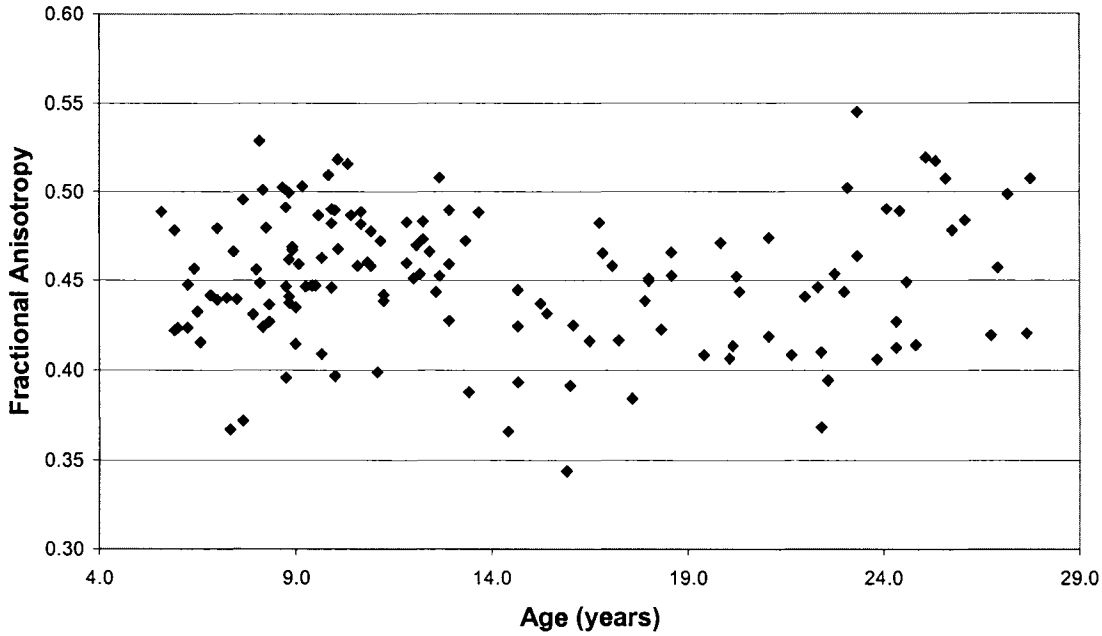

Figure 4.4g – FA trends for the centrum semiovale. Note that there is no increase of FA for this structure.

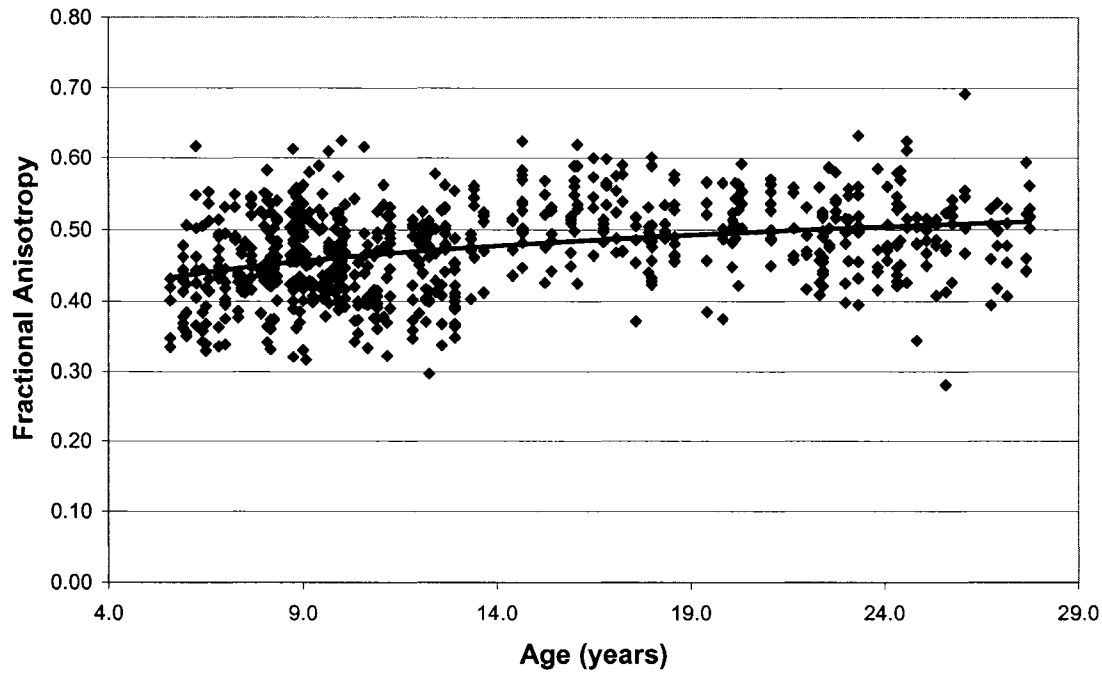

Figure 4.4h – FA trends for the subcortical white matter of the gyri (superior frontal gyrus, right supra marginal gyrus, right middle occipital gyrus, left superior temporal gyrus and the left postcentral gyrus).

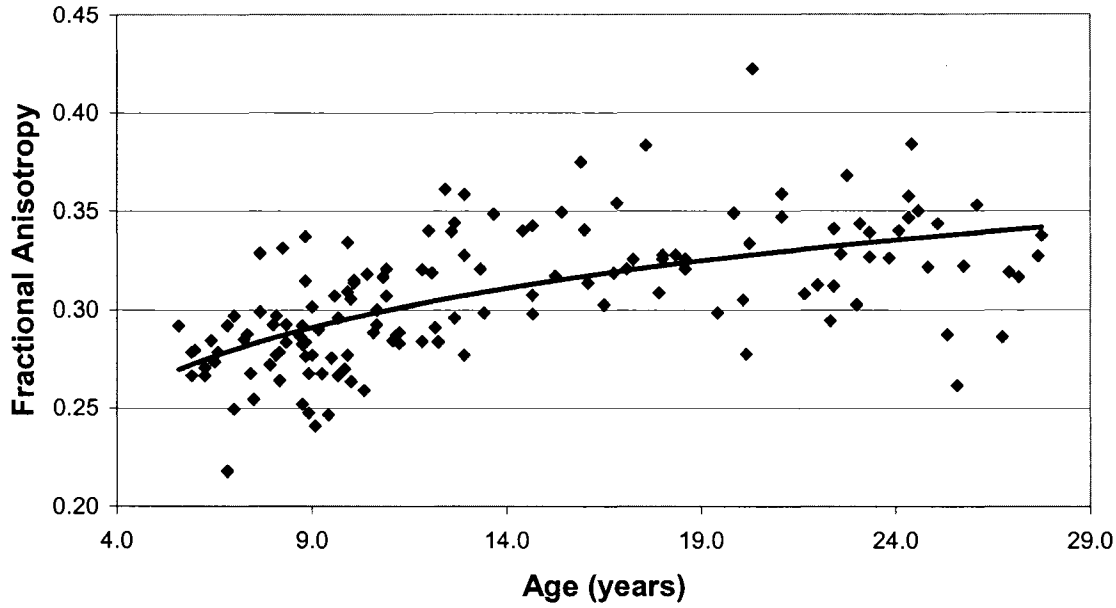

Figure 4.4i – FA trends for the thalamus.

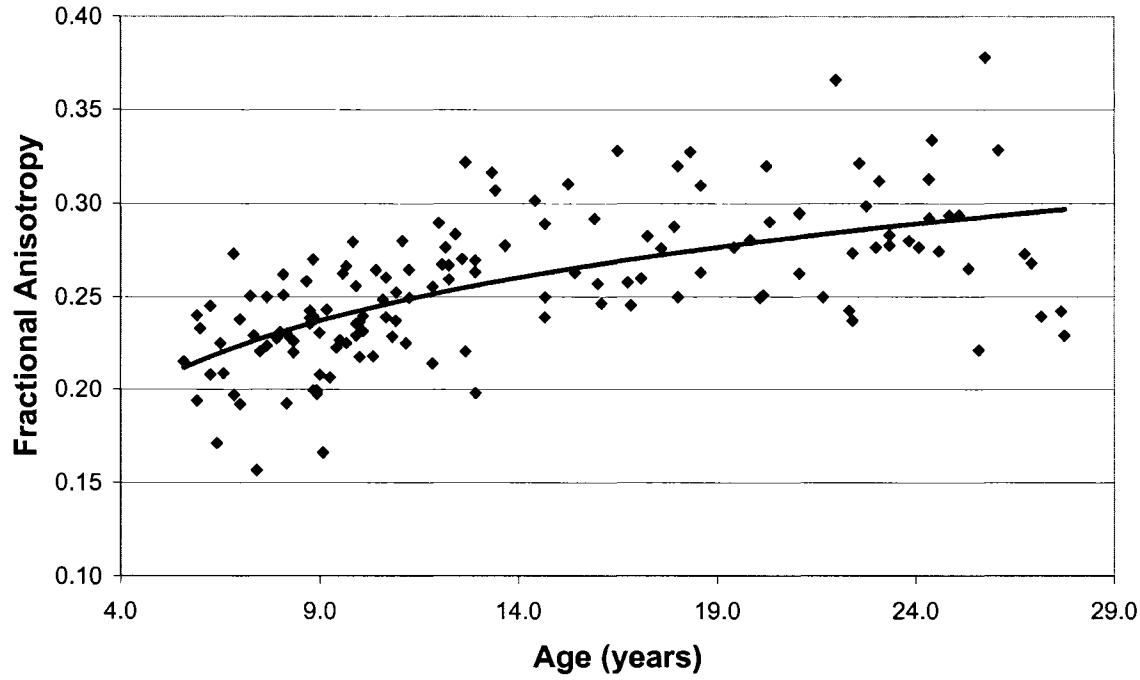

Figure 4.4j – FA trends for the globus pallidus.

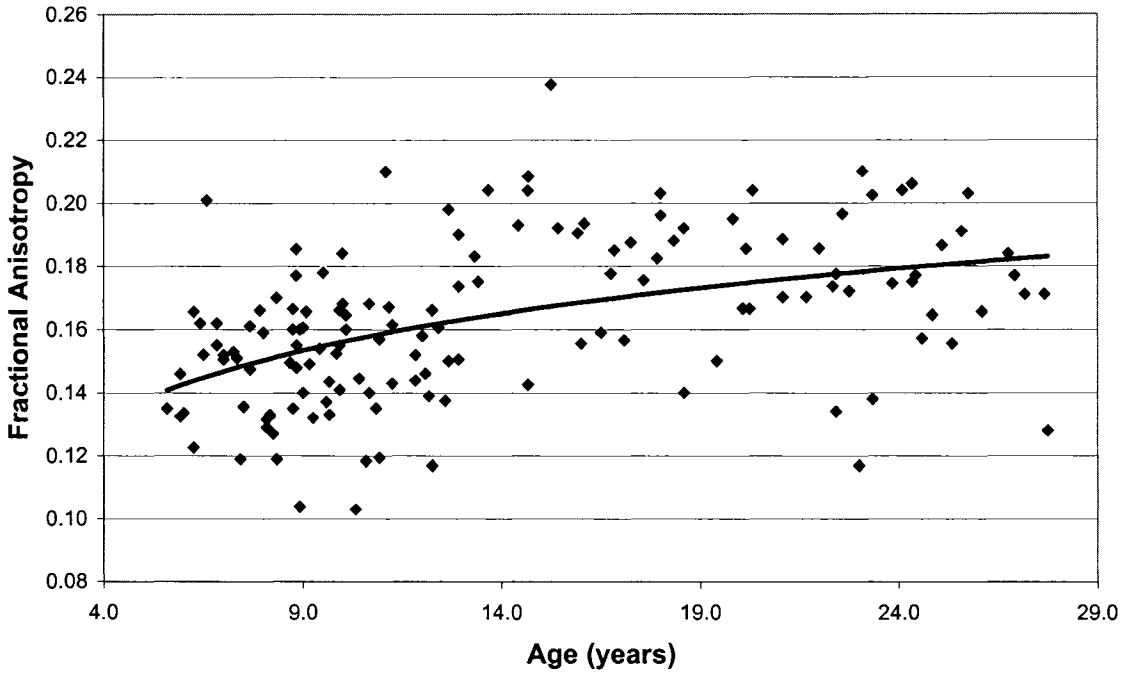

Figure 4.4k – FA trends for the putamen.

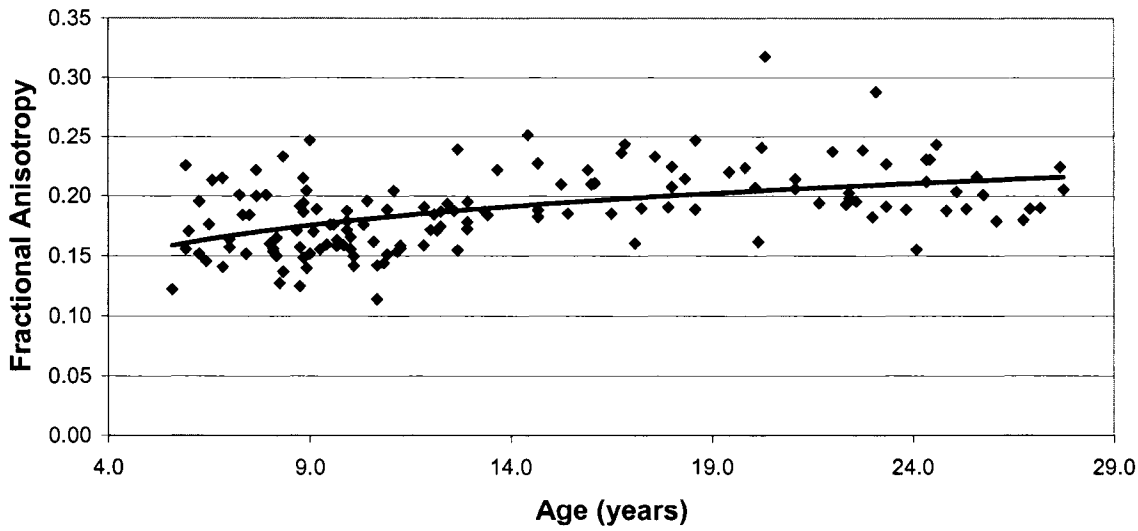

Figure 4.4l – FA trends for the caudate nucleus.

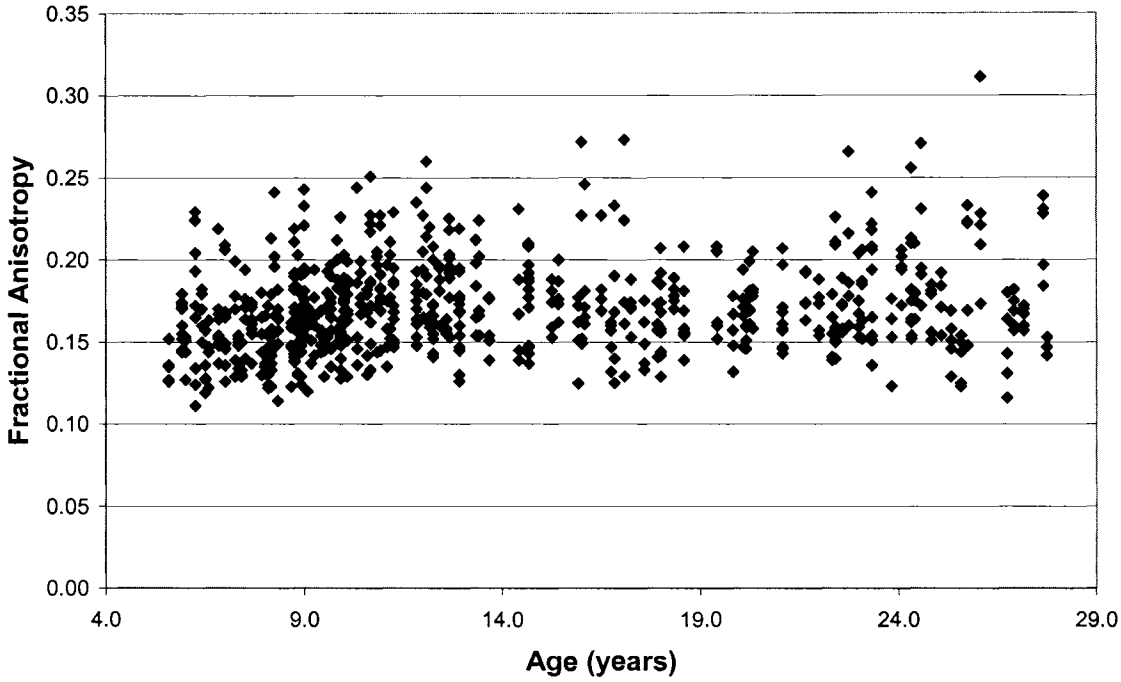

Figure 4.4m – FA trends for the cortical gray matter surrounding the gyri (superior frontal gyrus, right supra marginal gyrus, right middle occipital gyrus, left superior temporal gyrus and the left postcentral gyrus).

4.3.3 – Gender Differences

Female and male FA and Trace/3 ADC were compared visually, by plotting the male and female data sets on one graph, and drawing trend lines for both sets independently (linear trend lines for Trace/3 ADC, and linear or logarithmic, as determined in Table 4.1 for FA). The trend lines were nearly perfectly aligned in Trace/3 ADC for all 13 structures (plots not shown). For FA, however, there were some marked differences.

Three white matter regions showed obvious gender differences for FA (i.e. separation between regression lines): the anterior limb of the internal capsule, the posterior limb of the internal capsule and the corona radiata. The gray matter regions did not have perfectly overlapping trend lines; however, the differences were not as marked as the plots shown (Figure 4.5). Perhaps with the inclusion of all subjects, gender differences, if any, will become clearer.

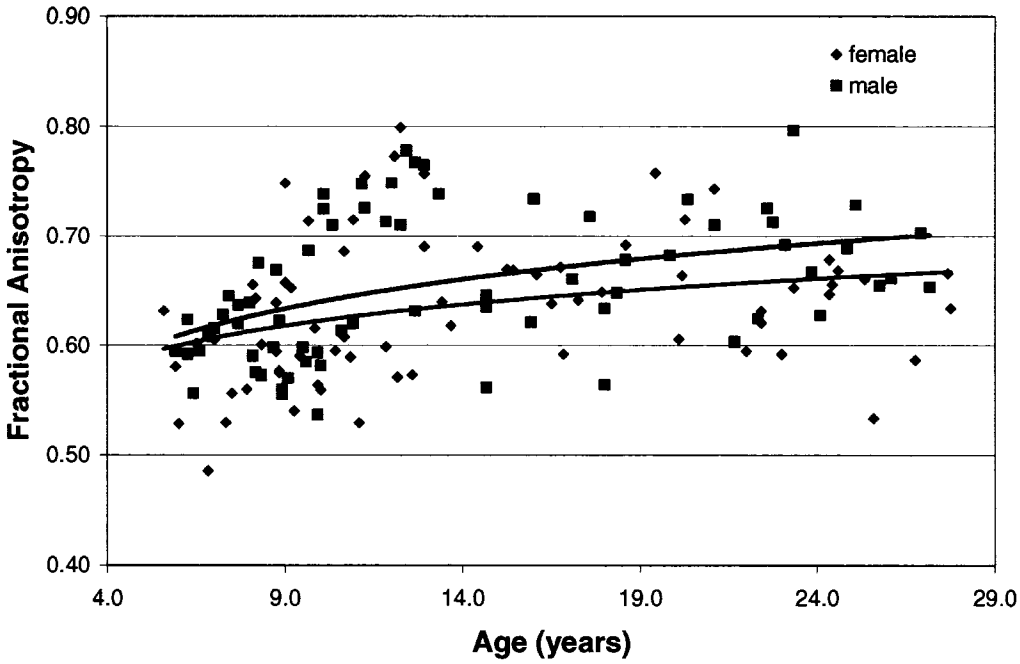

Figure 4.5a – Male and female trends for the anterior limb of the internal capsule, with separate logarithmic trend lines.

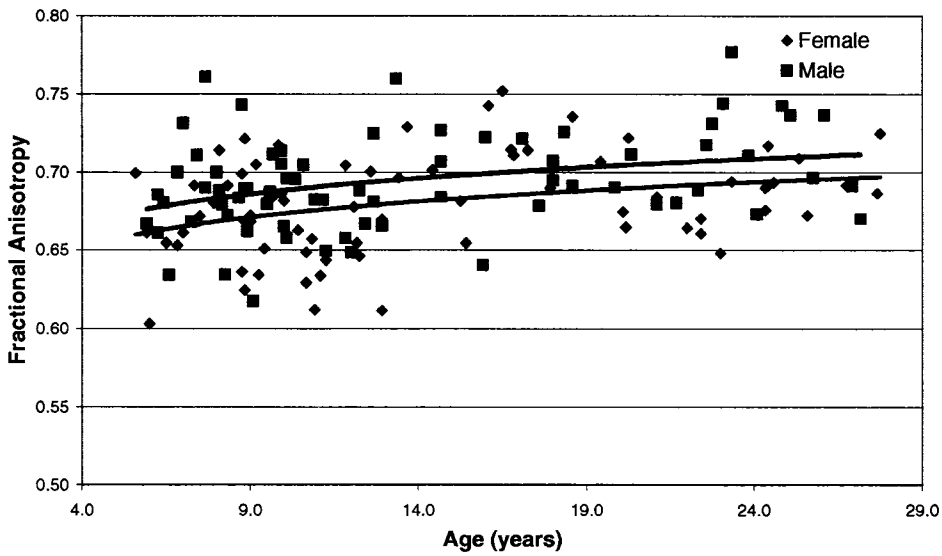

Figure 4.5b – Male and female trends for the posterior limb of the internal capsule, with separate logarithmic trend lines.

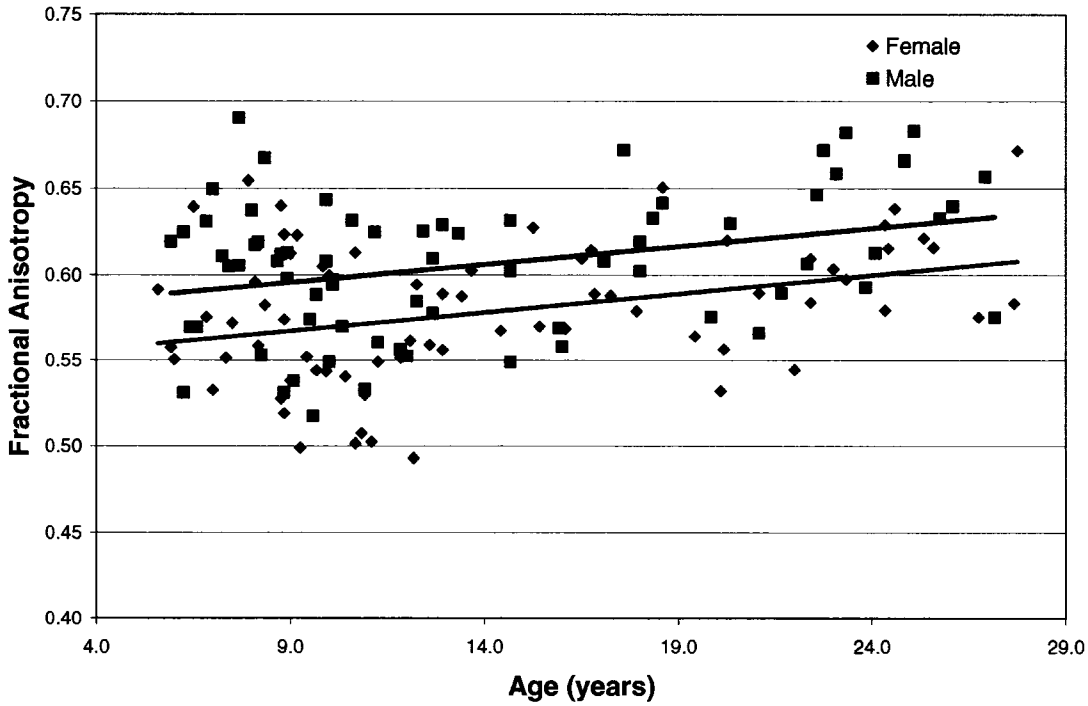

Figure 4.5c – Female and male trends for the corona radiata, with separate linear trend lines.

4.4 – Discussion

4.4.1 – Signal-to-Noise in the Brain with Age

One concern with using such a large age range of subjects is potential systematic variations in the signal to noise ratio (SNR). This is because it has been shown that for lower values of SNR, the eigenvalues quickly diverge from their "true" values (Pierpaoli and Basser, 1996). This is especially true of SNR < 20 (Bastin et al., 1998). At low values of SNR, λ_1 is higher than expected and λ_3 is lower than expected, causing an over-estimation of FA. However, since we are dealing with SNR values much greater than 20, we can be quite confident in our measurements of FA and Trace/3 ADC with age.

SNR was measured on the b0 images, by taking an average signal of gray and white matter from approximately ¼ of the brain, in the posterior left portion of the image, on a central slice. No CSF was sampled. This average signal is divided by the standard deviation of

the noise. Note that the noise is measured such as to avoid any areas of ghosting along the phase encode direction. Younger brains tend to show higher SNR (Figure 4.6). Over 5 – 27 years, SNR shows a power function decrease (SNR α age (years)$^{-0.16}$, r = 0.71).

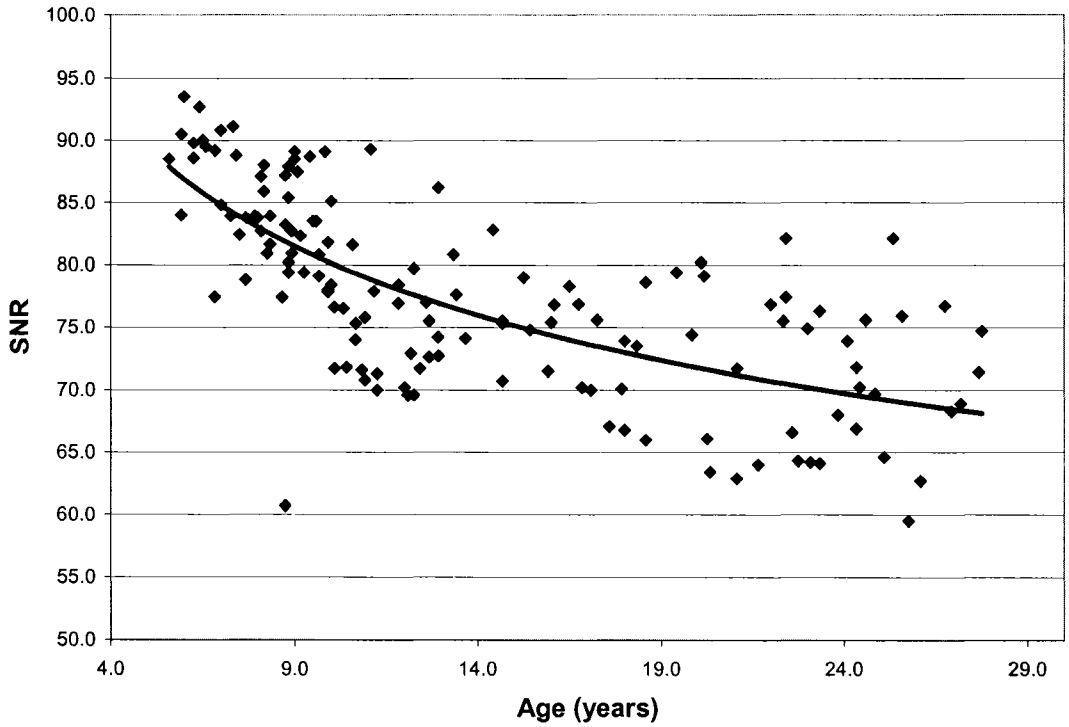

Figure 4.6 – SNR decreases with age.

There are a few potential reasons for this variation of SNR with age. Transverse relaxation time (T2) shortens with age (Kreis et al., 1993) which potentially would cause lower signal at older ages. However, by the age of 5 years, T2 has reached close to adult values (for example, using the bi-exponential fitting values of Ding, et al, T2 = 113 ms at 5 years, and 109 ms at 20 years), and would not account for the degree of change we are seeing (Ding et al., 2004). Another possibility is the fact that the water content of the brain decreases by 14 – 18% between birth and young adulthood (Mukherjee et al., 2001). This has been shown by MR Spectroscopy (Kreis et al., 1993), as well as by a decrease in proton density signal intensity (Autti et al., 1994). Again, this would decrease the total amount of signal available from the older brains. Any additional SNR differences, not accounted for by

proton density differences can be attributed to the difference in noise created by the varied volume exposed to the RF coil due to the systematic variation in size from 5 years to 27 years.

4.4.2 – Analysis Methods

More sophisticated statistical analysis techniques are required to determine a true fit to our data. From this, we hope to be able to determine at what age we see the greatest increases of FA (i.e. at what point the slope is the greatest). Potentially, SPM analysis of FA could be performed on this entire age range although a linear correlation analysis is likely to underestimate the changes, due to the observed non-linearity of the data.

4.5 – Conclusions

With the group results of Chapters 2 and 3, we hypothesized that Trace/3 ADC would decrease and FA would increase over the teenage years, however, the time course of their changes with brain development is not known. Our preliminary results show that Trace/3 ADC continues to decrease linearly with age until the mid- to late 20s. However, FA shows much more complicated mathematical trends. The true nature of these trends will not be completely elucidated until all 196 (or greater) subjects have been analyzed. This will fill in the sparse data in the middle teenage years, and make clear what is happening in those formative years.

Chapter 5 ♦ Diffusion Tensor Imaging and Neurodevelopment – Implications for the Future

5.1 – Comments on Neurodevelopment

5.1.1 – Postmortem studies

Early post-mortem neurodevelopment studies show continued myelination into adulthood (Yakovlev and Lecours, 1967; Benes et al., 1994). In this study we have confirmed these findings using diffusion tensor imaging between the ages of 5 – 27 years. Increases of FA with age were seen in the corpus callosum, many association fibres such the inferior longitudinal fasciculus, and the thalamus. Increases of FA were also seen in the fornix and possibly the cingulum. Yakovlev and Lecours saw continued myelination in these areas as well, with the exception of the fornix, where they were unclear as to when the development of the fornix completed (Yakovlev and Lecours, 1967). We saw increases throughout the brain stem and cerebellum, which could correspond to the reticular formation. The reticular formation is composed of tiny structures of the brain stem, specifically in the medulla, pons and midbrain and their respective connections, which is known to be highly organized. The medullary and pontine areas send fibres down the spinal cord to motor neurons, including the motor control of breathing. The midbrain sends fibres up into the cerebral hemispheres and while not much is known about their function, they are known to control consciousness. Injury to this area results in a coma (Lindsley and Holmes, 1984). Therefore, it is likely that the developing white matter tracts we are detecting in the brain stem are likely the connections of the highly organized reticular formation.

5.1.2 – DTI Studies

Quite a few DTI studies have been done on the subject of neurodevelopment. Each study comes to the same general conclusions that mean diffusivity decreases with development, and that anisotropy increases with development. However, the specific regional results seem to vary based on the age range of the subjects studied, the number of subjects and the

analysis method employed. When using an ROI based analysis, we are limited by the number of regions measured, and when using a voxel based analysis technique we are limited by the ability to properly normalize the images to a common stereotactic space. While each study may give a different answer as to what parts of the brain are developing, each study on its own is not the entire story (Table 5.1). Perhaps each study offers complementary information about the normal development of the brain. Recurring structures are the corticospinal tracts, internal capsule, and frontal white matter. However, the specifics of each study are slightly different. All these DTI studies see more regions than previous T1- weighted studies (Paus et al., 1999) who reported that only the posterior limb of the internal capsule and the left arcuate fasciculus changes over 4 – 17 years (N=111). Our results do agree in general with previous studies. However, we have found a much larger number of structures showing increases in anisotropy with age.

Table 5.1 – Summary of DTI Studies of the Developing Brain

Study	Ages	Analysis	Regions of Anisotropy Changes
Klingberg et al., 1999	8-12 & 20-31 yrs	VOI[13]	frontal white matter
Mukherjee et al., 2001	1 day – 11 years	ROI	corpus callosum, internal capsule, basal ganglia, thalamus
Schmithorst et al., 2002	5 – 18 years	SPM	internal capsule, corticospinal tract, arcuate fasciculus (L), inferior longitudinal fasciculus (R)
Suzuki et al., 2003	1-10 & 18-34 yrs	ROI	parietal white matter, frontal white matter
Schneider et al., 2004	1 day – 16 years	ROI	pons, crus, centrum semiovale, subcortical white matter
Barnea-Goraly et al., 2005	6 – 19 years	SPM	arcuate fasciculus, motor areas, internal capsule, prefrontal regions, corpus callosum, basal ganglia, thalamocortical connections, ventral-visual pathways
Snook et al., 2005	8-12 & 21-27 yrs	ROI	corpus callosum, internal capsule, external capsule, corona radiata, cortical white matter, thalamus, basal ganglia
Chapter 3 – To be published	8-12 & 21-27 yrs	SPM	cerebellum, brain stem, frontal white matter, inferior longitudinal fasciculus, inferior fronto-occipital fasciculus, internal capsule, external capsule, corpus callosum, cingulum, superior fronto-occipital fasciculus, superior longitudinal fasciculus, corona radiata

[13] Volume of interest, defined on T1-weighted images

5.2 – Implications for Cognition

While it is well know that the largest neurodevelopment changes occur in the first four years of life, the continued development of various regions of the brain has several implications for behavioural and cognitive development.

5.2.1 – Motor Development

SPM analysis showed continued development of the cerebellum, brainstem, internal capsule, external capsule, corona radiata, and centrum semiovale. The combined development of these tracts suggests that the corticospinal tracts are developing through the teenage years, as they are all projection fibres leading out of the brain stem. Also, ROI analysis showed continued development of the basal ganglia (globus pallidus, putamen and caudate) which are thought to be motor in function (Lindsley and Holmes, 1984). Anyone who has spent a substantial amount of time with teenagers would not find this surprising. From the age of 5 years, motor coordination improves in leaps and bounds. As a child, it is learning fine motor skills, such as holding a pencil and learning proper handwriting. In teenagers, the brain needs to deal with large growth spurts, essentially needing to recalculate the body's center of gravity, until we finally hit young adulthood, and motor coordination seems to be fairly stable.

5.2.2 – Learning and Memory

Several of our findings implicate those parts of the brain that are in charge of memory and learning. The limbic system is well known to be involved in these processes. As well, the long association fibres, the superior longitudinal fasciculus and the associated arcuate fasciculus, are thought to connect Wernicke's and Broca's language areas of the brain (Dronkers and Baldo, 2001). This implies that childhood and adolescence are the ideal time for education.

Interestingly, the development of the corpus callosum early in life (generally in the second year) is thought to contribute to one's ability to read and write. This is suggested due to the fact that the language areas are thought to be on the left side of the brain and the perception areas on the right side of the brain. Thus, to be able to put words and meanings together, we must have a good integration of left and right brain (Kagan and Baird, 2004). This integration is entirely provided by the left-right connections of the corpus callosum. One could see that this would be important for more than just reading and language, but for all aspects of learning. Thus, the continued development of the corpus callosum through adolescence is logical. It allows for better integration of the different learning and perception centers of the brain.

5.2.3 – Discussion

The biggest jumps in development occur in the early years of childhood (as do the largest changes of FA and Trace/3 ADC (Schneider et al., 2004)), however; there is continued white matter development into adolescence (Barnea-Goraly et al., 2005) and even young adulthood (Snook et al., 2005), as evidenced by DTI. This continued brain development is also known to occur in cortical gray matter (Sowell et al., 2004). There are several logical reasons for brain development during adolescence, mainly a refinement of the cortical connections as we become more specialized, and hormonal releases that are known to occur during puberty. It has been well documented that the adolescent years are a time of cortical pruning; a process thought to increase brain functionality by eliminating irrelevant connections. As well, it is a time of great change in both hormone and neurotransmitter levels in the brain (Walker and Bollini, 2002). While we may expect the biggest changes to be occurring very early in life, these post-pubertal physiological changes match up well with neuroimaging studies.

5.3 – Future Work

Our lab is currently undertaking several projects involving DTI, including advanced analysis techniques, as well as comparative clinical studies, using the 196 subjects of this body of work as the healthy controls.

5.3.1 – Advances in DTI Analysis Techniques

Several advances in DTI analysis techniques are currently emerging. Mainly, these are ways to automate the current analysis techniques. While ROI analysis is a tried and true method, it has some limitations, mainly in the amount of time one needs to dedicate to manually drawing each region.

5.3.1.1 – Atlas Based Region of Interest Analysis

This technique of ROI analysis is almost fully automated. A brain atlas is created by imaging a brain several times and then averaging the images to create a template. Alternatively, an atlas could be created from an average of the subjects of the study itself, creating a template brain based on the subjects to be analyzed. Each of the subject brains is normalized to this template brain, creating a unique transformation matrix for each individual subject. An ROI is then drawn on the atlas. The transformation matrix is applied for each subject, respectively, transforming the ROI back to the native imaging space for each subject. The advantages of this method are clear: if there are 200 subjects in a study, and a minimum of 30 ROIs to be drawn per subject, that means 6,000 ROIs, but with the atlas based method, only 30 ROIs need to be drawn. With this method, ROIs will often span two or more slices, depending on the orientation of the raw DTI images. Therefore, it is not equivalent to a standard ROI analysis. However, this can be an advantage because most native images are not going to be aligned in exactly the same way from one subject to the next. In these cases, with a standard ROI technique, the portion of the structure to be sampled may not be the same from one subject to the next.

Similar methods have been applied to PET imaging (Ohyama et al., 2000), in a 3D volumetric MRI analysis (Mega et al., 2005) in the assessment of dementia.

5.3.1.2 – Tractography Based ROIs

A recent extension to DTI is diffusion tractography (Jones et al., 1999; Mori et al., 1999; Conturo et al., 1999; Basser et al., 2000). By following the direction of fastest diffusion (generally, the eigenvector associated with λ_1), and assuming that water will preferentially diffuse in a direction parallel to white matter fibres, the white matter tracts can be reconstructed and visualized 3 dimensionally. This method offers a big advantage over 2 dimensional methods. If we take, for example, the cingulum and try to draw an ROI on a 2D FA image, it will be indistinguishable from the body of the corpus callosum (although it will appear green on a 2D colour map, allowing for easier identification (Hermoye et al., 2006)). However, based on our knowledge of basic neuroanatomy, we can place a seed point so that we can follow the cingulum (which runs anterior posterior) instead of the corpus callosum (which runs left-right). Thus smaller structures, and structures that are hard to identify on 2D images are easily drawn with tractography (Figure 5.1).

Figure 5.1 – Fibre tracking of the cingulum of a 7 year old male subject, shown on the central slice of a normalized FA map.

ROIs can then be defined along a tract, and multiple ROIs can be drawn in one tract to show regional changes within one structure. A recent study on newborns has shown that not only is this possible, but that it provides much improved reproducibility than a manual, 2D ROI method (Partridge et al., 2005).

5.3.2 – Normative Database for Comparison to Disorders Affecting Brain Connectivity

With nearly 200 subjects, over the ages of 5 – 27 years, we have a small gold mine of normative data. Because of DTI's ability to probe the microstructure of the brain's white matter, it is the most logical current method of studying many white matter related diseases and disorders. Our data set can be used as a control group for many of these disorders.

5.3.2.1 – Dyslexia and other Literacy Based Disorders

It has long been known that there is a neurologic basis to language. Over a century ago, Broca discovered lesions in the inferior part of the frontal lobe in a patient with a severe speech disorder (Dronkers and Baldo, 2001). This area of the cortex is now known as Broca's area. Thus, it is believed that language is produced in both Broca's area and in another part of the cortex named Wernicke's area. Therefore, it is logical to assume that there is a connection (white matter fibre tract) between these areas that is important for the proper development of literacy. In fact, a subset of our subjects (8 – 12 years, N=32) has been used for a reading study (Beaulieu et al., 2005) in which reading ability as measured by the Word Identification (Word ID) subtest of the Woodcock Reading Mastery Test-Revised (WRMT-R, American Guidance Service) is correlated with FA using SPM. This study found a region of significant correlation in the left temporo-parietal white matter. These results are in agreement with the results of 2 other studies of dyslexia, one in adults (N=6 poor readers, with 11 controls) (Klingberg et al., 2000) and the other in 7 – 13 year old children (N=14) (Deutsch et al., 2005). We are currently analyzing another subset of

our subjects (5 – 8 years, N = 48) who have had both DTI scans and cognitive assessments to see if the correlative results can be confirmed in even younger children.

5.3.2.2 – Prader-Willi Syndrome

Prader-Willi Syndrome (PWS) is a genetic disorder that involves a deletion of a band of the paternal chromosome 15 (and occasionally a maternal uniparental disomy of this region). It is characterized by hypotonia, polyphagia, obesity, hypogonadism, mental retardation and characteristic facial features, as well as an insatiable appetite. Abnormalities of the central nervous system, including poor myelination have been reported in neuropathologic investigations of humans with PWS (Hayashi et al., 1992). A recent study of PWS observed anatomical defects including irregular projections of axons, and dystrophic axons in prenatal mice (Pagliardini et al., 2005). Evidence of these defects of myelination in an animal model makes PWS of particular interest for a DTI study.

While a few MRI studies have been performed on patients with PWS with various findings such as enlarged ventricles, cortical atrophy, small brain stem and small pituitary glands (Miller et al., 1996; Hashimoto et al., 1998; Yoshii et al., 2002; Shapira et al., 2005), only one abstract has been presented using DTI to study PWS. With selective ROIs they found significantly reduced FA in the posterior limb of the internal capsule and the splenium of the corpus callosum of PWS subjects compared to age matched controls (Yamada et al., 2005), indicating that DTI is a tool capable of detecting the developmental differences of white matter between controls and PWS patients.

At the NMR Facility at the University of Alberta, we have scanned 11 PWS subjects (7 – 41 years) who will be gender and age matched to controls from our normative database of DTI data.

5.4 – Concluding Remarks

Diffusion tensor magnetic resonance imaging is a very powerful tool, which has many possible uses in medical research. It is a powerful tool for determining the time course of white matter development beyond the early developmental years, but into adolescence and even young adulthood. By truly understanding the course of normal development, we can hope to better understand abnormal development caused by various diseases and disorders. Above and beyond the suggestions made here, DTI could be useful in the study of autism, fetal alcohol spectrum disorder, Tourette's syndrome, and stuttering. There is so much about the brain that we do not know. Being able to elucidate information about the vital connections between brain areas, and how they malfunction in certain diseases and disorders can teach us so much about what is happening in our own brains. It can lead not only to a better understanding of how our brains function and develop, but can also lead to better interventions for cognitive impairments like dyslexia, or clinical treatments for the symptoms of disorders such as Prader-Willi Syndrome.

BIBLIOGRAPHY

Abe, O., Aoki, S., Hayashi, N., Yamada, H., Kunimatsu, A., Mori, H., Yoshikawa, T., Okubo, T. and Ohtomo, K., 2002. Normal aging in the central nervous system: quantitative MR diffusion-tensor analysis. Neurobiol Aging. 23, 433-441.

Aboitiz, F., Scheibel, A. B., Fisher, R. S. and Zaidel, E., 1992. Fiber composition of the human corpus callosum. Brain Res. 598, 143-153.

Ashburner, J. and Friston, K. J., 2000. Voxel-based morphometry--the methods. Neuroimage. 11, 805-821.

Ashburner, J. and Friston, K. J., 2001. Why voxel-based morphometry should be used. Neuroimage. 14, 1238-1243.

Autti, T., Raininko, R., Vanhanen, S. L., Kallio, M. and Santavuori, P., 1994. MRI of the normal brain from early childhood to middle age. II. Age dependence of signal intensity changes on T2-weighted images. Neuroradiology. 36, 649-651.

Barkovich, A. J., 2000. Concepts of myelin and myelination in neuroradiology. AJNR Am J Neuroradiol. 21, 1099-1109.

Barkovich, A. J., Kjos, B. O., Jackson, D. E., Jr. and Norman, D., 1988. Normal maturation of the neonatal and infant brain: MR imaging at 1.5 T. Radiology. 166, 173-180.

Barnea-Goraly, N., Kwon, H., Menon, V., Eliez, S., Lotspeich, L. and Reiss, A. L., 2004. White matter structure in autism: preliminary evidence from diffusion tensor imaging. Biol Psychiatry. 55, 323-326.

Barnea-Goraly, N., Menon, V., Eckert, M., Tamm, L., Bammer, R., Karchemskiy, A., Dant, C. C. and Reiss, A. L., 2005. White matter development during childhood and adolescence: a cross-sectional diffusion tensor imaging study. Cereb Cortex. 15, 1848-1854.

Basser, P. J., 1995. Inferring microstructural features and the physiological state of tissues from diffusion-weighted images. NMR Biomed. 8, 333-344.

Basser, P. J., Mattiello, J. and LeBihan, D., 1994a. Estimation of the effective self-diffusion tensor from the NMR spin echo. J Magn Reson B. 103, 247-254.

Basser, P. J., Mattiello, J. and LeBihan, D., 1994b. MR diffusion tensor spectroscopy and imaging. Biophys J. 66, 259-267.

Basser, P. J., Pajevic, S., Pierpaoli, C., Duda, J. and Aldroubi, A., 2000. In vivo fiber tractography using DT-MRI data. Magn Reson Med. 44, 625-632.

Basser, P. J. and Pierpaoli, C., 1996. Microstructural and physiological features of tissues elucidated by quantitative-diffusion-tensor MRI. J Magn Reson B. 111, 209-219.

Bastin, M. E., Armitage, P. A. and Marshall, I., 1998. A theoretical study of the effect of experimental noise on the measurement of anisotropy in diffusion imaging. Magn Reson Imaging. 16, 773-785.

Beaulieu, C., 2002. The basis of anisotropic water diffusion in the nervous system - a technical review. NMR Biomed. 15, 435-455.

Beaulieu, C., Plewes, C., Paulson, L. A., Roy, D., Snook, L., Concha, L. and Phillips, L., 2005. Imaging brain connectivity in children with diverse reading ability. Neuroimage. 25, 1266-1271.

Behrens, T. E., Johansen-Berg, H., Woolrich, M. W., Smith, S. M., Wheeler-Kingshott, C. A., Boulby, P. A., Barker, G. J., Sillery, E. L., Sheehan, K., Ciccarelli, O., Thompson, A. J., Brady, J. M. and Matthews, P. M., 2003. Non-invasive mapping of connections between human thalamus and cortex using diffusion imaging. Nat Neurosci. 6, 750-757.

Ben Bashat, D., Ben Sira, L., Graif, M., Pianka, P., Hendler, T., Cohen, Y. and Assaf, Y., 2005. Normal white matter development from infancy to adulthood: comparing diffusion tensor and high b value diffusion weighted MR images. J Magn Reson Imaging. 21, 503-511.

Benes, F. M., Turtle, M., Khan, Y. and Farol, P., 1994. Myelination of a key relay zone in the hippocampal formation occurs in the human brain during childhood, adolescence, and adulthood. Arch Gen Psychiatry. 51, 477-484.

Berg, H. C., 1983. Random Walks in Biology. Princeton University Press, Princeton, N.J.

Bhagat, Y. A. and Beaulieu, C., 2004. Diffusion anisotropy in subcortical white matter and cortical gray matter: changes with aging and the role of CSF-suppression. J Magn Reson Imaging. 20, 216-227.

Bookstein, F. L., 2001. "Voxel-based morphometry" should not be used with imperfectly registered images. Neuroimage. 14, 1454-1462.

Brody, B. A., Kinney, H. C., Kloman, A. S. and Gilles, F. H., 1987. Sequence of central nervous system myelination in human infancy. I. An autopsy study of myelination. J Neuropathol Exp Neurol. 46, 283-301.

Büchel, C., Raedler, T., Sommer, M., Sach, M., Weiller, C. and Koch, M. A., 2004. White matter asymmetry in the human brain: a diffusion tensor MRI study. Cereb Cortex. 14, 945-951.

Chenevert, T. L., Brunberg, J. A. and Pipe, J. G., 1990. Anisotropic diffusion in human white matter: demonstration with MR techniques in vivo. Radiology. 177, 401-405.

Conturo, T. E., Lori, N. F., Cull, T. S., Akbudak, E., Snyder, A. Z., Shimony, J. S., McKinstry, R. C., Burton, H. and Raichle, M. E., 1999. Tracking neuronal fiber pathways in the living human brain. Proc Natl Acad Sci U S A. 96, 10422-10427.

Cooper, R. L., Chang, D. B., Young, A. C., Martin, C. J. and Ancker-Johnson, D., 1974. Restricted diffusion in biophysical systems. Experiment. Biophys J. 14, 161-177.

Courchesne, E., Chisum, H. J., Townsend, J., Cowles, A., Covington, J., Egaas, B., Harwood, M., Hinds, S. and Press, G. A., 2000. Normal brain development and aging: quantitative analysis at in vivo MR imaging in healthy volunteers. Radiology. 216, 672-682.

Davatzikos, C., 2004. Why voxel-based morphometric analysis should be used with great caution when characterizing group differences. Neuroimage. 23, 17-20.

Deutsch, G. K., Dougherty, R. F., Bammer, R., Siok, W. T., Gabrieli, J. D. and Wandell, B., 2005. Children's reading performance is correlated with white matter structure measured by diffusion tensor imaging. Cortex. 41, 354-363.

Ding, X. Q., Kucinski, T., Wittkugel, O., Goebell, E., Grzyska, U., Gorg, M., Kohlschutter, A. and Zeumer, H., 2004. Normal brain maturation characterized with age-related T2 relaxation times: an attempt to develop a quantitative imaging measure for clinical use. Invest Radiol. 39, 740-746.

Dronkers, N. F. and Baldo, J. V., 2001. Neural Basis of Speech Production. In: Smelser, N. J. and Baltes, P. (Eds.), International Encyclopedia of the Social and Behavioral Sciences. Pergamon Press, Oxford, pp. 14875-14879.

Einstein, A., 1956. Investigations on the Theory of the Brownian Movement. Dover Publications Inc, New York

Evans, A. C., 2005. The NIH MRI study of normal brain development. Neuroimage.

Filley, C. M., 2001. The Behavioral Neurology of White Matter. Oxford University Press, Oxford

Flechsig, P., 1901. Developmental (myelogenetic) localisation of the cerebral cortex in the human subject. Lancet. 158, 1027-1030.

Giedd, J. N., Blumenthal, J., Jeffries, N. O., Castellanos, F. X., Liu, H., Zijdenbos, A., Paus, T., Evans, A. C. and Rapoport, J. L., 1999. Brain development during childhood and adolescence: a longitudinal MRI study. Nat Neurosci. 2, 861-863.

Giuliani, N. R., Calhoun, V. D., Pearlson, G. D., Francis, A. and Buchanan, R. W., 2005. Voxel-based morphometry versus region of interest: a comparison of two methods for analyzing gray matter differences in schizophrenia. Schizophr Res. 74, 135-147.

Greenstein, B. and Greenstein, A., 2000. Color Atlas of Neuroscience: Neuroanatomy and Neurophysiology. Theime, Stuttgart

Haghir, H., Sadeghi, Y., Hosseini, A. and Mehraein, P., 2001. A Histological Comparison of Myelinated Nerve Fibers between The External and Extreme Capsules in Human Brain. Yahkteh. 3, 123-130.

Hahn, E. L., 1950. Spin Echoes. Physical Review. 80, 580-594.

Hashimoto, T., Mori, K., Yoneda, Y., Yamaue, T., Miyazaki, M., Harada, M., Miyoshi, H. and Kuroda, Y., 1998. Proton magnetic resonance spectroscopy of the brain in patients with Prader-Willi syndrome. Pediatr Neurol. 18, 30-35.

Hayashi, M., Itoh, M., Kabasawa, Y., Hayashi, H., Satoh, J. and Morimatsu, Y., 1992. A neuropathological study of a case of the Prader-Willi syndrome with an interstitial deletion of the proximal long arm of chromosome 15. Brain Dev. 14, 58-62.

Hermoye, L., Saint-Martin, C., Cosnard, G., Lee, S. K., Kim, J., Nassogne, M. C., Menten, R., Clapuyt, P., Donohue, P. K., Hua, K., Wakana, S., Jiang, H., van Zijl, P. C. and Mori, S., 2006. Pediatric diffusion tensor imaging: Normal database and observation of the white matter maturation in early childhood. Neuroimage. 29, 493-504.

Hildebrand, C., Remahl, S., Persson, H. and Bjartmar, C., 1993. Myelinated nerve fibres in the CNS. Prog Neurobiol. 40, 319-384.

Huppi, P. S. and Barnes, P. D., 1997. Magnetic resonance techniques in the evaluation of the newborn brain. Clin Perinatol. 24, 693-723.

Innocenti, G. M., 1986. Functions of the Corpus Callosum. In: Lepore, F., Ptito, M. and Jasper, H. H. (Eds.), Two Hemispheres - One Brain. Alan R. Liss, New York, pp. 75-82.

Ito, R., Mori, S. and Melhem, E. R., 2002. Diffusion tensor brain imaging and tractography. Neuroimaging Clin N Am. 12, 1-19.

Jancke, L. and Steinmetz, H., 2003. Anatomical Brain Asymmetries and Their Relevance for Functional Asymmetries. In: Hugdahl, K. and Davidson, R. J. (Eds.), The Asymmetrical Brain. Massachusetts Institute of Technology, Cambridge, pp. 187-229.

Jones, D. K., Simmons, A., Williams, S. C. and Horsfield, M. A., 1999. Non-invasive assessment of axonal fiber connectivity in the human brain via diffusion tensor MRI. Magn Reson Med. 42, 37-41.

Jones, D. K., Symms, M. R., Cercignani, M. and Howard, R. J., 2005. The effect of filter size on VBM analyses of DT-MRI data. Neuroimage. 26, 546-554.

Kagan, J. and Baird, A., 2004. Brain and Behavioral Development During Childhood. In: Gazzaniga, M. (Ed.), The Cognitive Neurosciences III. The MIT Press, Cambridge, pp. 93-103.

Klingberg, T., Hedehus, M., Temple, E., Salz, T., Gabrieli, J. D., Moseley, M. E. and Poldrack, R. A., 2000. Microstructure of temporo-parietal white matter as a basis for reading ability: evidence from diffusion tensor magnetic resonance imaging. Neuron. 25, 493-500.

Klingberg, T., Vaidya, C. J., Gabrieli, J. D., Moseley, M. E. and Hedehus, M., 1999. Myelination and organization of the frontal white matter in children: a diffusion tensor MRI study. Neuroreport. 10, 2817-2821.

Kreis, R., Ernst, T. and Ross, B. D., 1993. Development of the human brain: in vivo quantification of metabolite and water content with proton magnetic resonance spectroscopy. Magn Reson Med. 30, 424-437.

Kubicki, M., McCarley, R., Westin, C. F., Park, H. J., Maier, S., Kikinis, R., Jolesz, F. A. and Shenton, M. E., 2005. A review of diffusion tensor imaging studies in schizophrenia. J Psychiatr Res, In Press.

Kubicki, M., Shenton, M. E., Salisbury, D. F., Hirayasu, Y., Kasai, K., Kikinis, R., Jolesz, F. A. and McCarley, R. W., 2002. Voxel-based morphometric analysis of gray matter in first episode schizophrenia. Neuroimage. 17, 1711-1719.

Le Bihan, D., 2003. Looking into the functional architecture of the brain with diffusion MRI. Nat Rev Neurosci. 4, 469-480.

Le Bihan, D., Breton, E., Lallemand, D., Grenier, P., Cabanis, E. and Laval-Jeantet, M., 1986. MR imaging of intravoxel incoherent motions: application to diffusion and perfusion in neurologic disorders. Radiology. 161, 401-407.

Le Bihan, D., Mangin, J. F., Poupon, C., Clark, C. A., Pappata, S., Molko, N. and Chabriat, H., 2001. Diffusion tensor imaging: concepts and applications. J Magn Reson Imaging. 13, 534-546.

Lindsley, D. F. and Holmes, J. E., 1984. Basic Human Neurophysiology. Elsevier Science Publishing Co., Inc., New York

Maas, L. C., Mukherjee, P., Carballido-Gamio, J., Veeraraghavan, S., Miller, S. P., Partridge, S. C., Henry, R. G., Barkovich, A. J. and Vigneron, D. B., 2004. Early laminar organization of the human cerebrum demonstrated with diffusion tensor imaging in extremely premature infants. Neuroimage. 22, 1134-1140.

Mangin, J. F., Poupon, C., Clark, C., Le Bihan, D. and Bloch, I., 2002. Distortion correction and robust tensor estimation for MR diffusion imaging. Med Image Anal. 6, 191-198.

Mansfield, P., 1977. Multi-Planar Image Formation using NMR Spin Echoes. J Phys C. 10, L55-L58.

McKinstry, R. C., Mathur, A., Miller, J. H., Ozcan, A., Snyder, A. Z., Schefft, G. L., Almli, C. R., Shiran, S. I., Conturo, T. E. and Neil, J. J., 2002. Radial organization of developing preterm human cerebral cortex revealed by non-invasive water diffusion anisotropy MRI. Cereb Cortex. 12, 1237-1243.

Mega, M. S., Dinov, I. D., Mazziotta, J. C., Manese, M., Thompson, P. M., Lindshield, C., Moussai, J., Tran, N., Olsen, K., Zoumalan, C. I., Woods, R. P. and Toga, A. W., 2005. Automated brain tissue assessment in the elderly and demented population: construction and validation of a sub-volume probabilistic brain atlas. Neuroimage. 26, 1009-1018.

Miller, J. H., McKinstry, R. C., Philip, J. V., Mukherjee, P. and Neil, J. J., 2003. Diffusion-tensor MR imaging of normal brain maturation: a guide to structural development and myelination. AJR Am J Roentgenol. 180, 851-859.

Miller, L., Angulo, M., Price, D. and Taneja, S., 1996. MR of the pituitary in patients with Prader-Willi syndrome: size determination and imaging findings. Pediatr Radiol. 26, 43-47.

Mori, S., Crain, B. J., Chacko, V. P. and van Zijl, P. C., 1999. Three-dimensional tracking of axonal projections in the brain by magnetic resonance imaging. Ann Neurol. 45, 265-269.

Morriss, M. C., Zimmerman, R. A., Bilaniuk, L. T., Hunter, J. V. and Haselgrove, J. C., 1999. Changes in brain water diffusion during childhood. Neuroradiology. 41, 929-934.

Moseley, M., 2002. Diffusion tensor imaging and aging - a review. NMR Biomed. 15, 553-560.

Moseley, M. E., Cohen, Y., Kucharczyk, J., Mintorovitch, J., Asgari, H. S., Wendland, M. F., Tsuruda, J. and Norman, D., 1990a. Diffusion-weighted MR imaging of anisotropic water diffusion in cat central nervous system. Radiology. 176, 439-445.

Moseley, M. E., Cohen, Y., Mintorovitch, J., Chileuitt, L., Shimizu, H., Kucharczyk, J., Wendland, M. F. and Weinstein, P. R., 1990b. Early detection of regional cerebral ischemia in cats: comparison of diffusion- and T2-weighted MRI and spectroscopy. Magn Reson Med. 14, 330-346.

Mukherjee, P., Miller, J. H., Shimony, J. S., Conturo, T. E., Lee, B. C., Almli, C. R. and McKinstry, R. C., 2001. Normal brain maturation during childhood: developmental trends characterized with diffusion-tensor MR imaging. Radiology. 221, 349-358.

Mukherjee, P., Miller, J. H., Shimony, J. S., Philip, J. V., Nehra, D., Snyder, A. Z., Conturo, T. E., Neil, J. J. and McKinstry, R. C., 2002. Diffusion-tensor MR imaging of gray and white matter development during normal human brain maturation. AJNR Am J Neuroradiol. 23, 1445-1456.

Neil, J., 1997. Measurement of Water Motion (Apparent Diffusion) in Biological Systems. Concepts of Magnetic Resonance. 9, 385-401.

Neil, J., Miller, J., Mukherjee, P. and Huppi, P. S., 2002. Diffusion tensor imaging of normal and injured developing human brain - a technical review. NMR Biomed. 15, 543-552.

Nelson, E., 1967. Dynamical Theories of Brownian Motion. Princeton University, Princeton, N.J.Second Edition published 2001, http://www.math.princeton.edu/~nelson/books.html

Nomura, Y., Sakuma, H., Takeda, K., Tagami, T., Okuda, Y. and Nakagawa, T., 1994. Diffusional anisotropy of the human brain assessed with diffusion-weighted MR: relation with normal brain development and aging. AJNR Am J Neuroradiol. 15, 231-238.

Ohyama, M., Senda, M., Mishina, M., Kitamura, S., Tanizaki, N., Ishii, K. and Katayama, Y., 2000. Semi-automatic ROI placement system for analysis of brain PET images based on elastic model: application to diagnosis of Alzheimer's disease. Keio J Med. 49 Suppl 1, A105-106.

Pagliardini, S., Ren, J., Wevrick, R. and Greer, J. J., 2005. Developmental abnormalities of neuronal structure and function in prenatal mice lacking the prader-willi syndrome gene necdin. Am J Pathol. 167, 175-191.

Partridge, S. C., Mukherjee, P., Berman, J. I., Henry, R. G., Miller, S. P., Lu, Y., Glenn, O. A., Ferriero, D. M., Barkovich, A. J. and Vigneron, D. B., 2005. Tractography-based quantitation of diffusion tensor imaging parameters in white matter tracts of preterm newborns. J Magn Reson Imaging. 22, 467-474.

Partridge, S. C., Mukherjee, P., Henry, R. G., Miller, S. P., Berman, J. I., Jin, H., Lu, Y., Glenn, O. A., Ferriero, D. M., Barkovich, A. J. and Vigneron, D. B., 2004. Diffusion tensor imaging: serial quantitation of white matter tract maturity in premature newborns. Neuroimage. 22, 1302-1314.

Paus, T., Collins, D. L., Evans, A. C., Leonard, G., Pike, B. and Zijdenbos, A., 2001. Maturation of white matter in the human brain: a review of magnetic resonance studies. Brain Res Bull. 54, 255-266.

Paus, T., Zijdenbos, A., Worsley, K., Collins, D. L., Blumenthal, J., Giedd, J. N., Rapoport, J. L. and Evans, A. C., 1999. Structural maturation of neural pathways in children and adolescents: in vivo study. Science. 283, 1908-1911.

Pfefferbaum, A., Sullivan, E. V., Hedehus, M., Lim, K. O., Adalsteinsson, E. and Moseley, M., 2000. Age-related decline in brain white matter anisotropy measured with spatially corrected echo-planar diffusion tensor imaging. Magn Reson Med. 44, 259-268.

Pierpaoli, C. and Basser, P. J., 1996. Toward a quantitative assessment of diffusion anisotropy. Magn Reson Med. 36, 893-906.

Ramenghi, L. A., Childs, A. M., Evans, D. J., Tanner, S., Arthur, R., Martinez, D., Saysell, M. and Levene, M. I., 1998. Magnetic resonance of the neonatal brain. Croat Med J. 39, 132-135.

Reese, T. G., Heid, O., Weisskoff, R. M. and Wedeen, V. J., 2003. Reduction of eddy-current-induced distortion in diffusion MRI using a twice-refocused spin echo. Magn Reson Med. 49, 177-182.

Rutherford, M. A., Cowan, F. M., Manzur, A. Y., Dubowitz, L. M., Pennock, J. M., Hajnal, J. V., Young, I. R. and Bydder, G. M., 1991. MR imaging of anisotropically restricted diffusion in the brain of neonates and infants. J Comput Assist Tomogr. 15, 188-198.

Sakuma, H., Nomura, Y., Takeda, K., Tagami, T., Nakagawa, T., Tamagawa, Y., Ishii, Y. and Tsukamoto, T., 1991. Adult and neonatal human brain: diffusional anisotropy and myelination with diffusion-weighted MR imaging. Radiology. 180, 229-233.

Schmithorst, V. J., Wilke, M., Dardzinski, B. J. and Holland, S. K., 2002. Correlation of white matter diffusivity and anisotropy with age during childhood and adolescence: a cross-sectional diffusion-tensor MR imaging study. Radiology. 222, 212-218.

Schmitt, F., Stehling, M. K. and Turner, R., 1998. Echo-Planar Imaging Theory, Technique and Application. Springer-Verlag, Berlin

Schneider, J. F., Il'yasov, K. A., Hennig, J. and Martin, E., 2004. Fast quantitative diffusion-tensor imaging of cerebral white matter from the neonatal period to adolescence. Neuroradiology. 46, 258-266.

Shapira, N. A., Lessig, M. C., He, A. G., James, G. A., Driscoll, D. J. and Liu, Y., 2005. Satiety dysfunction in Prader-Willi syndrome demonstrated by fMRI. J Neurol Neurosurg Psychiatry. 76, 260-262.

Shimony, J. S., McKinstry, R. C., Akbudak, E., Aronovitz, J. A., Snyder, A. Z., Lori, N. F., Cull, T. S. and Conturo, T. E., 1999. Quantitative diffusion-tensor anisotropy brain MR imaging: normative human data and anatomic analysis. Radiology. 212, 770-784.

Snook, L., Paulson, L. A., Roy, D., Phillips, L. and Beaulieu, C., 2005. Diffusion tensor imaging of neurodevelopment in children and young adults. Neuroimage. 26, 1164-1173.

Sowell, E. R., Thompson, P. M., Holmes, C. J., Jernigan, T. L. and Toga, A. W., 1999. In vivo evidence for post-adolescent brain maturation in frontal and striatal regions. Nat Neurosci. 2, 859-861.

Sowell, E. R., Thompson, P. M., Tessner, K. D. and Toga, A. W., 2001. Mapping continued brain growth and gray matter density reduction in dorsal frontal cortex: Inverse relationships during postadolescent brain maturation. J Neurosci. 21, 8819-8829.

Sowell, E. R., Thompson, P. M. and Toga, A. W., 2004. Mapping changes in the human cortex throughout the span of life. Neuroscientist. 10, 372-392.

Sowell, E. R., Trauner, D. A., Gamst, A. and Jernigan, T. L., 2002. Development of cortical and subcortical brain structures in childhood and adolescence: a structural MRI study. Dev Med Child Neurol. 44, 4-16.

Stejskal, E. O., 1965. Use of spin echoes in a pulsed magnetic-field gradient to study anisotropic, restricted diffusion and flow. Journal of Chemical Physics. 43, 3597 - 3603.

Stejskal, E. O. and Tanner, J. E., 1965. Spin diffusion measurements: spin echoes in the presence of a time-dependent field gradient. Journal of Chemical Physics. 42, 288 - 292.

Sundgren, P. C., Dong, Q., Gomez-Hassan, D., Mukherji, S. K., Maly, P. and Welsh, R., 2004. Diffusion tensor imaging of the brain: review of clinical applications. Neuroradiology. 46, 339-350.

Suzuki, M., Hagino, H., Nohara, S., Zhou, S. Y., Kawasaki, Y., Takahashi, T., Matsui, M., Seto, H., Ono, T. and Kurachi, M., 2005. Male-specific volume expansion of the human hippocampus during adolescence. Cereb Cortex. 15, 187-193.

Suzuki, Y., Matsuzawa, H., Kwee, I. L. and Nakada, T., 2003. Absolute eigenvalue diffusion tensor analysis for human brain maturation. NMR Biomed. 16, 257-260.

Takeda, K., Nomura, Y., Sakuma, H., Tagami, T., Okuda, Y. and Nakagawa, T., 1997. MR assessment of normal brain development in neonates and infants: comparative study of T1- and diffusion-weighted images. J Comput Assist Tomogr. 21, 1-7.

Tapp, P. D., Head, K., Head, E., Milgram, N. W., Muggenburg, B. A. and Su, M. Y., 2006. Application of an automated voxel-based morphometry technique to assess regional gray and white matter brain atrophy in a canine model of aging. Neuroimage. 29, 234-244.

Tapp, P. D., Siwak, C. T., Gao, F. Q., Chiou, J. Y., Black, S. E., Head, E., Muggenburg, B. A., Cotman, C. W., Milgram, N. W. and Su, M. Y., 2004. Frontal lobe volume, function, and beta-amyloid pathology in a canine model of aging. J Neurosci. 24, 8205-8213.

Taylor, D. G. and Bushell, M. C., 1985. The spatial mapping of translational diffusion coefficients by the NMR imaging technique. Phys Med Biol. 30, 345-349.

Testa, C., Laakso, M. P., Sabattoli, F., Rossi, R., Beltramello, A., Soininen, H. and Frisoni, G. B., 2004. A comparison between the accuracy of voxel-based morphometry and hippocampal volumetry in Alzheimer's disease. J Magn Reson Imaging. 19, 274-282.

Thompson, P. M., Giedd, J. N., Woods, R. P., MacDonald, D., Evans, A. C. and Toga, A. W., 2000. Growth patterns in the developing brain detected by using continuum mechanical tensor maps. Nature. 404, 190-193.

Thompson, P. M., Sowell, E. R., Gogtay, N., Giedd, J. N., Vidal, C. N., Hayashi, K. M., Leow, A., Nicolson, R., Rapoport, J. L. and Toga, A. W., 2005. Structural MRI and brain development. Int Rev Neurobiol. 67, 285-323.

Torrey, H. C., 1956. Bloch Equations with Diffusion Terms. Physical Review. 104, 563-565.

Tuch, D. S., 2004. Q-ball imaging. Magn Reson Med. 52, 1358-1372.

Tucker, K. A., Robertson, K. R., Lin, W., Smith, J. K., An, H., Chen, Y., Aylward, S. R. and Hall, C. D., 2004. Neuroimaging in human immunodeficiency virus infection. J Neuroimmunol. 157, 153-162.

Turner, R., Le Bihan, D., Maier, J., Vavrek, R., Hedges, L. K. and Pekar, J., 1990. Echo-planar imaging of intravoxel incoherent motion. Radiology. 177, 407-414.

Wakana, S., Jiang, H., Nagae-Poetscher, L. M., van Zijl, P. C. and Mori, S., 2004. Fiber tract-based atlas of human white matter anatomy. Radiology. 230, 77-87.

Walker, E. and Bollini, A. M., 2002. Pubertal neurodevelopment and the emergence of psychotic symptoms. Schizophr Res. 54, 17-23.

Wesbey, G. E., Moseley, M. E. and Ehman, R. L., 1984a. Translational molecular self-diffusion in magnetic resonance imaging. I. Effects on observed spin-spin relaxation. Invest Radiol. 19, 484-490.

Wesbey, G. E., Moseley, M. E. and Ehman, R. L., 1984b. Translational molecular self-diffusion in magnetic resonance imaging. II. Measurement of the self-diffusion coefficient. Invest Radiol. 19, 491-498.

Woessner, D. E., 1963. N.M.R. spin-echo self-diffusion measurements on fluids undergoing restricted diffusion. Journal of Physical Chemistry. 67, 1365 - 1367.

Worsley, K. J., Evans, A. C., Marrett, S. and Neelin, P., 1992. A three-dimensional statistical analysis for CBF activation studies in human brain. J Cereb Blood Flow Metab. 12, 900-918.

Xing, D., Papadakis, N. G., Huang, C. L., Lee, V. M., Carpenter, T. A. and Hall, L. D., 1997. Optimised diffusion-weighting for measurement of apparent diffusion coefficient (ADC) in human brain. Magn Reson Imaging. 15, 771-784.

Yakovlev, P. and Lecours, A., 1967. The myelogenetic cycles of regional maturation of the brain. In: Minkowski, A. (Ed.), Regional development of the brain in early life. Blackwell, Oxford.

Yamada, K., Matsuzawa, H., Fujii, Y., Kwee, I. L. and Nakada, T., 2005. Brain Developmental Abnormalities in Prader-Willi Syndrome Detected by Diffusion Tensor Imaging. Proceedings of the Society for Neuroscience, Washington, DC, pp. 565.3.

Yoshii, A., Krishnamoorthy, K. S. and Grant, P. E., 2002. Abnormal cortical development shown by 3D MRI in Prader-Willi syndrome. Neurology. 59, 644-645.

Yoshiura, T., Mihara, F., Tanaka, A., Togao, O., Taniwaki, T., Nakagawa, A., Nakao, T., Noguchi, T., Kuwabara, Y. and Honda, H., 2005. Age-related structural changes in the young adult brain shown by magnetic resonance diffusion tensor imaging. Acad Radiol. 12, 268-275.